

https://dspace.org/

Preparation of (Ti,Ta)(C,N) by mechanical alloying

Naidoo, Melisha

2013-01-31
http://hdl.handle.net/10539/12352

Downloaded from a DSpace repository. https://dspace.org/

Preparation of (Ti,Ta)(C,N) by Mechanical Alloying

Melisha Naidoo

A dissertation submitted to the Faculty of Engineering and the Built Environment, University of the Witwatersrand, Johannesburg, in fulfilment of the requirements for the degree of Master of Science in Engineering.

August 2012

Declaration

I declare that this dissertation is my own unaided work. It is being submitted to the degree of Master of Science to the University of the Witwatersrand, Johannesburg. It has not been submitted before for any degree or examination to any other university.

_____

Melisha Naidoo

_____ day of _____2012

Extracts of this research has been published in:

1. M. Naidoo, J. Raethel, I. Sigalas, and M. Herrmann, "Preparation of (Ti,Ta)(C,N) by Mechanical Alloying," *International Journal of Refractory Metals and Hard Materials*, 2012.

2. M. Naidoo, I. Sigalas, and M. Herrmann, "Preparation of Ti-Ta-(C,N) by Mechanical Alloying Ti(C,N) and TaC," *International Journal of Refractory Metals and Hard Materials*, in press 2012.

Dedicated to

my parents

Acknowledgements

First and foremost, I would like to offer the highest thanks to Lord Shri Krsna, for the opportunities I have been given and the capability to follow through successfully. Thank you for giving me the strength and power to persevere.

I would like to thank my supervisor, Prof Sigalas, for giving me the opportunity to carry out this research. Thank you for your guidance, suggestions and steadfast encouragement to complete this research.

My deepest and sincerest gratitude to my co-supervisor, Dr. Herrmann. Without your knowledge and expertise this dissertation would not have been possible. Your contribution has been invaluable and I thank you for the use of your facilities when we needed them.

A special thank you to Jan Raethel for his help in running my experiments. Your time and effort is greatly appreciated.

I would like to acknowledge the financial support of the DST/NRF Centre of Excellence in Strong Materials and Element six. Thank you for the opportunity as well as the facilities to work in.

To all my colleagues and friends, many thanks for contributing to a stimulating work environment. Thanks for all the laughs and afternoons at the PIG.

To Rinesh, a heartfelt thanks for your support and encouragement over the past six years. Your belief and confidence in me was all the inspiration I needed. Thank you for your suggestions and advice during the writing up of this dissertation and for your skill with formatting.

Last, but certainly not least, to my amazing parents and brother. Thank you for your patience and encouragement through all these years of studying. I could never repay all the sacrifices you have made for me but I thank you from the bottom of my heart for everything. I would not be who I am today had it not been for your love and support. Thank you.

Abstract

The research described in this dissertation concerns an investigation into the development of new/modified Ti(C,N)-based cermet materials for applications relating to the metal machining industry.

Ti(C,N)-based cermets are widely employed for high speed machining owing to their attractive properties such as high hot hardness, chemical stability and excellent wear resistance. However, the increasing demand for high performance, advanced materials has steered research towards the development of novel tooling materials using unconventional processing methodologies. The mechanical alloying technique has shown promising results in this regard. The technique has been identified as a powerful tool for the development of advanced engineering materials including equilibrium, non-equilibrium and composite materials. By understanding the composition-microstructure-property relationship, guidelines can be provided with regard to producing materials possessing desirable mechanical properties. As such, the synthesis of the (Ti,Ta)-carbonitride solid solution was investigated by mechanically alloying brittle-ductile and brittle-brittle components.

When brittle-ductile Ti(C,N) and Ta powders were mechanically alloyed, the (Ti,Ta)-carbonitride solid solution was successfully obtained. Mechanical alloying greatly improved the sinterability of the Ti(C,N)-Ta powders and full densification was obtained in solid state. As a result of high energy milling, nanocrystalline Ti(C,N) was obtained. Consequently, cermets produced with these mechanically alloyed powders showed a fine microstructure and possessed superior mechanical properties, as compared to conventional ball milled sintered cermets.

Conversely, formation of the (Ti,Ta)(C,N) solid solution phase was unsuccessful by the mechanical alloying of brittle-brittle Ti(C,N) and TaC powders. Owing to the brittleness of the powders and the low diffusion coefficients in the carbide lattices, the mechanical alloying process served only to refine the grain size of the Ti(C,N) and TaC phases, whilst both phases remained unreacted by the end of milling. Consequently, only partial dissolution was achieved during sintering of the mechanically alloyed Ti(C,N)-TaC powders. As such, poor densification was obtained in these samples which served to lower their mechanical properties.

Table of Contents

Declaration ..... *i*

Acknowledgements ..... *iii*

Abstract ..... *iv*

Chapter 1: Introduction *1*

Chapter 2: Literature Review *4*

2.1. Transition Metal Carbides and Nitrides **4**

2.1.1. Properties of Tantalum Metal Carbides 6

2.2. Cermets **7**

2.2.1. Titanium carbonitride-based cermets 9

2.3. Mechanical Alloying **19**

2.3.1. Introduction to Mechanical Alloying 19

2.3.2. The Process of Mechanical Alloying 23

2.3.3. The Mechanisms of Alloying 25

2.3.4. Systems for Mechanical alloying 29

2.3.5. Diffusion in Mechanical Alloying 34

Chapter 3: Experimental Method *38*

3.1. Raw Materials **39**

3.2. Powder Processing **39**

3.2.1. Ball-Milling 39

3.2.2. Mechanical Milling 40

3.3. Powder Characterisation **41**

3.3.1. Sample Preparation 41

3.3.2. Scanning Electron Microscopy 41

3.3.3. X-Ray Diffraction 42

3.4. Sintering Experiments **43**

3.4.1. Spark Plasma Sintering (SPS) 44

3.5. Cermet Characterisation **44**

3.5.1. Sample Preparation 44

3.5.2. Optical Microscopy 45

3.5.3. Physical property measurements 45

Chapter 4: Experimental Results *47*

4.1. Milling Process **47**

4.1.1. Ball Milling 47

4.1.2. Mechanical Alloying 50

4.2. Sintering Experiments **59**

4.2.1. Ti(C,N)-(Ta)-Ni Ball-MilledCermets 59

4.2.2. Ti(C,N)-Ta Mechanically Alloyed Cermets 63

4.2.3. Ti(C,N)-TaC Mechanically Alloyed Cermets 66

4.3. Microstructural Analysis **68**

4.3.1. Ball-Milled Cermets 68

4.3.2. Mechanically Alloyed Cermets 70

4.4. Mechanical Properties **73**

4.4.1. Ball-Milled Cermets 73

4.4.2. Mechanically Alloyed Cermets 74

Chapter 5: Discussion *75*

5.1. Fundamental Reactions in Mechanical Alloying of Ductile-Brittle and Brittle-Brittle Components **75**

5.2. Effect of Composition and Processing on Cermet Sinterability **79**

5.2.1. Ni-Binder containing Materials 79

5.2.2. Binder-free Materials 83

5.3. Effect of Composition and Processing on the Microstructural and Mechanical Properties of Ti(C,N)-based Cermets **91**

5.3.1. Ni-Binder containing Materials 91

5.3.2. Binder-free Materials 94

Chapter 6: Conclusions *96*

Chapter 7: References *97*

List of Figures

Figure 2-1: Illustration of the crystal structure of Ti(C,N) [25] 9
Figure 2-2: (a) Lattice parameter of Ti(C,N) as a function of nitrogen content[29] (b) Microhardness of Ti(C,N) as a function of nitrogen content[29] (c) Thermal conductivity dependence of Ti(C,N) on nitrogen content[28] 11
Figure 2-3: Schematic diagram of cermet cutting tool properties as a function of composition (after [1]) 13
Figure 2-4: Schematic representation of a SEM image of a Ti(C,N)-based cermet [4] 14
Figure 2-5: Variation of Hardness with the content of metallic binder [34] 15
Figure 2-6: SEM (BSE) micrographs of Ti(C,N)-10MC-30Ni, where MC is (a) HfC, (b) TaC and (c) WC 16
Figure 2-7: Synthesizing capabilities of the Mechanical Alloying process [44] 20
Figure 2-8: Schematic representation of the main factors affecting the MA process [44] 23
Figure 2-9: Common machines used for mechanical alloying [63] 25
Figure 2-10: Ball-powder-ball collision of powder mixtures during mechanical alloying [64] 26
Figure 2-11: The five stages of mechanical alloying according to Benjamin and Volin [66] 27
Figure 2-12: Narrow particle distribution achieved when a balance is maintained between the fracturing and welding processes [69] 28
Figure 2-13: SEM (BSE) micrograph of Ti(C,N)-Fe powder milled (a) 6Hr and (b) 12Hr[62] 30
Figure 2-14: SEM (BSE) images of the Ti(C,N)-W powders (a) starting powders and (b) powders milled for 12 hours [75] 33
Figure 2-15: SEM (BSE)image of cross-sectional Ti(C,N)-W powder mechanically alloyed for 24Hr[75] 33
Figure 2-16: Change in activation energy in the x-direction[79] 35
Figure 2-17: Dependence of diffusivity on surface, grain boundary and lattice diffusion at different temperatures [79] 37
Figure 3-1: Summary of experimental set-up 38
Figure 3-2: Schematic diagram of the SPS apparatus [86] 44
Figure 4-1: Diffractograms for the various ball-milled powder mixtures 48
Figure 4-2: SEM (BSE) micrographs of the ball-milled powder mixtures for (a) Cermet 3 (b) Cermet 4 and (c) Cermet 5 49
Figure 4-3: Diffractograms for the Ti(C,N)-Ta powders mechanically alloyed for different time intervals 51
Figure 4-4: Particle size refinement and lattice strain evolution with mechanical alloying 52
Figure 4-5: SEM (SE) micrographs of Ti(C,N)-Ta powders mechanically alloyed for 2h (a)-(b) and 12h (c)-(d) 53
Figure 4-6: EDX analysis of Ti(C,N)-Ta powders mechanically alloyed for 12 hours 54
Figure 4-7: Diffractograms for the Ti(C,N)-TaC powders mechanically alloyed for different time intervals 56
Figure 4-8: SEM (SE) micrographs of the Ti(C,N)-TaC powders after 0h MA(a) and (b); and 48h MA (c) and (d) 58
Figure 4-9: Densification curves for Cermet 3, Cermet 4 and Cermet 5 60
Figure 4-10: Diffractograms for the various cermets produced by ball milling 61
Figure 4-11: Densification curve for theTi(C,N)-Ta powders sintered after various times of MA 64
Figure 4-12: XRD pattern of the TiCN-Ta powders sintered at 1500°C 65
Figure 4-13: XRD profile of the mechanically alloyed Ti(C,N)-TaC powders sintered by SPS at 1500°C 67

Figure 4-14: SEM (BSE) micrographs of the various cermets sintered by SPS after ball-milling (a) Cermet 1: TiCN-10Ni, (b) Cermet 2: TiCN-Ta-10Ni, (c) Cermet 3: TiCN-5Ni, (d) Cermet 4: TiCN-Ta-5Ni and (e) Cermet 5: TiCN-Ta 69
Figure 4-15: SEM (SE) image of Cermet 3, with EDS spectra of various mircostructural phases 70
Figure 4-16: SEM (SE) micrographs of the Ti(C,N)-Ta powders sintered at 1500°C after (a) 2 hours MA (b) 4 hours MA (c) 8 hours MA and (d) 12 hours MA 71
Figure 4-17: SEM (SE) image of Ti(C,N)-Ta cermet prepared by MA, with EDS spectra of various mircostructural phases 71
Figure 4-18: SEM (BSE) micrographs of the Ti(C,N)-TaC powders sintered at 1500°C after (a) 24 hours MA and (b) 48hours MA 72
Figure 5-1: Ti(C,N) crystallite size refinement and lattice strain evolution with mechanical alloying of the Ti(C,N)-Ta and Ti(C,N)-TaC mixtures 77
Figure 5-2: Densification curves for Cermet 3, Cermet 4 and Cermet 5 79
Figure 5-3: Binary Ni-Ta phase diagram [92] 81
Figure 5-4: Densification curve for the Ti(C,N)-Ta powders sintered after ball-milling and various times of MA 85
Figure 5-5: Ti(C,N) lattice parameter changes of the BM and Ti(C,N)-Ta mixtures following MA and SPS, including the lattice parameters of the Ti(C,N) and TaC reference materials [28]-[90] 86
Figure 5-6: Ti(C,N) lattice parameter changes for the Ti(C,N)-Ta and Ti(C,N)-TaC mixtures following MA and SPS .. 89
Figure 5-7: Microstructures of binder-free Ti(C,N)-based cermets (a) Ti(C,N)-Ta MA 2Hr, (b) Ti(C,N)-Ta MA 4Hr, (c) Ti(C,N)-Ta MA 8Hr, (d) Ti(C,N)-Ta MA 12Hr, (e) Ti(C,N)-TaC MA 24Hr, (f) Ti(C,N)-TaC MA 48Hr and (g) Ti(C,N)-Ta BM 90
Figure 5-8: Mechanical properties of the Ni-binder containing Ti(C,N)-based cermets 91
Figure 5-9: Mechanical properties of the binder-free Ti(C,N)-based cermets 95

List of Tables

*Table 2-1: Properties of Group IV-VI transition metals, carbides and nitrides [10]. (*Values in brackets from [12])... 5*
Table 2-2: Development of titanium carbonitride-based cermets (after [21][22])... 7
Table 2-3: Comparison of properties between TiC-based cermets and Ti(C,N)-based cermets [24]... 8
Table 2-4: Properties of TiC and TiN... 10
Table 2-5: Density and mechanical properties of Ti(C,N)-based cermets [39][40]... 17
Table 2-6: Typical properties of Ti(C,N)-based cermets... 18
Table 3-1: Characteristics of raw powders in the as-received condition... 39
Table 3-2: A summary of the milling conditions used in this study... 40
Table 3-3: Composition design of cermet materials (wt%)... 43
Table 4-1: Sample Composition for ball-milled cermets... 47
Table 4-2: Sample Composition and Experimental Design for Ti(C,N)-Ta Mechanically Alloyed Cermets... 50
Table 4-3: Effect of mechanical alloying on the Ti(C,N) lattice parameter and crystallite size in the Ti(C,N)-Ta mixture... 51
Table 4-4: Sample Composition and Experimental Design for Ti(C,N)-TaC Mechanically Alloyed Cermets... 55
Table 4-5: Ti(C,N) and TaC lattice parameter and crystallite size evolution for the Ti(C,N)-TaC mixture after various times of mechanical alloying... 57
Table 4-6: Physical Properties of Ti(C,N)-based ball-milled cermets... 60
Table 4-7: Ti(C,N) Lattice parameter changes for the various cermets produced after ball milling... 62
Table 4-8: Physical Properties of Ti(C,N)-Ta Mechanically Alloyed cermets sintered at 1500°C... 63
Table 4-9: Physical Properties of Ti(C,N)-TaC Mechanically Alloyed cermets sintered at 1500°C... 66
Table 4-10: Ti(C,N) and TaC lattice parameter changes for the Ti(C,N)-TaC cermets produced after different times of mechanical alloying... 67
Table 4-11: Mechanical properties of the various cermets produced after ball-milling... 73
Table 4-12: Mechanical properties of the mechanically alloyed Ti(C,N)-Ta cermets... 74
Table 4-13: Mechanical properties of the mechanically alloyed Ti(C,N)-TaC cermets... 74
Table 5-1: Comparison of properties between mechanically alloyed powders and reference materials... 75
Table 5-2: Summary of results for the mechanically alloyed cermets sintered at 1500°C... 83

Chapter 1: Introduction

Titanium carbonitride (TiCN)-based cermets are widely used in metal machining applications, as both bulk materials and protective hard coatings for cutting tool inserts. Ti(C,N)-based cermets are competitors to conventional tungsten carbide-cobalt (WC-Co) cutting tools owing to their higher hot hardness, thermal and chemical stability, resistance to plastic deformation at elevated temperatures and excellent creep and wear resistance [**1**]-[**2**].

Optimisation of the mechanical properties of Ti(C,N)-based cermets is possible due to its complex microstructure [**3**]-[**4**]. Generally, these cermets are composed of Ti(C,N) solid solutions as the hard ceramic phase and Ni/Co as the metal binder. The carbide phases typically exhibit a core-rim microstructure where the rims are partially dissolved raw material grown through dissolution-reprecipitation processes on undissolved cores. This core-rim structure significantly influences the materials properties, since the undissolved Ti(C,N) cores are responsible for excellent wear resistance, while crack interactions between the solid solution rim structure and the binder phase determine the cermets toughness and integrity [**5**]. Ti(C,N) cermets can be reinforced with different transition metal carbides in order to enhance specific properties which improve their performance. Usually Mo_2C and WC are added to Ti(C,N) cermets to enhance densification and fracture toughness, whilst Ta/Nb carbide additions improve cutting performance by enhancing hot hardness and thermal shock resistance [**1**].

In addition, Ti(C,N)-based materials have been employed as a binder for the sintering of polycrystalline cubic boron nitride (PcBN) tools. Cubic boron nitride (cBN) is the second hardest material after diamond, and its superhard properties account for its widespread usage as a cutting tool, mainly for the machining of ferrous materials that would chemically attack diamond under the same conditions [**6**]-[**7**]. During high speed machining, PcBN remains inert and retains its high hardness and fracture toughness; and its low coefficient of thermal expansion allows it to be less sensitive to thermal shock compared to most ceramic materials [**8**].

Despite its attractive properties, uninterrupted and prolonged machining finds PcBN tools susceptible to chemical wear. It has been proposed that one possible way of improving the chemical wear resistance of these sintered hard materials is through modification of their binder phases. Incorporating binders based on titanium carbonitrides of transition metals as their hard components improves the operating characteristics of PcBN tools compared to those tools containing traditional aluminium binders.

Although diamond, cBN and WC have their stable place in industry, they each have their limitations as cutting tool materials. The increasing demand for 'stronger,' 'stiffer,' 'harder' and 'tougher' materials has led to the design and development of advanced materials. As such, scientific investigations by competitors have been continuously directed towards improving the properties and performance of materials in order to improve their hold on the global cutting tool market.

It is well recognised that the structure and constitution of advanced materials can be better controlled by processing them under non-equilibrium (or far-from equilibrium) conditions [**9**]. Amongst these processes, rapid solidification from the liquid state, mechanical alloying, plasma processing and vapour deposition have received much attention by researchers for commercial use. The underlying theme in all these techniques is to synthesize materials in a non-equilibrium state by 'energizing and quenching'. The energization involves bringing the materials into a highly non-equilibrium (metastable) state by some external dynamic force e.g. through melting, evaporation, irradiation, application of pressure or storing of mechanical energy by plastic deformation. The material is then quenched into a configurationally frozen state, which can then be used as a precursor to obtain the desired chemical constitution and/or microstructure by subsequent heat treatment/processing [**9**]. It has been shown that materials processed in this way possess improved physical and mechanical characteristics compared to conventional ingot (solidification) processed materials [**9**].

In this study, the synthesis of (Ti,Ta)(C,N) by the mechanical alloying technique is investigated. Mechanical alloying has received serious attention as a powerful tool for the fabrication of advanced engineering materials including equilibrium, non-equilibrium and composite materials. This high energy ball milling process involves repeated cold welding, fracturing and rewelding processes to plastically deform and mix the constituent

components. The extreme deformations experienced by the milled powders are an intrinsic part of the mechanical alloying process, leading to microstructural refinement and consequently enhanced physical and mechanical properties.

As such, the objectives of the study are to evaluate the mechanical alloying process as a promising route to develop Ti(C,N)-based cermets and to investigate if this processing technology offers significant improvement to alloy design with respect to microstructural-property relationships.

The dissertation begins with a review of Ti(C,N)-based cermets, which is presented in Chapter 2, along with a detailed description of the mechanical alloying process. Chapter 3 contains the method of investigation, including the experimental techniques and equipment used. The results of the investigation are presented in Chapter 4, followed by a discussion of these results in Chapter 5. Finally, based on the results and discussion, conclusions are drawn and presented in Chapter 6.

Chapter 2: Literature Review

2.1. Transition Metal Carbides and Nitrides

Carbon and nitrogen form strong bonds with the transition metals in Groups IVb – VIb, producing an interesting class of materials which possess both properties that are inherent of the parent metal lattice, as well as properties that result from the strong metal-to-carbon/nitrogen bonds. Alloys based on the carbides and nitrides of the transition metals exhibit unique physical and mechanical properties that result from manipulation of their composition and manufacturing process [**10**].

Table 2-1 lists the selected properties of the Group IV-VI transition metals, carbides and nitrides. These materials are collectively referred to as refractory materials owing to their extremely high melting points (2000-4000°C). In addition, these compounds are extremely hard (1200-3000 kg/mm^2), have high elastic modulus (300-700 GPa) and good thermal and electrical conductivity. Their hardness is retained to very high temperatures, they have low chemical reactivity and retain good corrosion resistance at high temperatures. For these reasons, transition metal carbides, nitrides and their solid solutions find widespread industrial use as cutting tools and wear-resistant parts [**10**].

Although all elements of Groups IV – VI are capable of forming refractory carbides, the number and complexity of these carbide systems increases with group number. The Group IV and V carbides have NaCl (B1) crystal structure, whereas the structures of the Group VI carbides are more complex. The carbon atom occupies the interstitial lattice sites and at 100% site occupancy the stoichiometry of the carbide is MC (where M is the transition metal). The concentration that results from a sub-stoichiometric M:C ratio greatly affects the thermodynamic, mechanical, electronic and magnetic properties of the metal carbide [**11**]. This effect is shown in Table 2-1, showing that the microhardness of the sub-stoichiometric carbides are higher than that of the stoichiometric carbides.

Table 2-1: Properties of Group IV-VI transition metals, carbides and nitrides [10]. (*Values in brackets from [12])

	Crystal Structure	Melting Point (K)	Micro-Hardness (kg/mm^2)	Modulus of Elasticity (GPa)
Group 4				
Ti	Hexagonal	1940	-	110
TiC	NaCl	3370	3000	451
TiN	NaCl	3220	2000	612
Zr	Hexagonal	2120	-	95
ZrC	NaCl	3670	2700	348
ZrN	NaCl	3250	1500	460
Hf	Hexagonal	2490	-	138
HfC	NaCl	4170	2600 (2700 $HfC_{0.99}$)*	352
HfN	NaCl	3660	1600	380
Group 5				
V	BCC	2170	-	130
VC	NaCl	2970	2900	422
VN	NaCl	2450	1500	-
Nb	BCC	2740	80	101
NbC	NaCl	3870	2000 (2400$NbC_{0.99}$)*	338
NbN	NaCl	2470	1400	-
Ta	BCC	3250	110	186
TaC	NaCl	4070	1800 (2500 $TaC_{0.99}$)*	285
TaN	NaCl	3360	1050	-
Group 6				
Cr	BCC	2130	-	248
Cr_3C_2	Orthorhombic	2070	1400	373
CrN	Hexagonal	1770	1100	-
Mo	BCC	2890	210	325
Mo_2C	Hexagonal	2770	1500	533
W	BCC	3670	400	345
WC	Hexagonal	3070	2350	696

2.1.1. Properties of Tantalum Metal Carbides

Tantalum metal carbide (TaC) shares a number of properties with other refractory carbides such as high hardness, fracture toughness and oxidation and wear resistance. However, among the transition metals, TaC has the highest melting point at 3983°C and is the most chemically stable of all the carbides [**13**]. As a result, TaC finds widespread usage in the field of cutting tools. It is commonly used as an additive for cemented carbides based on WC and Co, to improve the cutting characteristics of the alloy. TaC inhibits the grain growth of WC particles during liquid phase sintering and improves the alloys' properties such as hardness, strength, resistance to oxidation and fatigue [**14**]. TaC is also used for coating steel moulds for die casting of aluminium alloys. It provides a hard, wear resistant surface, which results in a low friction mould surface [**15**].

Mixed-metal carbides have also been examined for their high melting points and their hot hardness. It has been demonstrated that compositions of the ternary systems, namely those formed with TiC, TiN, ZrC, NbC , HfC and HfN are harder than the corresponding binary compounds [**16**]. Koester and Moak [**17**] compared the hot hardness of $(Ta_{0.8}Hf_{0.2})C_{1+x}$ with that of pure metal carbides TaC_{1-x} and HfC_{1+x}. Their results indicated that for temperatures up to 1400°C the hardness increased in the order $HfC_{1+x} < (Ta_{0.8}Hf_{0.2})C_{1+x} < TaC_{1-x}$, but at temperatures exceeding 1400°C the mixed carbide began to outperform tantalum carbide. The benefits of TaC addition to other alloy systems are further discussed in Section 2.2.1.3.

2.2. Cermets

A cermet (or a ceramic metal) is a structural material composed of a hard ceramic phase and a metal binding phase. Cermets are designed to incorporate the optimal properties of both the ceramic and metal phases. Consequently, cermets have high hardness and oxidation resistance provided by the ceramic phase, while the metal phase contributes ductility, toughness and thermal shock resistance [**18**].

Cermet materials are successfully employed in high speed machining of high strength steel grades and ductile cast irons. Recently, more and more conventional WC-based hardmetals are being replaced by carbide-based cermets, accompanied with the trend of high speed machining [**19**]. While similar in many aspects to WC-based hardmetals, cermets are more wear resistant, have higher performance reliability, give a better surface quality finish and have better edge strength and edge sharpness in these applications [**20**].

Table 2-2: Development of titanium carbonitride-based cermets (after [21**] [**22**])**

Year of establishment	Hard Phase	Binder Phase
1929	Ti(C)	Ni
1931	Ti(C,N)	Ni(Co,Fe)
1970	Ti(C,N)	Ni-Mo
1974	(Ti, Mo)(C,N)	Ni-Mo
1980-1983	(Ti, Mo, W)(C,N)	Ni-Mo-Al
1988	(Ti, Ta, Nb, V, Mo, W)(C,N)	(Ni,Co)-Ti_2AlN
1988	(Ti, Ta, Nb, V, W)(C,N)	Ni-Co
1991	(Ti, Ta, Nb, V, Mo, W, etc.)(C,N)	Ni-Cr

Table 2-2 provides a glance to the history of cermet development. Currently, there are two kinds of cermets available commercially, titanium carbide-based (TiC) and titanium carbonitride-based (Ti(C,N) cermets. As compared to titanium carbide-based cermets (Table 2-3), the titanium carbonitride-based cermets have higher hot hardness and transverse rupture strength (TRS), better oxidation resistance (less weight gain during oxidation tests) and higher thermal conductivity [**22**]-[**23**]. The relatively high enthalpy of formation of titanium carbonitride increases its resistance to built-up edges, scaling and crater formation. In cutting performance, Ti(C,N)-based cermets show improved surface finishing, tolerance control and prolonged tool life, even on superalloys and other difficult-to-machine materials for which TiC-based cermets cannot be used [**21**].

Consequently, due to their superior mechanical properties and chemical stability, titanium carbonitride is the major raw material in making high performance cermets and are quickly replacing titanium carbide-based cermets in metal machining applications.

Table 2-3: Comparison of properties between TiC-based cermets and Ti(C,N)-based cermets [24**]**

Cermets	1000°C Microhardness ($kgmm^{-2}$)	900°C Strength (TRS) (MPa)	Weight gain during oxidation tests at 1000°C ($mg.cm^{-2}h^{-1}$)	Therm. Cond ($Wm^{-1}deg^{-1}$)
TiC-cermet[a]	500	1050	11.8	24.7
Ti(C,N)-cermet[b]	600	1360	1.6	42.3

[a]TiC-16.5Ni-9Mo; [b] TiC-20TiN-15WC-10TaC-5.5Ni-11Co-9Mo

2.2.1. Titanium carbonitride-based cermets

Titanium carbide (TiC) and titanium nitride (TiN) are the basis for titanium carbonitride. The crystal structures of TiC and TiN are illustrated in Figure 2-1, which shows a face-centered cubic (fcc) crystal structure formed by titanium atoms, with C or N atoms occupying interstitial octahedral sites (i.e. sodium chloride crystal structure type).

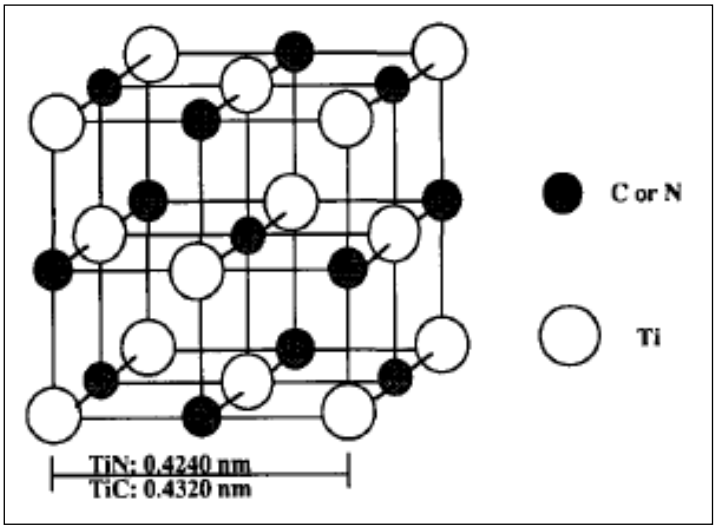


Figure 2-1: Illustration of the crystal structure of Ti(C,N) [25**]**

Considering that TiC and TiN are isomorphous, nitrogen can replace carbon on the TiC lattice in any proportion. Thus a continuous series of solid solutions can be produced i.e. $Ti(C_{1-x}N_x)$, where $0 \leq x \geq 1$.

The physical and mechanical properties of titanium carbonitride are strongly dependent on nitrogen content, as shown by Figure 2-2.

Figure 2-2(a) shows that as *x* increases, the lattice parameter of Ti(C,N) decreases linearly. This linearity is further supported by Table 2-4, showing that TiN has a slightly lower lattice parameter then TiC. Thus, as the nitrogen content (*x*) increases, the lattice parameter of Ti(C,N) decreases. A lower lattice parameter allows the TiN material greater thermal conductivity, thus Ti(C,N)-based cermet materials are more thermally conductive and therefore more thermal-shock resistant then their TiC counterpart [**25**].

Table 2-4: Properties of TiC and TiN

	Melting temp (°C)	Micro hardness $HK_{0.01}$ ($kgfmm^{-2}$)	Density (gcm^{-3})	Lattice parameter (Å)	Lattice parameter (Å)
TiC	3140	3200	4.92	4.322	4.320
TiN	2930	2000	5.22	4.242	4.240
Ref.	[**26**]	[**26**]	[**26**]	[**27**]	[**28**]

Figure 2-2(b) and Figure 2-2(c) also illustrates the dependence of microhardness and thermal conductivity on nitrogen content in titanium carbonitride. Since TiN has lower microhardness and higher thermal conductivity than TiC, in titanium carbonitride microhardness decreases and thermal conductivity increases as the nitrogen content increases.

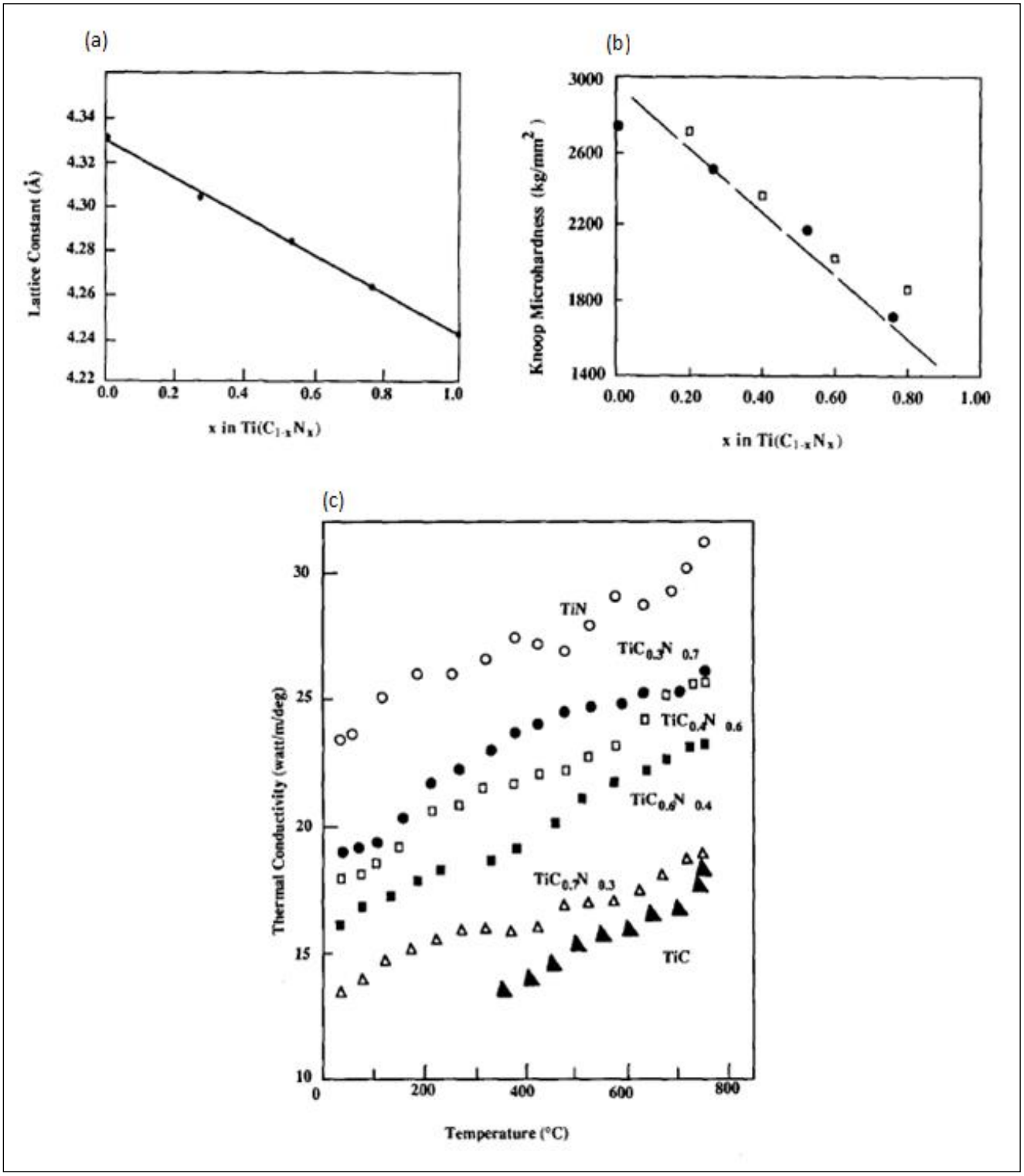


Figure 2-2: (a) Lattice parameter of Ti(C,N) as a function of nitrogen content [29] **(b) Microhardness of Ti(C,N) as a function of nitrogen content** [29] **(c) Thermal conductivity dependence of Ti(C,N) on nitrogen content** [28]

2.2.1.1. Processing of Ti(C,N)-based cermets

Despite its attractive properties, a sintered body of pure titanium carbonitride is rarely used as a material for cutting tools or wear resistance machine parts because of its brittleness and low breaking strength. As a result, to overcome these shortcomings metals or metal alloys are added as binders to form the cermet material [**25**].

Titanium carbonitride-based cermets are typically prepared by the powder metallurgy process. This involves powder preparation, mixing, compaction and densification. In order to obtain cermets with the desired mechanical properties, it is necessary that each of these processing steps be properly controlled.

In the production of titanium carbonitride-based cermets, the starting materials are typically Ti(C,N) and a metal binder that is usually Ni, Co or a combination of the two. For industrially important cermets carbides, nitrides or carbonitrides of elements from groups IVb (Zr, Hf), Vb (V, Nb, Ta) or VIb (Cr, Mo, W) of the Periodic Table are generally added as additional hard phases. These elements (i.e. Mo,V,W,Nb,Ta,Zr,Hf and Cr) form carbonitride solid solutions which improve the sinterability, high-temperature hardness, and thermal shock resistance of the hard phase by solid solution mechanisms.

Figure 2-3 schematically outlines the function of the individual elemental compounds in cermets. Hardness increases with increasing TiC and TiN contents, Ta/Nb additions improve cutting performance and Mo_2C and WC improve sinterability of the cermet [**1**].

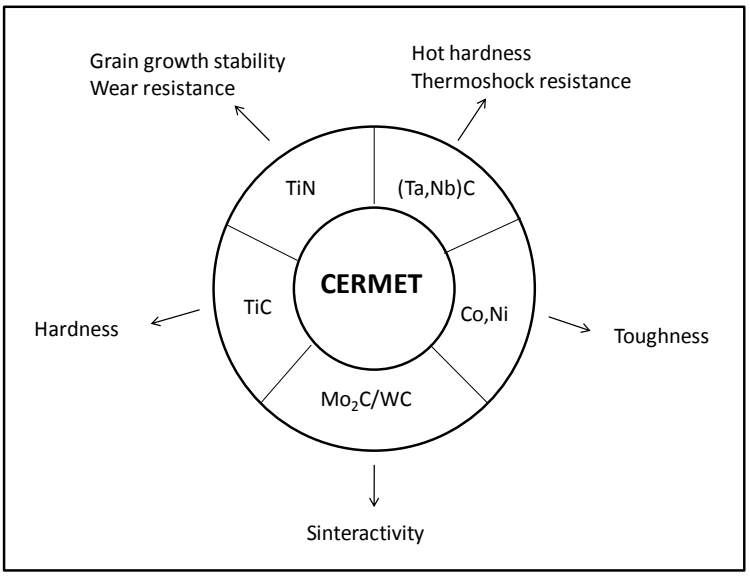


Figure 2-3: Schematic diagram of cermet cutting tool properties as a function of composition (after [1])

2.2.1.2. Microstructure and Properties of Ti(C,N)-based cermets

Many authors [**3**]-[**5**] have identified that the key to optimising the mechanical properties of Ti(C,N)-based cermets lies in its complex microstructure.

Ti(C,N) cermets possess a fine-grained, stable microstructure, in which the equiaxed fine grains of the hard phase are embedded in the tough metallic binder. The typical microstructure of Ti(C,N)-based cermets display core-rim morphology, which enhances wetting of the carbonitrides to the metal binder and inhibits the coalescence and growth of the carbonitride grains during sintering [**30**]. Generally, the cores are partially dissolved raw material particles on which the rim structures have grown through dissolution-reprecipitation processes. Figure 2-4 shows a schematic SEM image of the microstructure of a commercial Ti(C,N)-based cermet, which consists of black undissolved Ti(C,N) cores surrounded by grey (Ti, W, Mo, Nb, Ta,…)(C, N) complex carbonitride solid-solution rims [**31**].

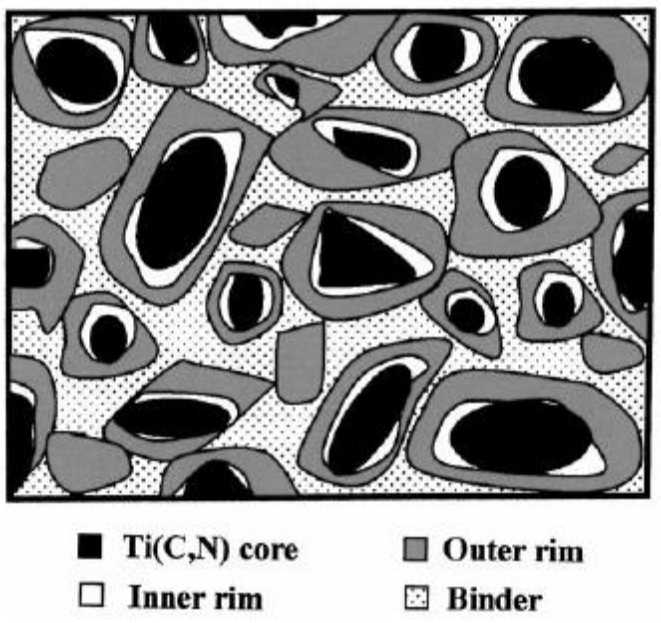


Figure 2-4: Schematic representation of a SEM image of a Ti(C,N)-based cermet [4]

Cermets are composite materials, thus their physical properties depend strongly on their constituent materials. The characteristics of the microstructure (in terms of size/shape of the core-rim structure and chemical composition) are influenced greatly by the starting materials. As a result, careful consideration is given to the addition of appropriate binder and secondary carbide phases, which enables adjustment of the mechanical and physical properties in order to obtain the desired requirements for cutting applications.

Typically, the undissolved Ti(C,N) cores are responsible for excellent wear resistance, while crack interactions between the solid solution rim structure and the binder phase determine the cermets toughness and integrity [**5**]. Investigations by Lindahl *et al*. [**32**] supported the theory that the physical properties of the cutting tools depend strongly on the starting materials. By using pre-alloyed starting powders, as opposed to as-mixed elemental powders, they were able to significantly improve the wear resistance and fracture toughness of the sintered cermet.

With regard to the binder, it is important that the amount of binder is sufficient enough to achieve full densification during liquid phase sintering and produce cermets with good machining characteristics. Conversely, too high a binder content is detrimental to the mechanical properties of the material. Xiong *et al*. [**33**] suggested that when Ti(C,N)-based cermets are used as finish machining tools, a lower binder content is required to achieve

excellent hardness and abrasion resistance. Investigations by Gong *et al*. [**34**] proved to support this statement. Gong *et al*. examined the hardness characteristics for a series of hot-pressed Ti(C,N) cermets with varying binder content.

Their results, as shown in Figure 2-5, illustrate that hardness decreases with increasing concentrations of metallic binder, explaining that this trend is easily explained when considering that the hardness of the individual metallic binder elements (Ni and/or Co) is significantly smaller than that of Ti(C,N). Thus increasing compositions of these metallic phases lower the overall hardness of the cermet material.

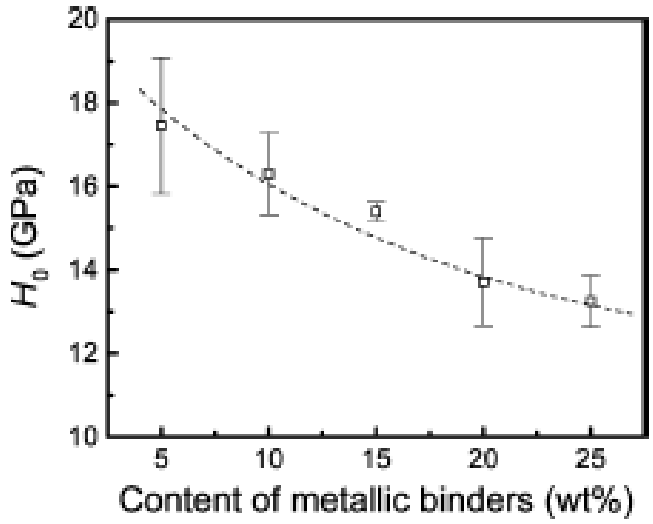


Figure 2-5: Variation of Hardness with the content of metallic binder [34**]**

Many authors [**35**]-[**36**] have reported on the effect of secondary carbide addition on the microstructure and properties of Ti(C,N)-based cermets. Ahn and Kang [**5**] studied the effect of various carbides on the dissolution behaviour of Ti(C,N). The microstructures of their various systems are shown in Figure 2-6. In accordance with Figure 2-4, the cermets exhibit microstructures with typical core-rim morphologies in all systems. Following EDX analysis, Ahn and Kang explained that the black cores comprised undissolved Ti(C,N), whilst the grey outer rim are solid solutions formed by the reactions between Ti(C,N) and the secondary carbides. The authors explained that although the systems exhibit core-rim morphologies, the characteristics of the core-rim (in terms of size and shape) differ greatly in appearance, depending on the type of carbide added. In the case of added HfC, the size of the Ti(C,N) core was the smallest and the development of the solid solution rim was distinct. Whereas

in the case of added TaC or WC, the frequency and size of the Ti(C,N) cores are increased, whilst the rim size has reduced.

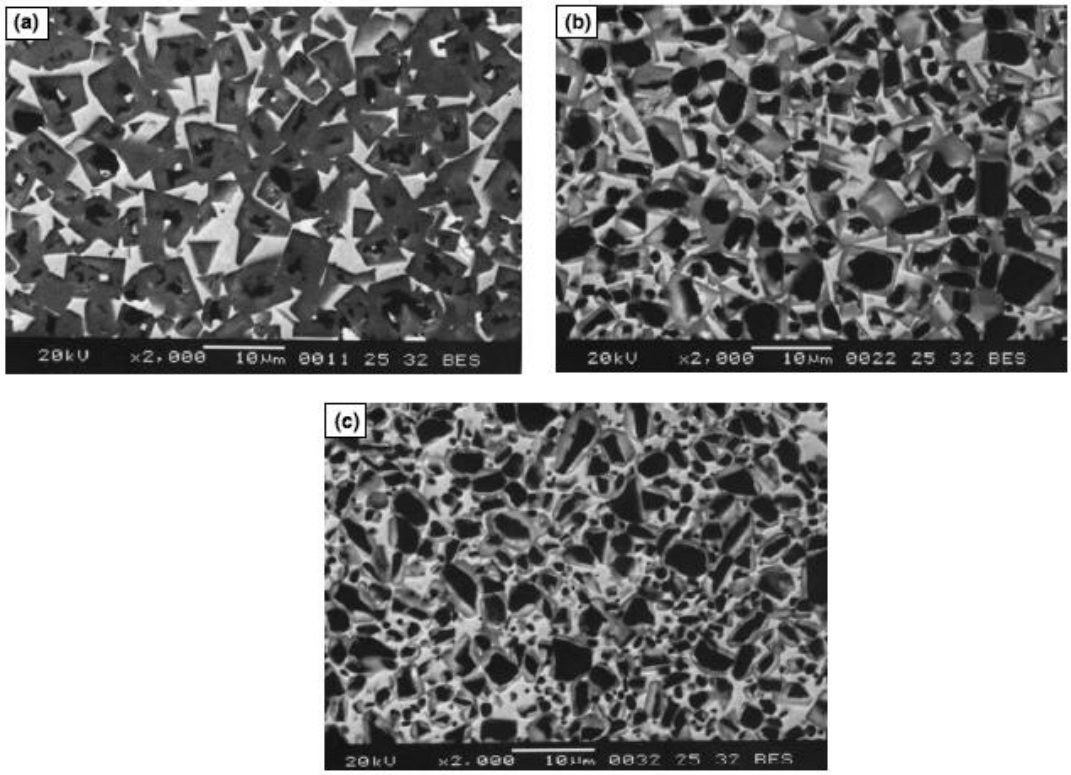


Figure 2-6: SEM (BSE) micrographs of Ti(C,N)-10MC-30Ni, where MC is (a) HfC, (b) TaC and (c) WC

These results support the theory that the solubility of Ti(C,N) in the binder controls grain growth during sintering. The authors attribute the different Ti(C,N) core-rim sizes to the relative affinity of the secondary carbides towards nitrogen from Ti(C,N). According to thermodynamic tables [**37**], the free energy of formation, ΔG_f of HfN, TaN and WN are -238, -114 and +51kJ/mol respectively (at 1500°C). This therefore suggests that Hf and Ta have a greater tendency to form a nitride compared to W. Thus, the dissolution of Ti(C,N) in the binder phase is reduced to a greater degree as a result of the WC addition and a smaller solid-solution rim is formed. Furthermore, the dissolution of Ti(C,N) in the TiCN-Ta/Ti(C,N)-Hf systems is facilitated more by the crystal structure similarities between the Ti(C,N) and Ta/Hf (which are all FCC), compared to W (which is HCP) [**38**].

These microstructural variations directly influence the mechanical properties of the material. Kumar *et al*. [**39**] studied the influence of different refractory carbides on the machining properties of Ti(C,N)-based cermets. The effect that the metal carbides have on the mechanical properties of these cermets is illustrated in Table 2-5.This shows that metal carbides (i.e. WC, NbC and TaC) play a significant role in the strengthening mechanism by increasing the hardness of the cermet when compared to cermets without metal carbides. Tantalum toughened cermets provided the greatest increase in hardness (≈2.6 GPa), and from their tribological tests, Kumar *et al*. concluded that cermets containing TaC phases exhibited lowest tool wear compared to WC and NbC containing cermets. Thus, TaC addition allows the wear rate of the baseline Ti(C,N) cermet to be retained whilst subsequently improving the mechanical properties of the material.

Table 2-5: Density and mechanical properties of Ti(C,N)-based cermets [39**] [**40**]**

Ti(C,N) Cermets	Density (g/cm^3)	Hardness HV_{30} (GPa)	K_{Ic} ($MPa.m^{1\backslash 2}$)	Wear rate of cermets ($x10^{-6}$ mm^3/Nm)
Ti(CN)-20Ni	5.33	9.9 ± 0.5	18.3 ± 0.9	3.2
Ti(CN)-10WC-20Ni	5.87	11.8 ± 0.6	17.3 ± 0.9	5.0
Ti(CN)-10NbC-20Ni	5.52	10.9 ± 0.5	13.4 ± 0.7	5.2
Ti(CN)-10TaC-20Ni	5.48	12.5 ± 0.6	16.1 ± 0.8	3.5

2.2.1.3. Influence on TaC on the properties of Ti(C,N)-based cermets

In addition to Kumar *et al*. [**39**], the effect of tantalum addition on the Ti(C,N)-based cermets has been reported by other authors. Kang and co-workers [**41**] examined the effect of TaC on the microstructure and mechanical properties of Ti(C,N). They found that TaC produces cubic carbides in the microstructure during sintering which lead to lower hardness, but higher fracture toughness values. Tret'yakov and Mashevskaya [**42**] also reported on the effect of tantalum in the Ti(C,N)-Ni-Mo-WC system. They found that the tantalum addition increased the bending strength and explained that this was the result of the formation of a complex carbonitride phase with higher strength properties. Gruss *et al*. [**43**] reported on the mechanical properties of two Ti(C,N)-based cermets. They explained that molybdenum carbide additions will generally produce cermets with a microhardness of 1650 $Kgmm^{-2}$, fracture toughness of 8.5$MPam^{1/2}$ and bending strength of 1500MPa. However tantalum additions, known as tantalum toughened Ti(C,N) cermets, produce a little lower hardness but result in higher strength and fracture toughness values, as compared in Table 2-6.

Table 2-6: Typical properties of Ti(C,N)-based cermets

Ti(C,N) cermets	Hardness ($Kgmm^{-2}$)	MOR (MPa)	K_{Ic} ($MPam^{1/2}$)	Young's Modulus (GPa)
Type A	1650	1500	8.5	450
Type B	1500	1800	10	410

Type A: (Ti, Mo/W)(C,N)-based cermets Type B: (Ti, Mo/W, Ta)(C, N)-based cermets

Rolander *et al*. [**36**] investigated the effect of tantalum additions on the machining properties of (Ti-W)(C,N)-Co cermets. The authors found that Ta additions enhanced the materials' resistance to plastic deformation, which consequently reduced flank wear during metal cutting applications. From their investigations, Rolander *et al*. [**36**] suggested that Ta influenced the interfacial energies of the system, thereby yielding a stronger hard phase skeleton which increased the materials resistance to plastic deformation. Hence, the tantalum addition to Ti(C,N) shows great promise for the production of a cermet with high hardness, which still exhibits an adequate degree of ductility.

2.3. Mechanical Alloying

2.3.1. Introduction to Mechanical Alloying

Mechanical alloying (MA) is a solid-state powder processing technique that allows for the production of homogenous materials, starting from a blend of elemental powders of various mixtures [**9**]. The process was originally developed by Benjamin of the International Nickel Company to produce oxide-dispersion strengthened (ODS) nickel and iron-based superalloys for applications in the aerospace industry. Nowadays, the popularity of the process has spread across all industries and the technique has been employed commercially and scientifically to develop a variety of novel materials. The increasing interest towards the mechanical alloying process stems from the many attributes offered by the process. These include the following:

- Production of fine dispersion of second phase particles
- Extension of solid solubility limits
- Refinement of grain sizes down to the nanometer range
- Disordering of ordered intermetallics
- Possibility of alloying of difficult to alloy elements
- Inducement of chemical reactions at low temperature
- Scaleable process

As a result, this simple yet effective processing technique is not only used to develop metal alloys, but now extends to ceramics, polymers and composite systems.

Fundamentally, the term *milling* may be referred to as the breaking down of relatively coarse materials to their ultimate fineness [**44**]. Over the past few decades, the milling process has progressed from its traditional purpose in the mineral processing and powder metallurgy industries. It is no longer used primarily for particle size reduction, but is fast becoming an important tool for the preparation of new engineering materials with enhanced mechanical and physical properties [**44**].

As such, the mechanical alloying (MA) process, using rod or ball-milling techniques, has received much attention as a powerful tool for the fabrication of several advanced materials (Figure 2-7), including equilibrium, non-equilibrium and composite materials.

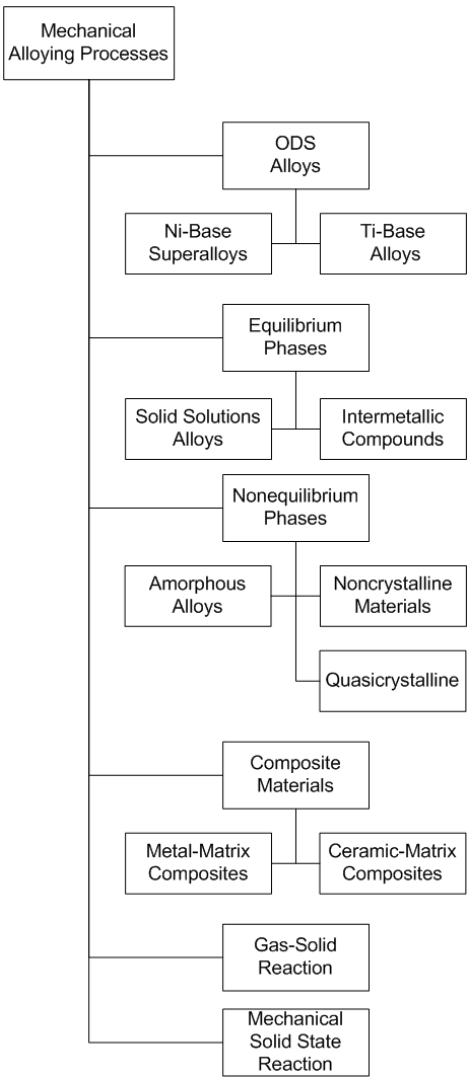


Figure 2-7: Synthesizing capabilities of the Mechanical Alloying process [44**]**

The mechanical alloying technique provides a fundamentally different approach to alloy design compared to conventional ingot (solidification) processed alloys. Whilst traditional technologies use heat treatments or chemical reactions to combine alloy components, mechanical alloying relies on deformation processes to mix the constituent materials. The extreme deformations experienced by the milled powders are an intrinsic part of the mechanical alloying process. The large amounts of distortion and the production of nanograin-boundaries increase the free energy, the volume of the atomic cavity and the number of atoms distributed on the nanograin-boundaries. All these effects reduce diffusion distances between the atoms and improve the sintering process substantially. Powder compressibility following mechanical milling is said to decrease due to particle cold welding and full densification can be obtained during solid state sintering processes [**45**]. The effect of mechanical alloying on the sintering process was illustrated by Lahiri and Bhargava [**46**]. They showed that powder products have high sinterability and catalytic effect, due to the high level of internal defects. During densification of Cu-Cr compacts, they found that mechanical alloying changed the sintering process from liquid to solid state sintering, thereby making the process more energy efficient.

Benjamin [**47**] reported that hard powders such as tungsten carbide, which normally do not form composites, can be made to form a solid with a soft powder such as cobalt or nickel, by milling a mixture of the powders in a high energy ball mill. Similarly, Gordo *et al*. [**48**], while working on the production of Fe-Ti(C,N) powders, encountered a number of difficulties incorporating the hard phase in the Fe matrix. They attributed these difficulties to agglomeration of the particles, which inhibit homogenous dispersion of the hard phase in the matrix, and the poor bonding between the added particles and the matrix. One of the options proposed to overcome these problems was also high-energy ball milling [**49**]-[**50**].

Matteazzi *et al*. [**51**] reported that many carbides could be synthesized by mechanical alloying of elemental powders to produce stable and metastable compounds with a high defect density. From their studies, they reported on the formation of the following carbide systems: TiC, VC, V_2C, Cr_3C_2, Mn_3C, Fe_3C, Nb_2C, NbC, HfC, $TaReC_2$, $NbTaMoReC_4$, ReC and SiC.

Several studies have shown that the properties of refractory materials can be further improved if the grain size of the constituent materials is reduced and the homogeneity of the structural elements is increased. In this respect, high-energy mechanical alloying is a

well-developed process for dispersing nanocrystalline reinforcing elements more uniformly in a metal matrix [**52**]. The ultrafine nanocrystalline nature of the reinforcing particles and their homogeneous distribution within the microstructure is therefore expected to improve the obtainable mechanical properties of materials prepared by the mechanical alloying route [**53**].

Choi [**54**] reported on the preparation of TiC-Ni cermets by mechanical alloying. He was able to synthesize TiC-Ni cermet powders by mechanically alloying pure titanium, nickel and carbon powders. In order to investigate the effectiveness of the process, Choi also developed TiC-Ni cermets by conventional ball milling. He found that the TiC-Ni cermet sintered from the mechanically alloyed powders contained TiC particles of 0.1-1.5 μm size, compared to 3-5 μm for a conventional cermet. As a result, mechanical alloying produced a cermet with finer microstructure, which possessed hardness comparable to ball milled cermets.

Bolokang *et al*. [**55**] proposed that the toughness of (V,W)C alloys can be greatly enhanced by reducing the grain size of (V,W)C powders to less than 2μm. The authors selected the mechanical alloying process for the production of these powders, due to its success in producing nanocrystalline TiC powder, and were successful in synthesizing nano-sized (V,W)C powders by mechanical alloying of W, V and C powders. Bolokang *et al*. [**55**] reported that the production of these nano-sized powders reduced the temperatures required for sintering, thereby preventing excessive grain growth during sintering and consequently improving the mechanical properties of the material.

Similarly, during their attempts to reduce the fabrication costs of WC-Co composites, Zhu *et al*. [**56**] reported on the mechanical alloying process as an inexpensive and faster processing route for the synthesis of WC composites. They were able to synthesize WC nanocomposites which offered a unique combination of high hardness and excellent fracture toughness.

Consequently, these investigations [**46**]-[**56**] illustrate that composite powders can be produced by mechanical alloying, whose component elements are homogenously distributed due to the repeated fracturing, cold welding and fast diffusion between the powders [**57**]. Furthermore, the production of finer microstructures leads to enhanced mechanical properties.

2.3.2. The Process of Mechanical Alloying

From the foregoing, it is apparent that the mechanical alloying technique is capable of developing a wide range of novel and advanced materials. Though the processing technique is relatively simple, it requires optimization of a number of variables in order to achieve the desired phase/microstructure and mechanical properties. The most important parameters that have an effect on the final constitution of the powders are schematically presented in Figure 2-8.

During MA, milling time is the most important process variable. Time is set to achieve a steady-state equilibrium between fracturing and cold welding of the powder particles. The time required to reach this equilibrium depends on the type of mill used, milling intensity (or speed) and the ball to powder ratio [**9**].

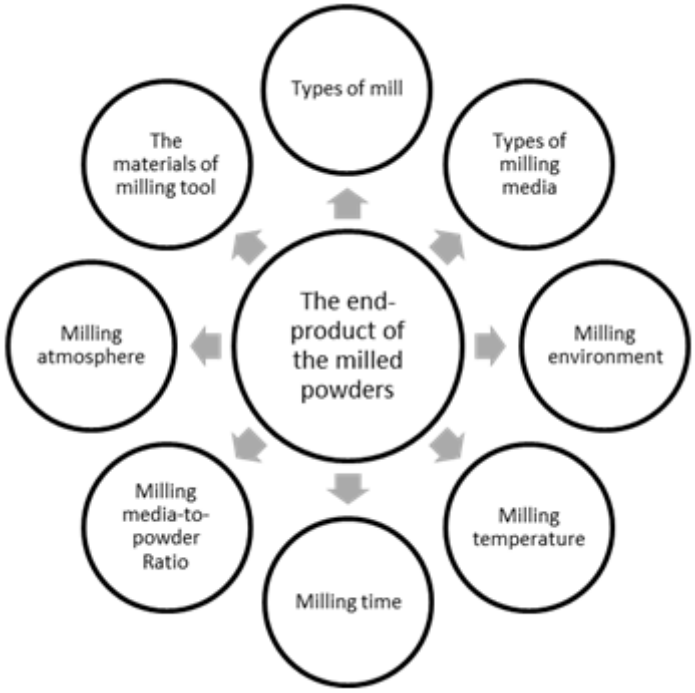


Figure 2-8: Schematic representation of the main factors affecting the MA process [44**]**

2.3.2.1. Ball-to-Powder weight ratio

The ball to powder weight ratio (BPR) has a significant effect on the time required to achieve a particular phase in the milled powder. Different authors have reported on the effects of the BPR, using values as low as 1:1 [**58**] to as high as 220:1 [**59**]. Generally, the higher the ratio, the shorter the time required for milling. When high BPR are used, the increase in weight proportion of the balls increases the number of collisions per unit time. Consequently, more energy is transferred to the powder particles, thus alloying takes place at a faster rate. However, this will also lead to increased contamination from the milling tools.

For milling of powders in small capacity mills such as a SPEX (SPEX is a trademark of Sytech Corporation, Houston, TX) mill a ratio of 10:1 is most commonly used.

2.3.2.2. Milling intensity

Milling speed is another important process variable to be considered. Suryanarayana [**9**] explained that the faster the mill rotates, the higher the energy input into the powders. Thus, low rotational speeds lead to very long periods of milling and a large inhomogeneity in the alloy because of insufficient kinetic energy input into the powders [**60**]. Depending on the design of the mill, there are certain limitations to the maximum speed that could be used. In the case of conventional ball mills, increasing the speed of rotation increases the speed at which the balls move. At rotational speeds above a critical point, the balls are pinned to the sides of the milling vial and do not fall down to exert any impact force. Therefore, the maximum speed mills should be operated at should be just below this critical value, so that balls fall down from a maximum height to produce the maximum collision energy [**9**].

Calka *et al*. [**61**] reported that when vanadium and carbon powders were milled together at different energy levels, the final constitutions of the powders were different. At very low milling energy (or speed), the powder consisted of nanometer-sized grains of vanadium and amorphous carbon, which on annealing formed either V_2C or a mixture of V + VC. At intermediate energy level, the as-milled powder contained a nanostructure, which on annealing transformed to VC. At the highest energy level, VC formed directly during milling.

2.3.2.3. Milling atmosphere

Mechanical alloying is mostly performed in an inert atmosphere. Since very fine powders have relatively large surface areas, they are highly reactive to oxygen, hydrogen and nitrogen gases, which at the smallest amounts will have a great influence on the final product.

Gordo *et al*. [**62**] studied the influence of milling parameters on the manufacturing of Fe-Ti(C,N) composite powders. They observed that milling in argon produced a finer and more homogenous microstructure than when milling was performed in nitrogen or air. They concluded that the milling atmosphere is most influential in determining the composition of powders after milling, whilst the milling time and type of mill influences the morphology and microstructure of the milled powders.

2.3.3. The Mechanisms of Alloying

Alloying is achieved by the repeated welding, fracturing and re-welding of a mixture of powder particles in a dry, highly energetic ball charge [**63**]. This is usually carried out in one of three mill configurations (Figure 2-9) i.e. a vertical ball mill such as the Szegvari attritor, a vibratory mill such as the SPEX shaker mill, or a conventional horizontal ball mill.

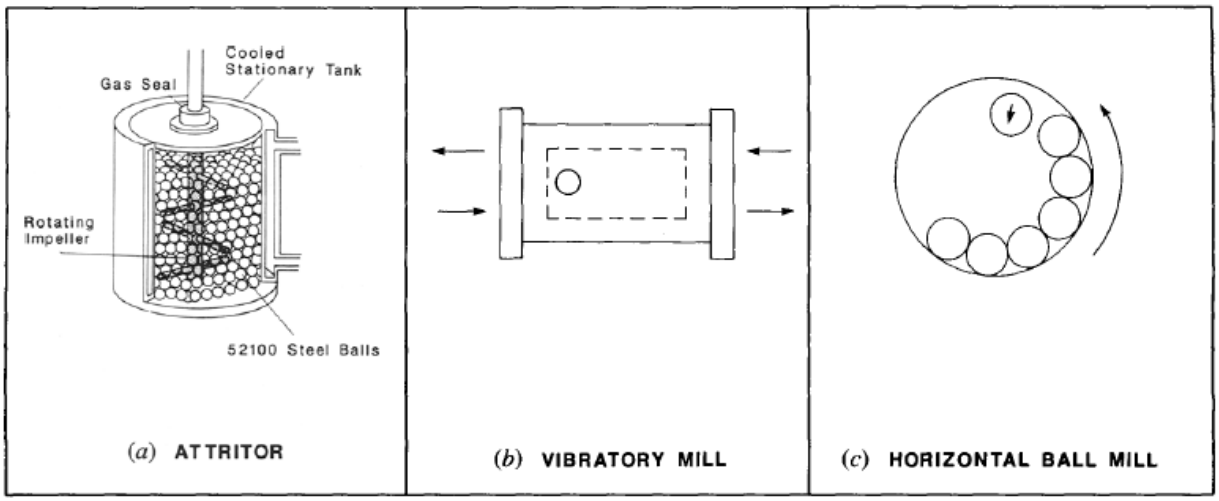


Figure 2-9: Common machines used for mechanical alloying [63**]**

Regardless of the mill used, the process is characterised by the collisions between the tools and the powders, which result in fragmentation and coalescence. As the grinding balls collide, some amount of powder becomes trapped between them. The force of such an impact causes the powder particles to plastically deform and mix together (Figure 2-10).

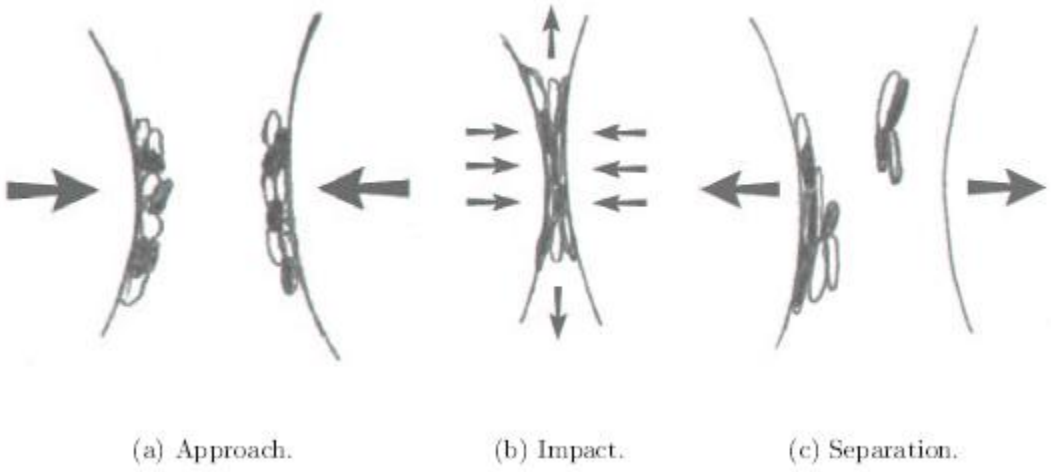


Figure 2-10: Ball-powder-ball collision of powder mixtures during mechanical alloying [64**]**

Benjamin and Volin [**65**] provided the most complete description of the mechanical alloying process, outlined in their five stage model below. This model describes the events taking place during mechanical alloying of an all-ductile system. The processes taking place in systems containing brittle components are detailed in Section 2.3.4.

Figure 2-11 shows the powder morphology and microstructure characteristic of each of the five stages [**65**]. **Stage 1** involves powder mixing, where concurrent deformation, fracturing and welding of the powder particles occurs. These processes cause the powder particles to flatten, allowing for the formation of large flake-shaped particles. At this stage, there is significant variability in the morphology and hardness of the powder particles. During **Stage 2**, welding of the powder particles predominates. The flattened particles weld together to form lamellar structures or composite particles containing layers of the alloying components. This subsequently leads to a decrease in the number of particles, as particle size increases due to the welding effect. The hardness of the powder particles continues to increase due to extensive plastic deformations taking place during mechanical alloying.

During **Stage 3**, the lamellar particles are no longer flake-like, instead they manifest into thicker and rounder morphologies. The work hardening effect accounts for the equiaxed nature of the powder particles during this stage of alloying. The continuing increase in particle hardness (and concurrent decrease in ductility) leads to an increased tendency for the particles to fracture. Thus, **Stage 4** is reached when fragments of the equiaxed particle fracture off and start to weld in different orientations and the lamellar structure becomes progressively finer. During **Stage 5,** the structure of the material is gradually refined and the composition of each particle converges to the overall starting composition.

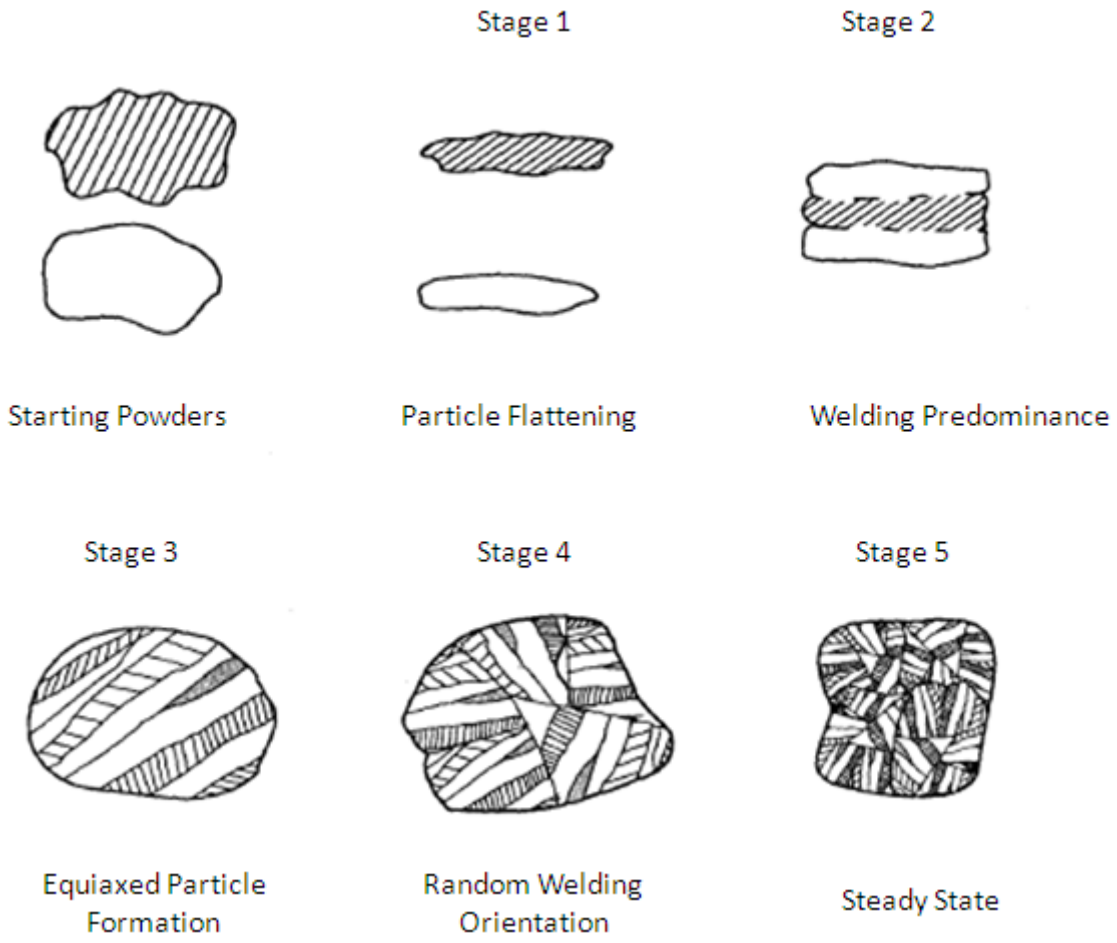


Figure 2-11: The five stages of mechanical alloying according to Benjamin and Volin [66**]**

Steady-state processing constitutes the 5th and final stage of mechanical alloying. After milling for a certain length of time, a steady-state equilibrium is reached when a balance is maintained between the rate of welding and the rate of fracturing. Very small particles behave in a ductile fashion and therefore a point is reached, termed the limit of comminution, when further reduction in size is not possible [**67**]. Thus, smaller particles are able to withstand deformations without fracturing and tend to be welded into larger sizes, with an overall tendency to drive both very fine and very large particles towards an intermediate size. Consequently, a narrow particle distribution (Figure 2-12) may be achieved due to the tendency for particles larger than average to reduce in size at the same rate that particles smaller than average grow due to agglomeration [**47**]. The final grain size achievable by mechanical alloying depends on a number of variables, namely the equipment used, the milling intensity, the ball-to-powder ratio, milling time, initial particle sizes etc. In most cases however, the rate of refinement of the internal structure (particle and crystallite size) is roughly logarithmic with processing time, so that within a few minutes to a hour the crystallite size is refined to nanometer dimensions [**9**]. Consequently, the ease at which nanostructured materials can be synthesized by this process is one of the reasons why mechanical alloying has been extensively employed to produce nanocrystalline materials [**68**].

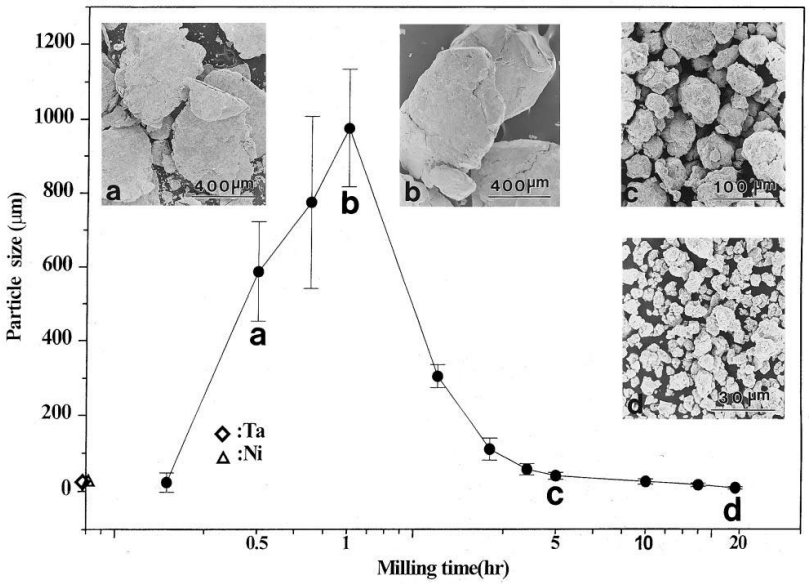


Figure 2-12: Narrow particle distribution achieved when a balance is maintained between the fracturing and welding processes [69**]**

2.3.4. Systems for Mechanical alloying

As mentioned in Section2.3.3, Benjamin and Volins' five stage model of the events taking place during mechanical alloying generally refers to systems which contain at least one ductile metal component. Benjamin [**47**] suggested that it was necessary to have at least 15% of a ductile component to achieve alloying. In this way, the metal acts as a binder to hold together all other components thus enabling the cold welding action indicative of the process. Consequently, the ideal systems for mechanical alloying will contain ductile-ductile or ductile-brittle components.

For ductile-ductile systems, the mechanism of alloying will be identical to those outlined in Benjamin and Volins' five stage model [**65**], where the resultant material is a solid-solution of the starting constituents and the microstructure becomes so refined that the layers of the different constituents are no longer visible under optical microscope.

However, in the case of ductile-brittle systems, the mechanism of alloying is different. Benjamin and others [**70**]-[**71**] described that during the initial stages of mechanical alloying, the ductile metal powder would be flattened by the ball-powder-ball collisions, while the brittle particles would be fragmented. These fragmented brittle particles become occluded by the ductile constituents and are trapped in the ductile particles. With further milling, the ductile particles are work hardened, the lamellar structure becomes convoluted and refined. If the brittle component is insoluble, the particles will be uniformly dispersed in the ductile matrix such as in the case of oxide dispersion-strengthened (ODS) alloys or WC and Co. If however they are soluble then alloying occurs between the ductile and brittle components and chemical homogeneity is achieved. Thus, alloying of ductile-brittle components during mechanical alloying requires not only fragmentation of the brittle particles to facilitate short-range diffusion, but also reasonable solid solubility in the ductile matrix component [**9**].

Gordo *et al*. [**62**] performed mechanical alloying on a ductile-brittle system and were able to manufacture Ti(C,N)-Fe composite powders. From their SEM and particle size analysis, they explained that the morphology and microstructure of the mechanically alloyed powders have an evolution with milling time that covers all the typical stages of mechanical alloying.

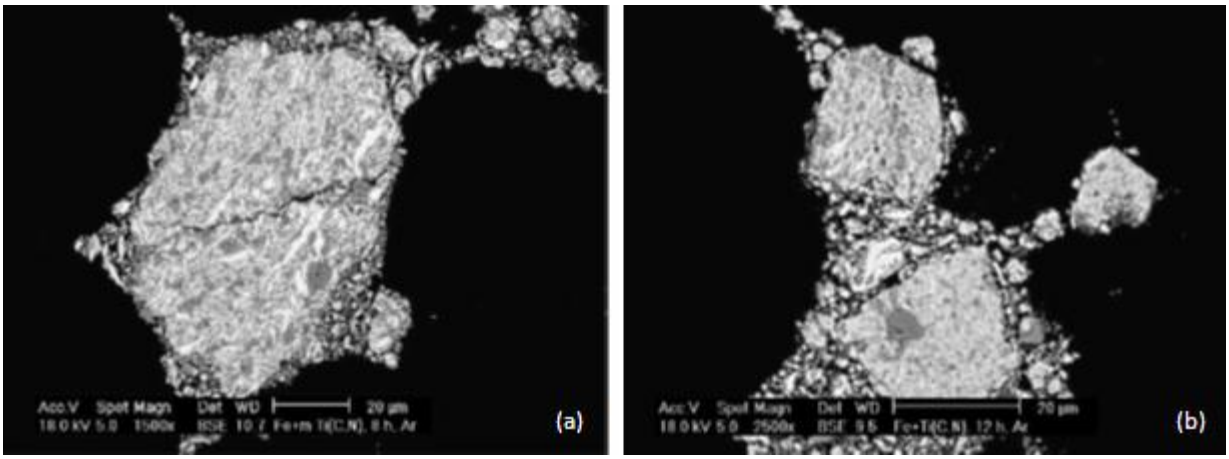


Figure 2-13: SEM (BSE) micrograph of Ti(C,N)-Fe powder milled (a) 6Hr and (b) 12Hr [62**]**

Gordo *et al*. [**62**] explained that in the early stages, the Fe particles suffered plastic deformation and acquired a flake-like morphology and a lamellar-type microstructure of Fe layers with carbonitride particles trapped among them. In Figure 2-13a, the Fe laminates (bright contrast) can be clearly distinguished from the Ti(C,N) particles trapped between them. As milling time increased, the particle shape becomes equiaxial due to the fracture and re-welding processes. The laminates within the microstructure became smaller and after 12 hours mechanical alloying the particles were rounded and the microstructure more homogenous as seen in Figure 2-14b. The Ti(C,N) particles (dark grey contrast) appear dispersed in a homogenous Fe-rich matrix.

Although Benjamin [**47**] proposed that it would be unlikely that alloying would occur in a system consisting of two or more brittle components, mechanical alloying has been reported to have successfully occurred in a number of brittle-brittle systems. Davis and Koch [**72**] and Davis *et al*. [**73**] both reported to have obtained solid solutions after mechanically alloying brittle Si-Ge and Mn-Bi systems respectively. During milling of these systems, it was suggested that the more brittle (harder) component becomes fragmented and embedded in the less brittle (softer) component.

In brittle-brittle systems, fracture predominates during the initial stages of milling [**65**]. Due to the absence of a ductile component, each ball-powder-ball collision causes both brittle components to fragment and the particle size to reduce continuously. As mentioned previously, after a certain period of milling, the powders reach their “limit of comminution,”

at which time fine particles behave in a ductile manner thereby allowing for intermixing and adhesion.

Compared to ductile systems, alloying in brittle systems may require longer milling times and higher milling intensities. This may be due to the longer diffusion distances in the brittle-brittle granular vs. ductile-ductile lamellar geometries [**9**]. The exact mechanism of alloying is unclear, although a number of explanations have been offered to explain alloying with brittle-brittle systems. The possible mechanisms which may contribute to material transfer during mechanical alloying of brittle components includes plastic deformation, induced by (a) local temperature rises, (b) microdeformation in defect-free volumes, (c) surface deformation and/or (d) hydrostatic stress state [**73**]. These temperature-induced microdiffusions or deformations may link the alloying mechanisms responsible in ductile systems to brittle systems [**60**].

The large diffusion coefficients and solubility of defects may have also contributed to the successful mechanical alloying of the brittle Si-Ge and Mn-Bi systems. These properties are not available to hard ceramic materials. However, Zhang *et al*. [**74**] performed the first study of an all ceramic $Ti(C_{0.3}N_{0.7})$ + WC + TaC system. They mixed ceramic powders in weight proportion of 70:20:10 and planetary ball milled the powders at a charge weight ratio of 20:1. X-Ray diffraction analysis performed after mechanical alloying for different times showed that the TaC peaks progressively reduced in intensity with milling and had disappeared after 88 hours. Zhang *et al*. [**74**] reported that although there was an overall peak intensity drop for every species, the WC peaks persisted and remained well defined, even after 131 hours MA. Also observed was the significant increase in half-peak-width of the powders after MA. This they attributed to the decrease in the coherent crystalline domain size.

SEM analysis performed by Zhang and co-workers [**74**] revealed different particle morphologies for samples milled for 19 hours and 131 hours. The microstructure after 19 hours MA was non-uniform, with many large facetted grains. Some particles were spherical, whilst others angular. They explained that because they worked on an all ceramic system, the microstructural lamella morphology was not observed as it would have been in ductile-ductile systems. Instead, they obtained a microstructure containing mainly fine grained particles with a granular morphology after 131 hours of MA.

From this study, Zhang *et al*. [**74**] found that Ti, Ta and W all existed in the same grain after 131 hours of MA, thereby indicating the progress of the solid solubility process. Although they found dissolution of both tungsten and tantalum atoms into the Ti(C,N) phase, the extent was considerably different for the two atoms. They explained that tungsten atoms are bigger, while tantalum atoms are the same size as titanium atoms, thus the dissolution of Ta into Ti(C,N) occurs quickly and without any lattice distortion, whereas the dissolution of tungsten is more difficult.

Maweja *et al*. [**75**] studied the alloying mechanisms in the Ti(C,N)-W system during high energy ball milling. By SEM analysis (Figure 2-14(a)-(b)), they showed that milling improved the mixing and the homogeneity of the powders by destroying agglomerates of the tungsten particles and dispersing these fine particles in the softer Ti(C,N) phase. By observing cross sections of the milled powders (Figure 2-15), Maweja *et al*. [**75**] were able to confirm the alloying ability of the mechanical alloying technique via the diffusion of W atoms into the Ti(C,N) particles. They explained that this diffusion was completed after 24 hours in particles smaller than 1µm. On the other hand, particles larger than 1µm showed a core-rim structure with the rim being richer in W. This indicated that 24 hours was not long enough for W atoms to diffuse completely into the Ti(C,N) grain.

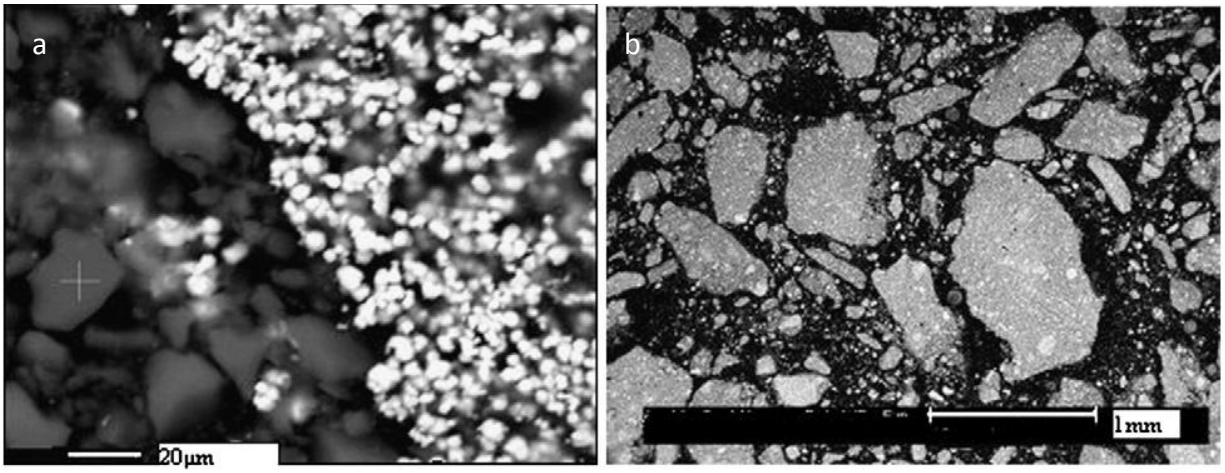


Figure 2-14: SEM (BSE) images of the Ti(C,N)-W powders (a) starting powders and (b) powders milled for 12 hours [75**]**

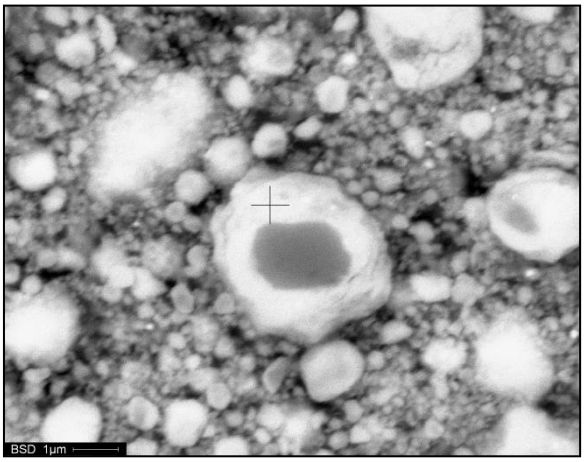


Figure 2-15: SEM (BSE)image of cross-sectional Ti(C,N)-W powder mechanically alloyed for 24Hr [75**]**

2.3.5. Diffusion in Mechanical Alloying

Diffusion is a fundamental process during mechanical alloying. Diffusion occurs in any system to decrease the Gibbs free energy of the bulk material and ceases when the chemical potential of all atoms are the same and the system is in equilibrium. There are two primary mechanisms by which atoms may diffuse through a solid; the vacancy or interstitial mechanism, depending on the type of site occupied in the lattice by the diffusing species.

The diffusion process can be represented mathematically by Ficks second law:

$$\frac{\partial C}{\partial t} = D_x \frac{\partial^2 C}{\partial x^2} + D_y \frac{\partial^2 C}{\partial y^2} + D_z \frac{\partial^2 C}{\partial z^2} \qquad \textbf{Equation 2-1}$$

where C is the concentration of the solute atom element, D_x D_y and D_z are the diffusivities of the solute atoms in the x, y and z directions respectively, and t is the diffusion time. For homogenous diffusion however, $D_x = D_y = D_z = D$. Thus Equation 2-1 can be rewritten as follows:

$$\frac{\partial C}{\partial t} = D\left(\frac{\partial^2 C}{\partial x^2} + \frac{\partial^2 C}{\partial y^2} + \frac{\partial^2 C}{\partial z^2} \right) \qquad \textbf{Equation 2-2}$$

Equation 2-2 indicates that the rate of diffusion is a function of diffusivity. Diffusivity is also a function of temperature according to the Arrhenius equation (Equation 2-3).

$$D = D_o \exp\left(\frac{-\Delta Q}{RT} \right) \qquad \textbf{Equation 2-3}$$

where D_o is a material constant, Q is the activation energy, R the universal gas constant and T the temperature. Thus, it follows that the diffusion rate is dependent on temperature.

Traditional solid-state reactions involve the formation of one or more product phases between reactants. The rates of these reactions are influenced by the initial contact areas and diffusion of the reactant species through the product phases [**76**]. Most solid-state reactions however, have fixed contact areas and limited diffusion rates. Thus solid-state processes are primarily temperature dependent.

This is not the case for mechanically alloyed induced reactions, since a reaction can actually increase with increase in mechanical alloying duration and with a change in phases [**77**], [**78**]. Due to the nature of the process, the particles are always in contact with each other with atomically clean surfaces and minimised diffusion distances. Consequently, reaction areas are increased, thereby allowing for an increase in chemical reactivity during MA.

During most mechanical alloying processes, temperature is not a dominating factor since the temperature generated by collisions is far from reaching the temperatures required to activate diffusion.

Zhang *et al*. [**74**] measured the temperature changes inside and outside the milling container after certain intervals of mechanical alloying. Their results indicated that the maximum temperature rise within the mill was around 120°C, which is far from the melting or diffusion temperatures of most ceramic materials such as WC, TiC and TiN. Consequently, MA relies on an alternative mechanism for developing advanced refractory materials.

During diffusion, an interstitial/substitutional atom is moved to an adjacent site. In order for this movement to occur, a high energy barrier has to be overcome, as shown in Figure 2-16a [**79**]. The increase in free energy is known as the activation energy, and for diffusion it is equal to the sum of the activation energy to form a vacancy and to move the vacancy (Figure 2-16b):

$$\Delta Q = \Delta Q_f + \Delta Q_m \qquad \textbf{Equation 2-4}$$

where ΔQ_f is the activation energy for creating vacancies, and ΔQ_m is the activation energy for moving vacancies.

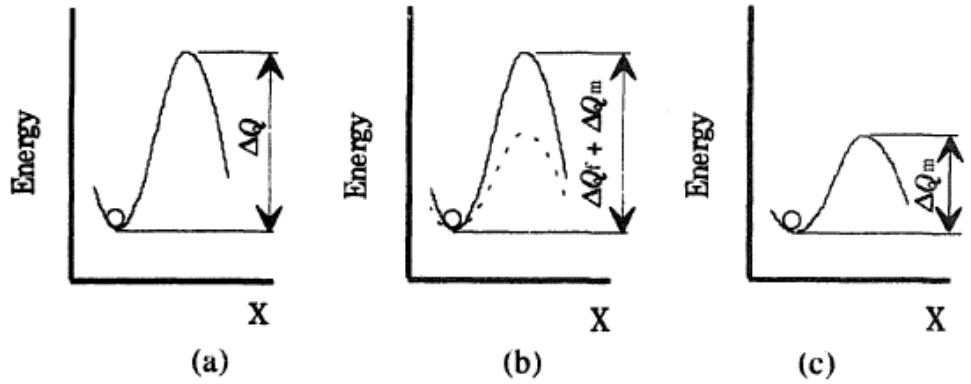


Figure 2-16: Change in activation energy in the x-direction [79**]**

As pointed out by Schaffer [**80**], mechanical alloying minimizes the effect of product barriers on the reaction kinetics and provides the conditions required for the promulgation of solid-state reactions at low temperature. Due to the nature of the process, heavy deformation is introduced into the milled particles during mechanical alloying. The fracturing effect generates a number of microcracks, which provide free surfaces that increase the internal energy of the system. In addition to cracking, a variety of crystal defects such as dislocations, vacancies, stacking faults and increased number of grain boundaries [**9**] are also introduced into the material.

The presence of this defect structure lowers the activation energy needed for diffusion by reducing the activation energy needed for the creation of vacancies as seen in Figure 2-16(c). It can also be seen, from Equation 2-3, that in order to achieve a certain value of D, either the activation energy should be decreased and/or the temperature increased. Mechanical alloying provides an opportunity to decrease the activation energy by the formation of more free surfaces, grain boundaries and sub-grain boundaries which is equivalent to increasing the diffusion temperature [**81**].

Another factor that influences diffusion is the difference in the diffusion modes [**82**]. At a given temperature, the magnitude of diffusivity along a grain boundary (D_b), a free surface ($D_{s)}$ and through a defect free lattice (D_l), are such that:

$$D_s > D_b > D_l \qquad \textbf{Equation 2-5}$$

Equation 2-5 reflects the relative ease with which atoms can migrate along a free surface compared to the grain boundary and lattice. Figure 2-17 shows the relationship between diffusion via the surface, the grain boundary and the lattice [**83**]. It can be seen that lattice diffusion has the largest slope, whilst surface diffusion the smallest. The surface tends to be a region of relatively high disorder and therefore the activation energy for diffusion tends to be low. The activation energy in grain boundaries is generally higher in comparison to surface diffusion, whilst lattice diffusion is the highest of all. As a result, at low temperatures, surface diffusion dominates over grain boundary and lattice diffusions. An increase in temperature allows grain boundary diffusion to become most significant and at even higher temperatures, lattice diffusion becomes the principal mode for diffusion [**83**].

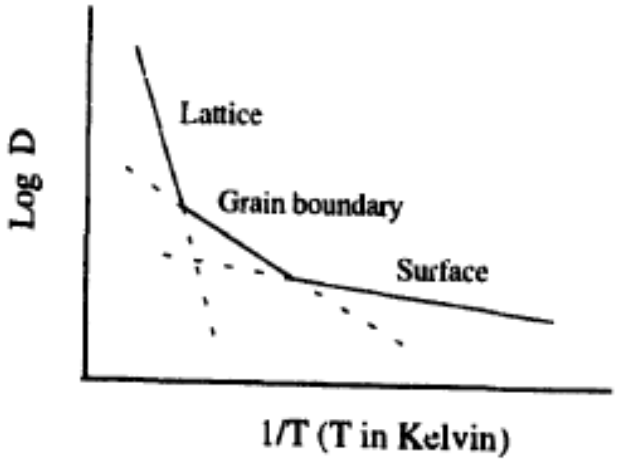


Figure 2-17: Dependence of diffusivity on surface, grain boundary and lattice diffusion at different temperatures [79**]**

Unique to the mechanical alloying process is its ability to change between all these diffusion modes at low temperatures. This is attributed to the grain refinement characteristic of the process. According to calculations by Lu et al. [**79**], diffusivity can be raised dramatically by reducing the grain size and increasing the temperature (within the range of temperature rise experienced by the MA process). In addition, due to the decrease in grain size and the subsequent increase in grain boundary area, diffusion mode is changed from lattice diffusion to grain boundary and surface diffusion. These diffusion mechanisms dominate during the mechanical alloying process, since they both are associated with much lower activation energies in comparison to lattice diffusion.

Chapter 3: Experimental Method

This chapter details the experimental procedures used to synthesize and characterise the (Ti,Ta)(C,N) powders produced by mechanical alloying and ball-milling.

An overview of the methodology is illustrated in the process flow chart as seen in Figure 3-1. A full description of the materials used, milling processes, as well as the individual powder characterisation techniques are detailed in the sections to follow.

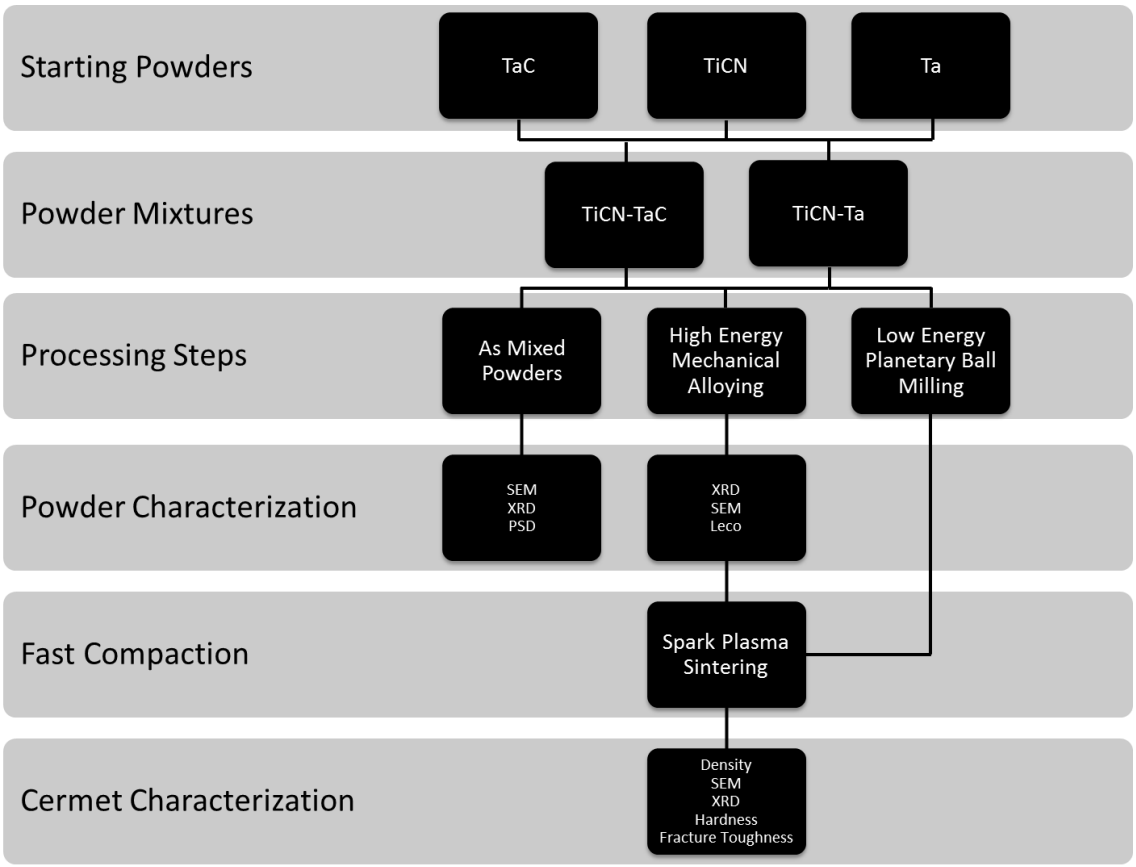


Figure 3-1: Summary of experimental set-up

3.1. Raw Materials

Specifications for the materials used in this research study are detailed in Table 3-1.

Table 3-1: Characteristics of raw powders in the as-received condition

Powder	Supplier	Grade	Particle size (um)			Stoichiometry
			D10	D50	D90	
Ti(C,N)	H.C. Starck	B	0.8	3.6	8.2	$Ti(C_{0.7}N_{0.3})$
TaC	H.C. Starck	B	1.1	2.4	5.2	TaC
Ta	Speciality Metals (Pty) Ltd	-	1.6	3.7	6.7	Ta
Ni	Alfa Aesar	-	11.7	25.0	50.2	Ni

3.2. Powder Processing

3.2.1. Ball-Milling

All ball-milling experiments were performed using the Fritsch Pulverisette ball mill. Powder mixtures (as given in Table 3-3) were wet milled in isopropanol for 3 hours, at a rotational speed of 300rpm. Milling was performed using WC milling pots and grinding balls, with a 10:1 ball-to-powder weight ratio.

3.2.2. Mechanical Milling

All mechanical alloying experiments were performed in the Retsch PM 400MA high energy ball mill. Pure titanium carbonitride was admixed with tantalum carbide or tantalum metal powder in a mass ratio of 60:40 wt% Steric acid (3 wt%) was also added to the powder mixture as a process control agent to reduce the effect of cold welding between the powder particles, the particles and balls; and to minimize adhesion of particles to the mill walls. Stainless steel balls were used as grinding media, with a charge ratio of 10:1. Milling was performed at a rotational speed of 400 rpm; for 12, 24 and 48 hour intervals for the Ti(C,N)-TaC mixture, and 2, 4, 8 and 12 hour intervals for the Ti(C,N)-Ta mixture. To minimize powder oxidation, all milling experiments and handling of powders were performed in a controlled argon inert environment. Table 3-2 provides a summary of the parameters for mechanical alloying.

Table 3-2: A summary of the milling conditions used in this study

Milling speed (rpm)	400
Ball-powder weight ratio	10:1
Number of milling balls	84
Diameter of milling balls (mm)	10
Weight of each milling ball (g)	4.09
Density of milling ball (g/cm^3)	7.81
Volume of milling vial (ml)	500
Milling ball/vial medium	Stainless steel

3.3. Powder Characterisation

Following mechanical alloying, the milled powders were washed, dried and sieved down to 75µm. Characterisation of the mechanically alloyed powders was done using the following techniques.

3.3.1. Sample Preparation

Samples were prepared for electron microscopy by first mounting powders in an EpoFix epoxy cold mounting resin, followed by grinding and polishing. Cold mounted samples were ground on successive SiC grit papers (240, 400, 600, 800 and 1200) and polished using diamond suspensions down to 1µm. Following polishing, all samples were rinsed with copious amounts of tap water, then rinsed with distilled water and ethanol, and finally force air dried.

3.3.2. Scanning Electron Microscopy

The Scanning Electron Microscope (SEM) used in this study was a Philips XL 30 ESEM-FEG, equipped with a detector for energy dispersive X-Ray spectroscopy (EDX). An average accelerating voltage of 15keV was used to generate images of magnifications ranging from 50-10000x.

Cross sections of the mechanically alloyed powders were analysed under backscattered electron mode to obtain an overview of their microstructure and the distribution of phases within the particles. Considering that atoms of higher atomic number generate a brighter contrast image under the backscattered electron mode, the large difference in atomic number between Ti, Ni and Ta made identification of the respective carbonitride and metal phases easier.

EDX analysis was performed to determine the phase composition in the particles of the milled powders. This, coupled with XRD analysis, provided an indication to the extent of mechanical alloying as well as the level of contamination introduced into the system during the milling process.

3.3.3. X-Ray Diffraction

X-Ray diffraction (XRD) was performed to identify the phases present in the milled powder mixtures. A Bruker AXS D2 phaser desktop powder diffractometer with monochromatic Cu Kα radiation produced at 30 kV and 10 mA was used in this investigation. Diffractograms were collected over a range of 2θ between 10 and 90^{o}, with a step size of 0.03^{o} 2θ, together with a scan step time of 0.15s.

The raw data obtained was recorded digitally and analyzed with an X'Pert High Score software package. The software enables several corrections to be made to the raw data. These include $K\alpha_2$-stripping, background subtraction, deconvolution of overlapping reflections and smoothing of the diffractograms. The software also has an automated phase identification application that allows direct comparison of the experimentally obtained data with the data in the 2002 Powder Diffraction File. Thus, the individual carbonitride and metal phases could be easily identified.

Data generated from the X'Pert High Score software was also used to compute the lattice parameter changes of the milled powders. The lattice parameter (*a*) of the Ti(C,N) phases detected was determined from the interplanar spacing (*d*)using the equation for a cubic phase [**84**]:

$$a = d\ \sqrt{h^2 + k^2 + l^2} \qquad \textbf{Equation 3-1}$$

where *hkl* are the Miller indices of the crystal planes.

The crystallite size and lattice strains were determined by means of the Scherrer formula [**85**]:

$$\textbf{Crystallite size} = \frac{k\lambda}{B\cos\theta} \qquad \textbf{Lattice strain} = \frac{B}{\tan\theta}$$

where K the Scherrer constant, λ the wavelength and B the FWHM (in radians).

3.4. Sintering Experiments

Following mechanical alloying and ball milling, the powders were sintered by spark plasma sintering (SPS) to prepare Ti(C,N)-based cermets. The compositions of the different cermets produced by both the mechanical alloying and ball milling processes are detailed in Table 3-3.

Table 3-3: Composition design of cermet materials (wt%)

Cermet Type		Ti(C,N)	Ta	TaC	Ni
Ball Milled	Cermet 1	90	-	-	10
	Cermet 2	54	36	-	10
	Cermet 3	95	-	-	5
	Cermet 4	57	38	-	5
	Cermet 5	60	40	-	-
Mechanically Alloyed	Cermet 6	60	40	-	-
	Cermet 7	60	40	-	-
	Cermet 8	60	40	-	-
	Cermet 9	60	40	-	-
	Cermet 10	60	-	40	-
	Cermet 11	60	-	40	-
	Cermet 12	60	-	40	-

3.4.1. Spark Plasma Sintering (SPS)

The spark plasma sintering experiments were performed using the SPS furnace (model HPD 25/1, FCT Systeme GmbH, Germany). Figure 3-2 shows a schematic drawing of this equipment. About 5g of powder sample was loaded in a graphite die (15mm diameter) and punch unit. To prevent reaction of the powders with the dies during sintering, the dies were coated with hBN. Samples were sintered at a heating rate of 200°C/min and a pressure of 30MPa, in a vacuum controlled environment. The dwell time for sintering was 5min at the respective sintering temperature.

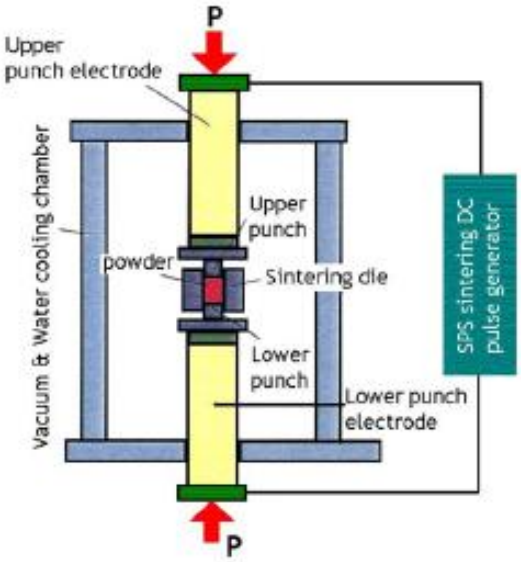


Figure 3-2: Schematic diagram of the SPS apparatus [86**]**

3.5. Cermet Characterisation

3.5.1. Sample Preparation

The sintered samples were prepared for electron microscopy, XRD and mechanical testing from cross-sections of the cermet materials that were cut, ground and polished. Samples were cut using diamond bonded cutting blades. The cross-sections were then ground to produce a planar surface, which was followed by polishing down to a 1µm finish.

XRD and SEM were performed as described in Sections 3.3.2 and 3.3.3 respectively. The methods of mechanical testing and density measurements are described below.

3.5.2. Optical Microscopy

The Zeiss Axiotech reflected-light microscope with an AxioVision image analysis program was used to measure the Vickers indent diagonals and the lengths of Palmqvist fractures at the corners of the indentations.

3.5.3. Physical property measurements

The physical properties measured were density, porosity and hardness. Fracture toughness was derived from the hardness measurements.

3.5.3.1. Density

The density and open porosity of sintered cermets were determined by Archimedes principle using Equation 3-2 and 3-3 respectively.

$$\boldsymbol{\rho = \frac{M_d \times \rho_{Water}}{M_W - M_s}} \qquad \textbf{Equation 3-2}$$

$$\boldsymbol{P_{Open} = \frac{M_W - M_d}{M_W - M_s}} \qquad \textbf{Equation 3-3}$$

where ρ is the density of water (0.998g/cm2 at room temperature), M_d the dry mass of the sample; M_w the water saturated mass and M_s the mass of the sample suspended in water.

The samples were boiled for 3h in distilled water, which was cooled to room temperature before the measurements were made. Each measurement was made three times and the average used in the equations above.

3.5.3.2. Hardness

The hardness of the SPS cermets was measured on smoothly polished cross-sections using the Vickers hardness (HV) indentation technique. Hardness was measured with a pyramidal diamond indenter, at a load of 5kg and an indenting time of 10s. After indentation, the lengths of the two diagonals of each indentation were measured by optical microscopy and recorded. The hardness was calculated from the average length of the two diagonals by Equation 3-4:

$$\mathbf{HV} = \frac{\mathbf{1.854}P}{d^2} \qquad \textbf{Equation 3-4}$$

Where *P* is the applied load in kg and *d* the indent diameter in mm.

At least five indentations were made on each sample and the reported values are the average of the measured values.

3.5.3.3. Fracture Toughness

Fracture toughness of the cermet materials was determined from the hardness measurements. The length of the radial cracks propagating from the edges of the Vickers indentation were measured by optical microscopy, and the formula of Shetty *et al*. [**87**] was used to estimate the fracture toughness.

$$\mathbf{K_{Ic}} = \overline{\frac{HP}{4a}} \qquad \textbf{Equation 3-5}$$

where *P* is the indentation load (in N) and *a* is the sum of the radial crack length (in μm).

Chapter 4: Experimental Results

As mentioned in Chapter 2, in order to obtain cermets with the desired physical and mechanical properties, optimization of the processing parameters is essential. The properties and microstructure of the cermet depend on the nature of the starting materials. Consequently, small changes in composition and/or processing parameters bring about significant change in the physical and microstructural properties of the resultant cermets. As such, the processing-microstructure-property relationship needs to be fully understood.

This chapter details the influence of powder processing on the starting powder mixtures, and the subsequent impact of this on the microstructure and physical properties of the cermets sintered from these mixtures.

4.1. Milling Process

4.1.1. Ball Milling

This section summarizes the results relating to all ball-milled (BM) samples. A description of the sample composition is illustrated in Table 4-1.

Table 4-1: Sample Composition for ball-milled cermets

Cermet Type	Composition (numbers represent wt%)	Milling Time (h)
Cermet 1	TiCN-10Ni	3
Cermet 2	TiCN-36Ta-10Ni	3
Cermet 3	TiCN-5Ni	3
Cermet 4	TiCN-38Ta-5Ni	3
Cermet 5	TiCN-40Ta	3

4.1.1.1. Phase Composition of the Ball-Milled Powders

The X-Ray diffraction patterns for the various ball-milled powder mixtures are shown in Figure 4-1. The XRD data confirms the phase composition of the starting powder mixtures for all cermet mixtures. The data show no significant broadening of the characteristics peaks and no distinguishable shift in peak position was observed after ball-milling. An additional phase was discerned from peak positions 31.4 and 48.3 °2theta. This phase was identified to be that of WC, resulting from contamination from the milling media.

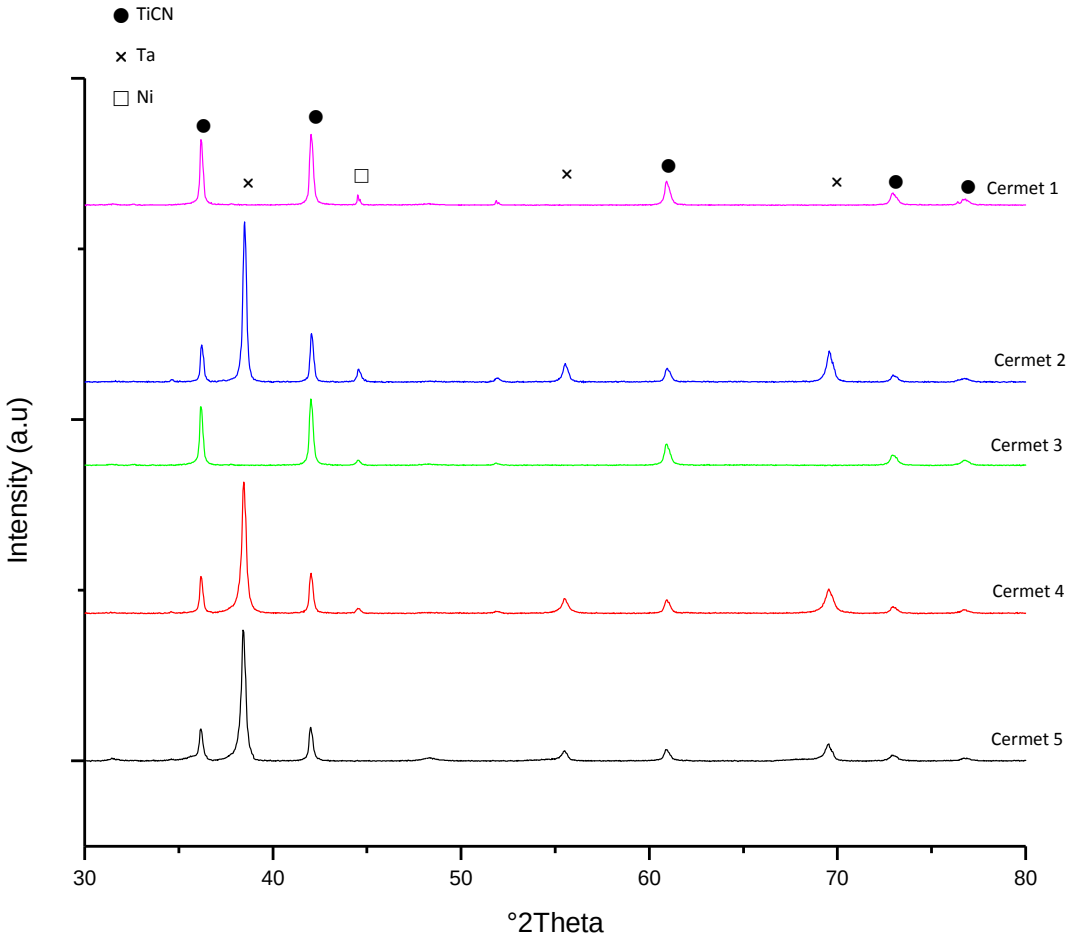


Figure 4-1: Diffractograms for the various ball-milled powder mixtures

4.1.1.2. SEM Analysis of Ball-Milled Powders

The SEM micrographs of the powder mixtures for Cermets 3-5 after ball-milling are shown in Figure 4-2. For Cermet 3, the particle size of the Ti(C,N) phase is seen to be approximately 3-4µm, similar to that of the starting particle size. Thus, no considerable reduction in particle size was observed after ball-milling. Similar observations can be made for Cermets 4 and 5. For these mixtures, the microstructure remains largely heterogeneous after ball-milling, with the Ti(C,N) and Ta phases easily identifiable in the micrographs (Figure 4-2(b)-(c)).

The micrographs of Cermet 1 and 2 have not been shown, as their characteristics closely resemble those of Cermets 3 and 4 respectively.

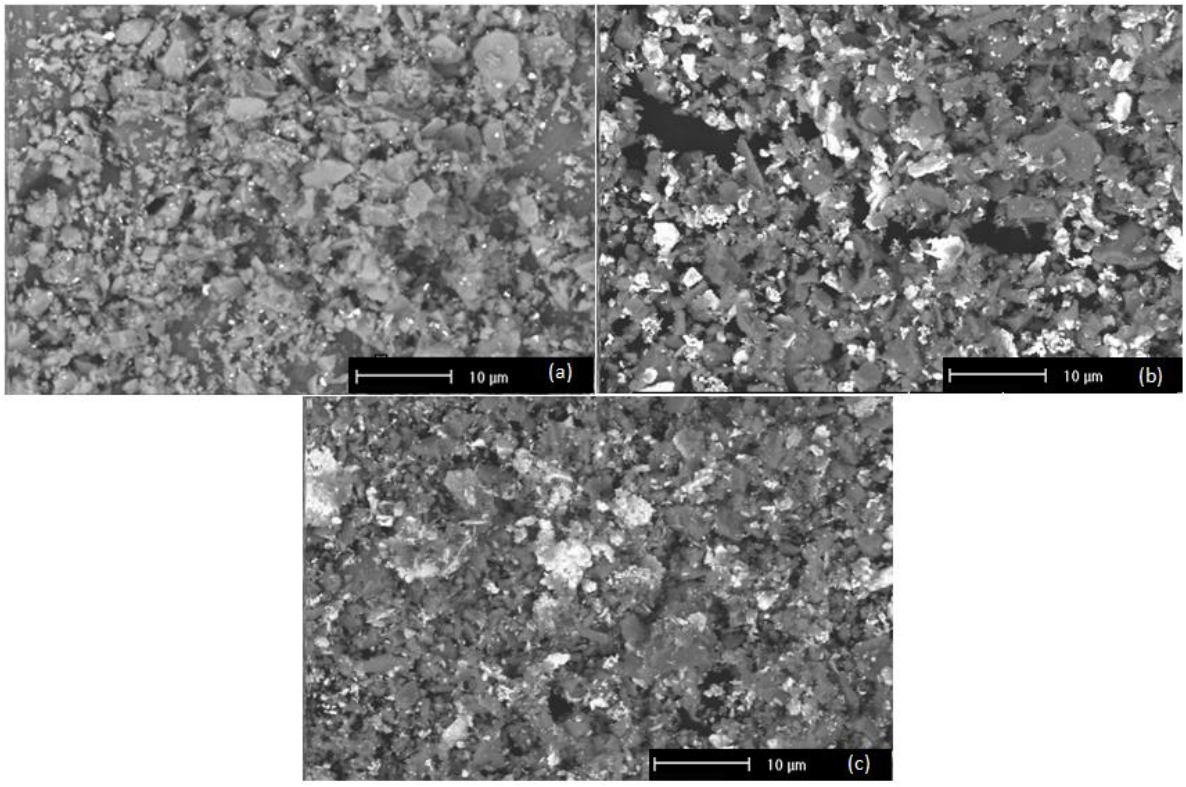


Figure 4-2: SEM (BSE) micrographs of the ball-milled powder mixtures for (a) Cermet 3 (b) Cermet 4 and (c) Cermet 5

4.1.2. Mechanical Alloying

This section details the results pertaining to all mechanically alloyed samples. Detailed analysis of the mechanical alloying process within the Ti(C,N)-Ta and Ti(C,N)-TaC mixtures is given in Sections 4.1.2.1 and 4.1.2.2 respectively.

4.1.2.1. The Ti(C,N)-Ta Mixture

A description of the sample composition and milling process for the Ti(C,N)-Ta mixture is given in Table 4-2.

Table 4-2: Sample Composition and Experimental Design for Ti(C,N)-Ta Mechanically Alloyed Cermets

Cermet No.	Composition (numbers represent wt%)	Milling Time (h)
Cermet 6	TiCN-40Ta	2
Cermet 7	TiCN-40Ta	4
Cermet 8	TiCN-40Ta	8
Cermet 9	TiCN-40Ta	12

4.1.2.1.1. Phase Composition of the Ti(C,N)-Ta Mechanically Alloyed Powders

The X-Ray diffraction pattern for the $TiC_{0.7}N_{0.3}$-Ta powder mixture and its evolution upon mechanical alloying is illustrated in Figure 4-3. The top-most pattern shows the as-mixed powder (i.e. 0h MA), in which the individual Ti(C,N) and Ta phase have been identified. After 2 hours mechanical alloying, the relative intensity of the Ta phase had significantly reduced and there was a distinguishable shift in peak position to lower 2θ angles by 1°. This trend continued with prolonged milling and after 8 hours, the Ta phase peak had completely merged with the neighbouring (111) Ti(C,N) peak. The characteristic peaks became broader with mechanical alloying, as the FWHM of the Ti(C,N) (111) peak reflection increased from 0.2 to 1 °2Theta after 12 hours mechanical alloying.

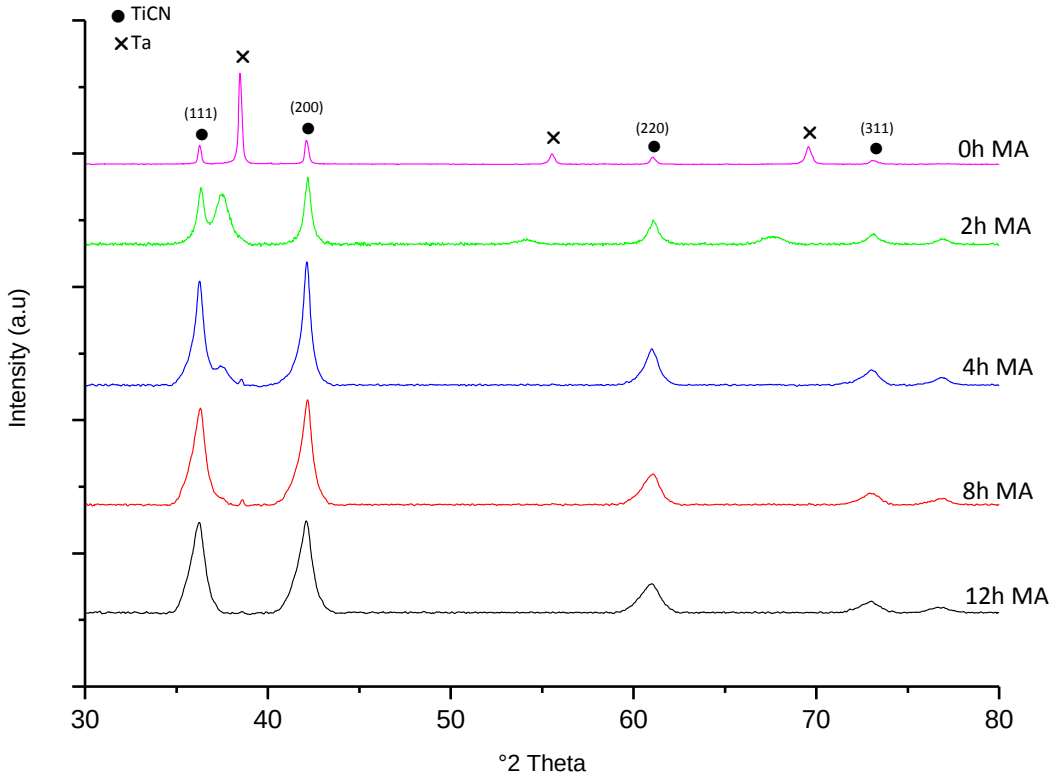


Figure 4-3: Diffractograms for the Ti(C,N)-Ta powders mechanically alloyed for different time intervals

Table 4-3: Effect of mechanical alloying on the Ti(C,N) lattice parameter and crystallite size in the Ti(C,N)-Ta mixture

Material/Milling time	Lattice Parameter (Å)	Crystallite size (nm)
0h	4.296 ± 0.002	54 ± 1.5
2h	4.299 ± 0.002	13 ± 1.2
4h	4.301 ± 0.003	12 ± 0.6
8h	4.294 ± 0.003	11 ± 0.3
12h	4.292 ± 0.003	8 ± 0.2

Table 4-3 gives the Ti(C,N) lattice parameter changes and crystallite size evolution with increasing time of mechanical alloying. The lattice parameter measurements showed no systematic change in the Ti(C,N) lattice parameter with increasing periods of mechanical alloying, when the errors of determination were considered (Table 4-3). The estimated crystallite size of Ti(C,N) showed that with increasing mechanical alloying time, the crystallite size strongly reduced. It was observed (Figure 4-4) that the reduction in size was mostly achieved within the first two hours of milling. Thereafter, as mechanical alloying time increased, the rate at which the crystallite size reduced slowed down. After 12 hours MA, the crystallite size had reduced from approximately 54nm to 8nm.

In contrast, lattice strain had an inverse relation with increasing mechanical alloying time. This trend is observed in Figure 4-4, which shows the change in lattice strain with increasing mechanical alloying time, calculated from the (220) Ti(C,N) peak. A maximum lattice strain of 0.9% was obtained after 12 hours mechanical alloying.

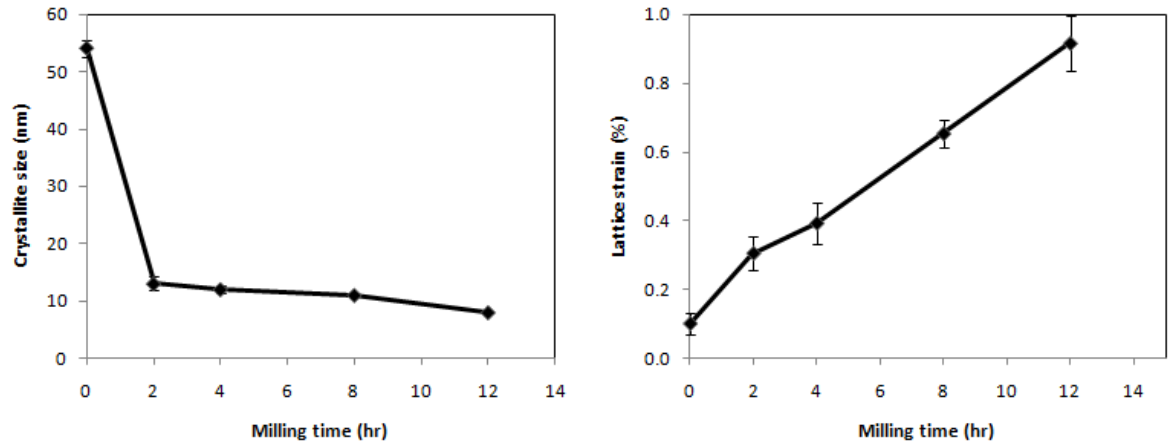


Figure 4-4: Particle size refinement and lattice strain evolution with mechanical alloying

4.1.2.1.2. SEM Analysis of the Ti(C,N)-Ta Mechanically Alloyed Powders

The morphology of the milled powders after various mechanical alloying times is shown in Figure 4-5. Examination of the SEM micrographs revealed different particle morphology for the powders mechanically alloyed for 2 and 12 hours. After 2 hours milling, the morphology of the particles was non-uniform, as some particles were spherical while others angular and some particles had apparently not been broken down by the milling process. Evidence of the early stage of alloying or reaction between the phases was clearly seen with numerous sub-micron particles embedded around larger ones. For powders mechanically alloyed for 12 hours, SEM investigation of the milled powder revealed a strong reduction in the tantalum phase and the formation of large aggregates. Similar to the 2 hour milled samples, many fine particles were embedded onto larger ones, with the sub-micron grains being well-fused together. EDX analysis (Figure 4-6) showed that the Ti(C,N) existed as the core of these aggregates which is surrounded by fine particles of the tantalum containing phase.

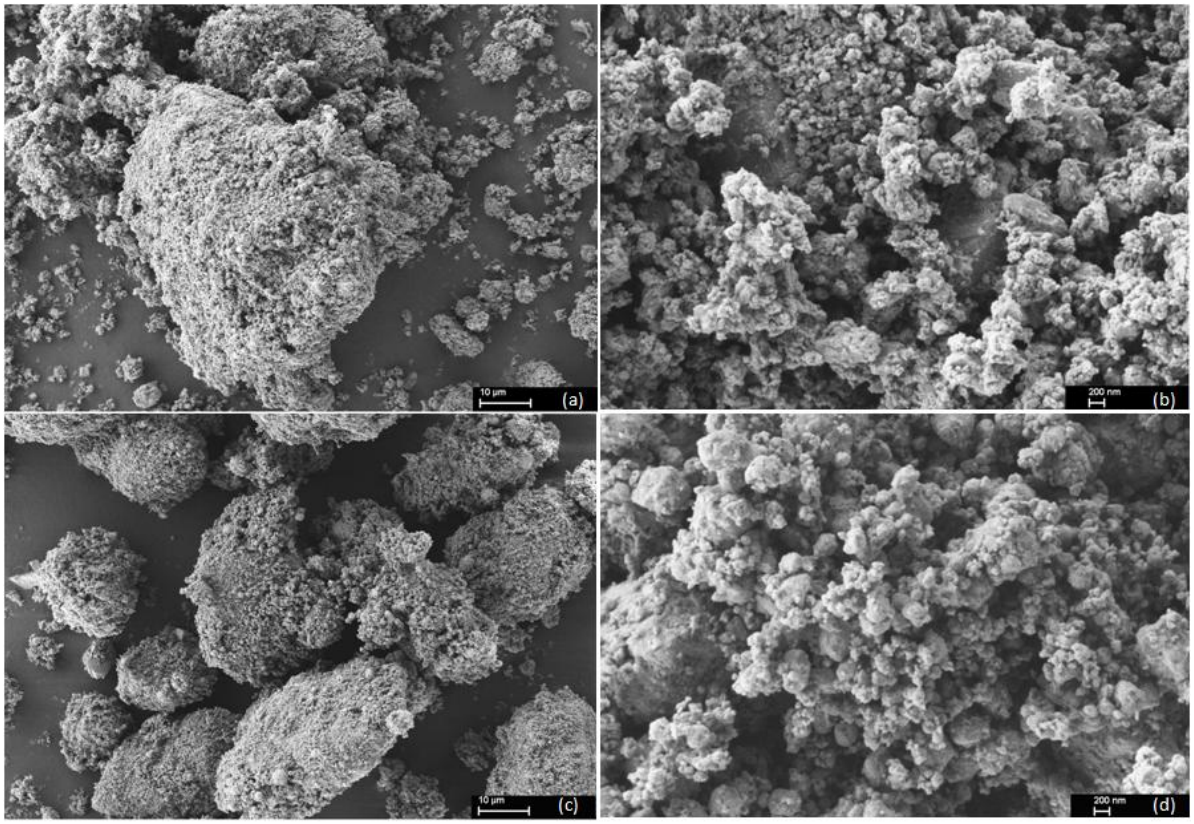


Figure 4-5: SEM (SE) micrographs of Ti(C,N)-Ta powders mechanically alloyed for 2h (a)-(b) and 12h (c)-(d)

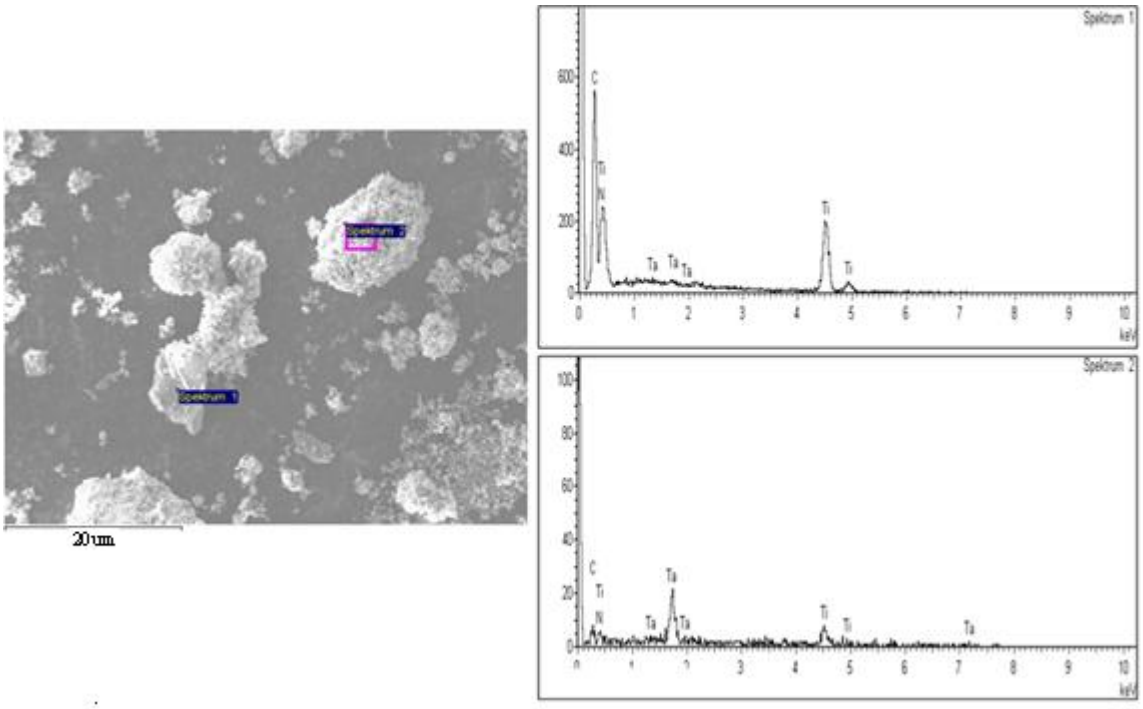


Figure 4-6: EDX analysis of Ti(C,N)-Ta powders mechanically alloyed for 12 hours

Chemical analysis of the powders before and after milling showed that the oxygen content increased from 0.54 ± 0.04 to 1.86 ± 0.07 wt% after 12 hours mechanical alloying. This increase was due to an increase in the amount of adsorbed oxygen as a result of the increased surface area of the powder particles following mechanical alloying.

4.1.2.2. The Ti(C,N)-TaC Mixture

A description of the sample composition and milling process for the Ti(C,N)-TaC mixture is provided in Table 4-4.

Table 4-4: Sample Composition and Experimental Design for Ti(C,N)-TaC Mechanically Alloyed Cermets

Cermet No.	Composition (numbers represent wt%)	Milling Time (h)
Cermet 10	TiCN-40TaC	12
Cermet 11	TiCN-40TaC	24
Cermet 12	TiCN-40TaC	48

4.1.2.2.1. Phase Composition of the Ti(C,N)-TaC Mechanically Alloyed Powders

Figure 4-7 shows the X-ray diffraction pattern of the Ti(C,N)-TaC powder mixture mechanically alloyed for different time intervals ranging from 0 to 48 hours. The top-most diffraction pattern shows the initial powder mixture (i.e. 0h MA), where sharp, high intensity peaks of the Ti(C,N) and TaC phases can be easily identified. After 12 hours mechanical alloying, there was a decrease in the intensity of the TaC peaks. This trend continued for both the 24 and 48 hour mechanically alloyed powders. In addition to the drop in peak intensity, mechanical alloying had also shown to increase the characteristic peak widths for both the Ti(C,N) and TaC phases.

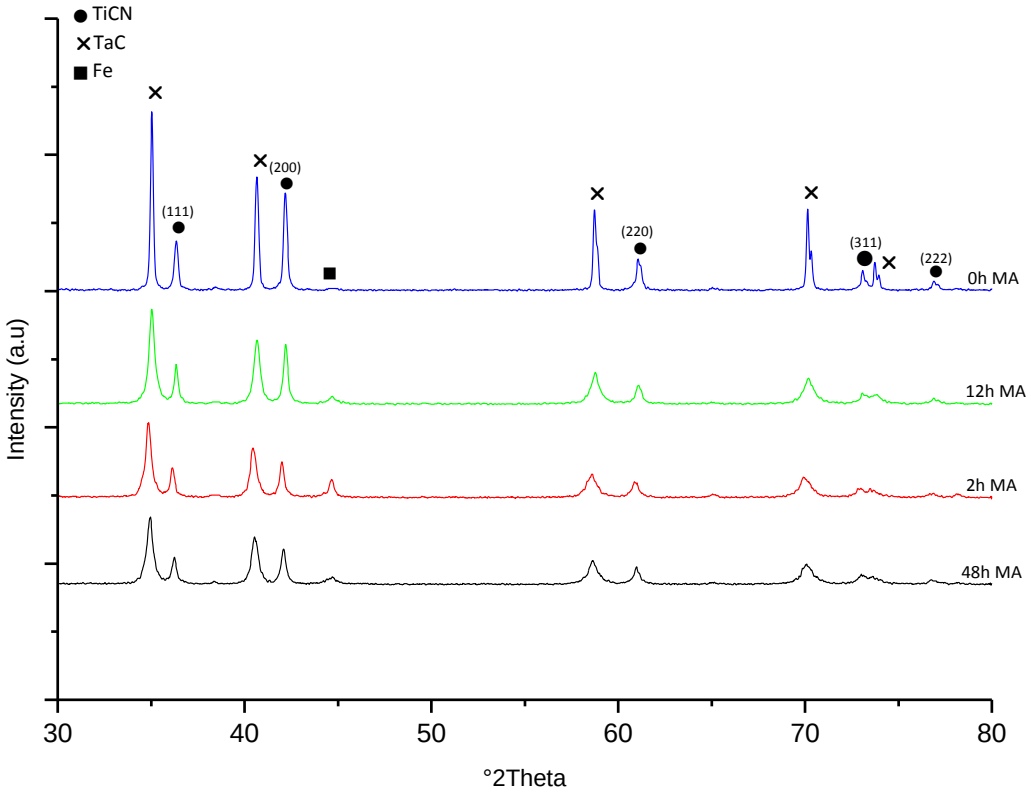


Figure 4-7: Diffractograms for the Ti(C,N)-TaC powders mechanically alloyed for different time intervals

Although there was an overall decrease in maximum peak intensity across all milled species, after 48 hours MA, the TaC phase peaks persisted and still remained well defined. Thus, this reduction in intensity may be attributed primarily to peak broadening caused by particle size reduction. Comparison of the ratio of relative peak intensity between the (200) Ti(C,N) and TaC peak reflections showed no distinct change with increasing milling time. The Ti(C,N):TaC peak ratio remained constant at approximately 1.4:1 after mechanically alloying for the different time intervals.

Figure 4-7 indicates no distinguishable shift in the Ti(C,N) phase peak positions after mechanical alloying for 48 hours. This correlates with the lattice parameter changes with increasing mechanical alloying time given in Table 4-5. These results show that the changes in both the Ti(C,N) and TaC lattice parameter were minimal and taking into account the errors of determination, these values remained relatively constant during the mechanical milling process.

Table 4-5: Ti(C,N) and TaC lattice parameter and crystallite size evolution for the Ti(C,N)-TaC mixture after various times of mechanical alloying

Sample	Lattice Parameter (Å)		Crystallite Size (nm)	
	Ti(C,N)	TaC	Ti(C,N)	TaC
0h MA	4.296 ± 0.002	4.453 ± 0.002	55± 1.5	55± 1.8
12h MA	4.295 ± 0.002	4.452 ± 0.002	50± 1.3	51± 1.5
24h MA	4.298 ± 0.003	4.451 ± 0.003	35± 0.4	37± 0.6
48h MA	4.299 ± 0.003	4.450 ± 0.003	33± 0.5	35± 0.4

Table 4-5 also shows the crystallite size evolution as a function of mechanical alloying time for both the Ti(C,N) and TaC phases. It is observed that the reduction in size was not as extensive as in the Ti(C,N)-Ta system, even though longer periods of mechanical milling were employed for this mixture. The data showed that after 24 hours mechanical alloying, the crystallite size had reduced by approximately 20nm and milling for periods longer than 24 hours showed no significant reduction in particle size. After 48 hours mechanical alloying the crystallite size had reduced from approximately 55nm to 33 and 35nm for the Ti(C,N) and TaC phases respectively.

4.1.2.2.2. SEM Analysis of the Ti(C,N)-TaC Mechanically Alloyed Powders

The morphologies of the Ti(C,N)-TaC powders mechanically alloyed for 0 and 48 hours are shown in Figure 4-8. The microstructure of the starting powder mixture (i.e. 0h MA) was largely heterogeneous, with the individual TaC and TiCN phases easily identifiable. After 48 hours mechanical alloying, the microstructure became more homogenous, as the TaC and Ti(C,N) phases were more evenly distributed within the overall microstructure as seen in Figure 4-8(b). However, both phases still existed as individual particles after 48 hours mechanical milling.

At higher magnification (Figure 4-8(d)), flattening, fracturing and welding mechanisms could be observed. Non-uniform particle morphology was seen, as the size of the ball milled powders was uneven and their shape irregular due to the continuous cold welding and fracturing process occurring during milling. Figure 4-8(d) also shows the TaC phase embedded around the Ti(C,N) phase particles after 48 hours mechanical alloying.

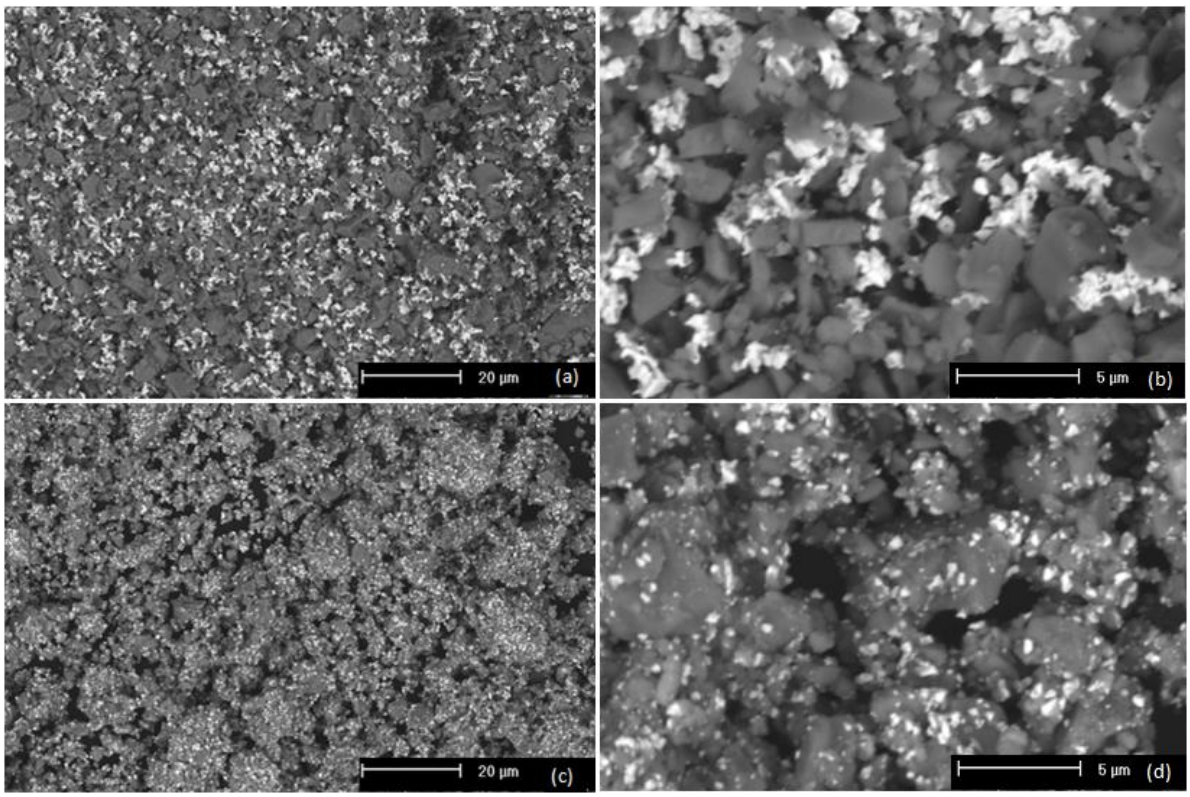


Figure 4-8: SEM (SE) micrographs of the Ti(C,N)-TaC powders after 0h MA(a) and (b); and 48h MA (c) and (d)

4.2. Sintering Experiments

4.2.1. Ti(C,N)-(Ta)-Ni Ball-Milled Cermets

The physical properties of the ball-milled cermets are given in Table 4-6. The results showed that the densities obtained for Cermets 1 and 2 were lower in comparison to the other samples. Since these samples contained a greater weight percentage of the metal binding phase, a higher volume of the liquid phase was produced during sintering. Consequently, this caused squeezing out of the liquid phase during densification, thus resulting in residual porosity and change in the theoretical densities of these samples. When the Ni binder was reduced to 5wt%, as in Cermets 3 and 4, much higher densities were obtained for these cermets, with significantly less porosity. Good densification was obtained for Cermet 5, by solid state sintering processes.

Figure 4-9 shows the densification curves of the ball-milled cermets. These curves display significantly different sintering behaviour as a result of the different starting compositions. For Cermet 5 (TiCN-Ta), densification started at approximately 1200°C. The shallowness of the gradient indicated that the rate of densification was slow, approximately 40% of which occurs during the isothermal sintering period. The addition of Ni to the cermet reduced the starting densification temperature, so that for Cermet 3 (TiCN-5Ni) and Cermet 4 (TiCN-Ta-5Ni), densification started earlier at approximately 900°C and 1100°C respectively. The rate of densification in these samples was much faster than that of Cermet 5, as indicated by the greater steepness in the curves as opposed to Cermet 5, with approximately 15% densification occurring during the isothermal sintering period.

The difference in sintering behaviour between the ball-milled cermets was due to the different sintering mechanisms occurring between the samples and the differences in the compositions of the starting powder mixtures. The addition of Ni to Cermet 3 and 4 enabled densification by liquid phase sintering processes, which subsequently accelerated transport and diffusion of elements through a liquid medium. This subsequently allowed densification to occur faster in these samples compared to Cermet 5.

Table 4-6: Physical Properties of Ti(C,N)-based ball-milled cermets

Cermet #	Sample	Sintering Temp (°C)	Density (g/cm^3)	% Theoretical	Open Porosity(%)
Cermet 1	TiCN-10Ni	1500	5.04	96.2	1.8
Cermet 2	TiCN-Ta-10Ni	1500	6.70	94.8	2.1
Cermet 3	TiCN-5Ni	1400	5.10	99.5	0.4
Cermet 4	TiCN-Ta-5Ni	1400	6.92	99.0	0.4
Cermet 5	TiCN-Ta	1500	6.88	99.6	0.3

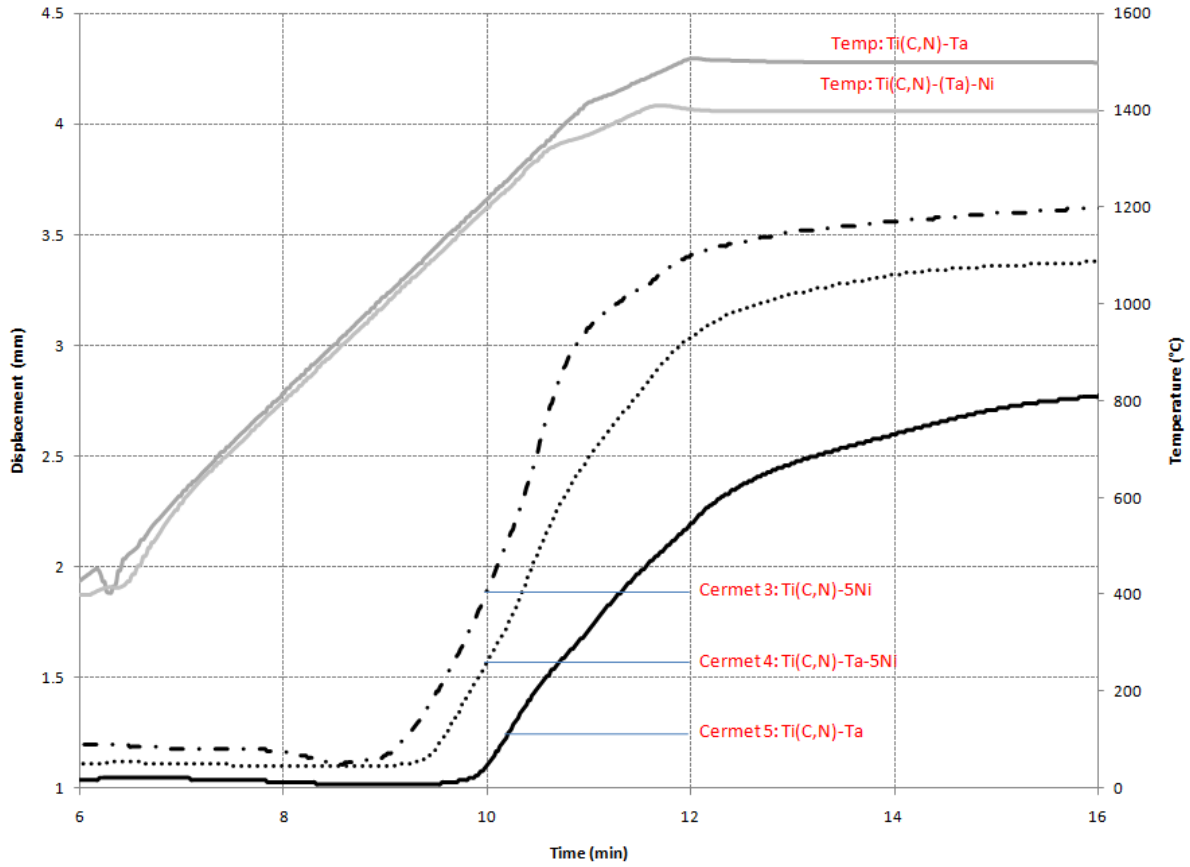


Figure 4-9: Densification curves for Cermet 3, Cermet 4 and Cermet 5

The XRD analysis of the cermets produced from ball milled powders is illustrated in Figure 4-10. The results of the XRD analysis showed the absence of the Ta phase peak in Cermet 2 following sintering at 1500°C. For Cermet 4 and 5 however, the Ta phase peak was still evident within the diffractograms, but with a distinguishable shift in peak position to higher °2θ by 1.6°. This indicated that Ni and maybe even Ti, C and N had dissolved into the Ta crystal lattice.

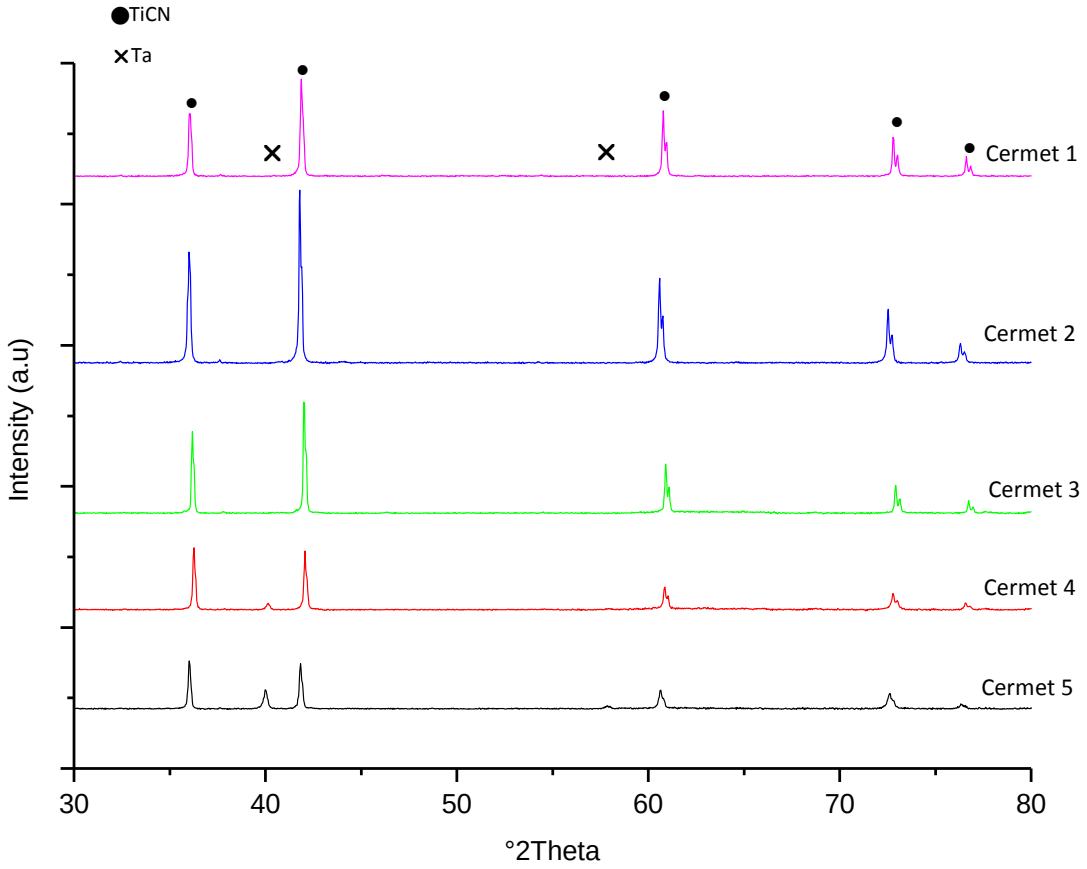


Figure 4-10: Diffractograms for the various cermets produced by ball milling

The lattice parameter measurements following densification showed an overall increase in the Ti(C,N) lattice parameter for all ball-milled cermets, as seen in Table 4-7. The greatest increase was observed in the Ta-containing cermets, as the lattice parameter tended to be closer to that of the TaC lattice parameter (4.45Å). For Cermets 1 and 3, the lattice parameter following densification was only slightly higher than the lattice parameter of the starting Ti(C,N) powder (4.296Å) when their errors of determination were taken into account. Thus, these changes may be due to denitrification resulting from the sintering conditions. Denitrification had been reported to occur when TiC and TiN react to form Ti(C,N) [**88**] or during the reaction between the Ti(C,N) phase and the binding metal [**89**]. For Cermets 1 and 3, Ni was used as the binding metal, therefore if denitrification had occurred within these samples the resultant cermet would be deficient in nitrogen. Considering the stoichiometry as $TiC_{1-x}N_x$, if x decreased the lattice parameter would increase linearly due to TiN having a slightly lower lattice parameter then TiC (Table 2-4). Consequently, denitrication would result in a slight increase in the Ti(C,N) lattice parameter as observed in Cermets 1 and 3.

Table 4-7: Ti(C,N) Lattice parameter changes for the various cermets produced after ball milling

Cermet #	Sample	Lattice Parameter (Å)
Cermet 1	TiCN-10Ni	4.308± 0.002
Cermet 2	TiCN-Ta-10Ni	4.319± 0.001
Cermet 3	TiCN-5Ni	4.303± 0.002
Cermet 4	TiCN-Ta-5Ni	4.314± 0.001
Cermet 5	TiCN-Ta	4.316± 0.001

4.2.2. Ti(C,N)-Ta Mechanically Alloyed Cermets

The densities and densification curves of the Ti(C,N)-Ta samples sintered at 1500°C are given in Table 4-8 and Figure 4-11 respectively. Although the densities achieved were similar, densification curves displayed significantly different sintering behaviour between the samples. For the 2 hours mechanically alloyed powders, densification started at approximately 900°C. Thereafter, there was a steep rise in densification, which was almost completed before entering the isothermal sintering period. For powders mechanically alloyed longer than 2 hours, there were only slight changes observable in densification behaviour between the 4, 8 and 12 hour samples. For these samples, densification occurred slightly later (at approximately 1000°C) and the rate of densification was much slower as compared to the 2 hour mechanically alloyed sample. Similar to the 2 hour mechanically alloyed sample, densification was near completion upon reaching the isothermal sintering temperature. These results showed the influence of the mechanical alloying process on the sinterability of the materials and are discussed in detail in Chapter 5.

Table 4-8: Physical Properties of Ti(C,N)-Ta Mechanically Alloyed cermets sintered at 1500°C

Sample	Density (g/cm^3)	% Theoretical
2h	6.89	99.7
4h	6.92	100
8h	6.90	99.9
12h	6.92	100

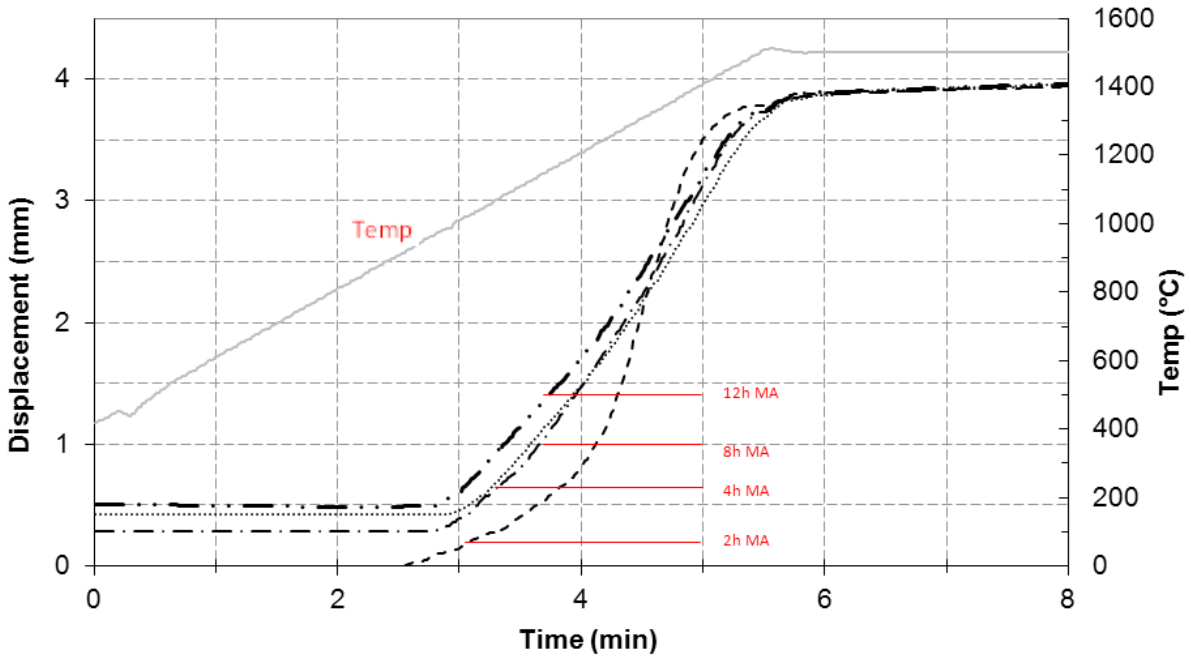


Figure 4-11: Densification curve for the Ti(C,N)-Ta powders sintered after various times of MA

Figure 4-12 shows the XRD pattern for the Ti(C,N)-Ta powders sintered after the various mechanical alloying times. Different features could be observed from the XRD traces. The most prominent feature for all traces was the complete disappearance of the Ta phase following densification. Also evident was the presence of a secondary phase in close proximity to the peaks of the main cubic carbide phase. The insert allows for easier examination of the ratio of relative peak intensity between the primary and secondary phase at 61 °2Theta, and its change with increasing milling time. After 2 hours mechanical alloying the secondary phase peak had an intensity that was $\frac{1}{5}$ that of the primary peak. With increasing times of mechanical alloying, the ratio of the two peaks decreased, so that after 12 hour the intensity of the secondary phase peak was $\frac{1}{10}$ that of the primary peak. This indicated a reduction of the secondary phase within the system. Consequently the primary and secondary phases had been identified as $Ti_{(1-x)}$-Ta_x(C,N) and unreacted Ti(C,N) respectively. The Fe peak identified at 44.5 °2Theta was due to contamination introduced by wear of the stainless steel milling media.

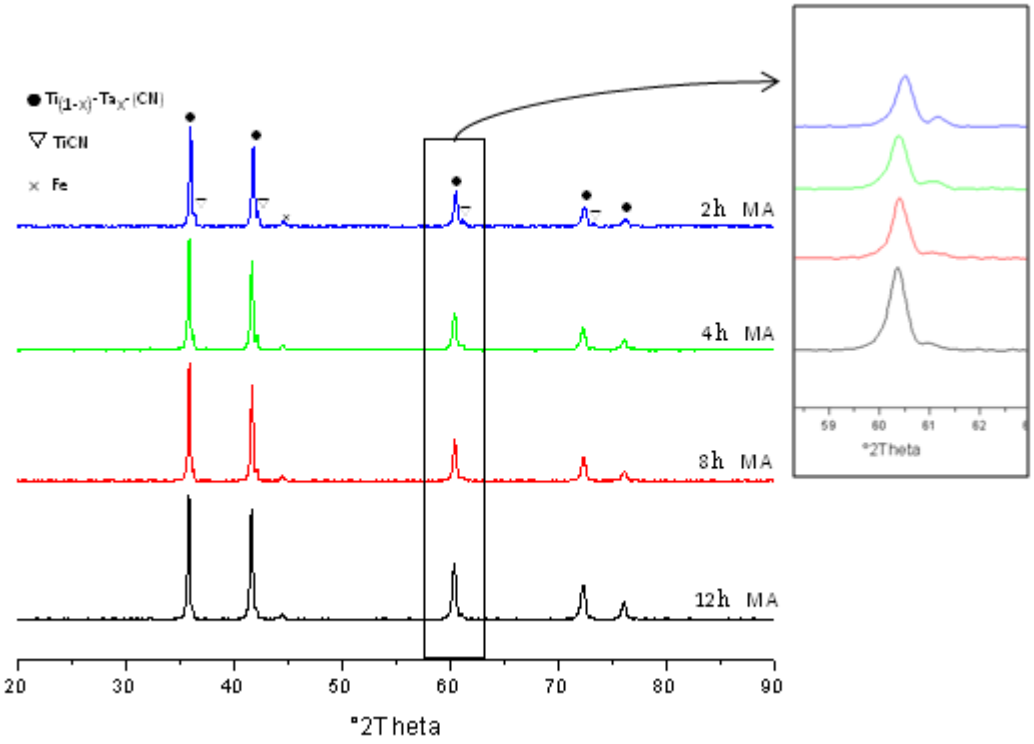


Figure 4-12: XRD pattern of the TiCN-Ta powders sintered at 1500°C

4.2.3. Ti(C,N)-TaC Mechanically Alloyed Cermets

The densities for the cermets produced from the mechanically alloyed Ti(C,N)-TaC powders are given in Table 4-9. For the 12 and 24 hour mechanically alloyed samples, the densities achieved were low and the percentage open porosity was high. Significantly improved densities was obtained for the 48 hour mechanically alloyed sample, as the densification increased by an average of approximately 21% compared to the 12 and 24 hours mechanically alloyed sample, and the open porosity was reduced to 0.1%.

Table 4-9: Physical Properties of Ti(C,N)-TaC Mechanically Alloyed cermets sintered at 1500°C

Sample	Density (g/cm^3)	% Theoretical	Open Porosity(%)
12h	5.25	77.3	15.8
24h	5.70	84.3	10.2
48h	6.72	99.0	0.1

Figure 4-13 shows the XRD pattern for the Ti(C,N)-TaC powders sintered after the various times of mechanical alloying. For the cermet produced from the powders sintered after 12 hours mechanical alloying, the XRD pattern showed the presence of two separate phases. The Ti(C,N) phase has been indexed in Figure 4-13 as the main cubic carbide phase. The peaks to the left of the Ti(C,N) peaks are those of the original TaC phase peaks, which have significantly shifted following densification. With increasing mechanical alloying time, the Ti(C,N) and TaC phases began to merge with one another as their peaks overlap at lower °2θ. However, at higher angles these phases remain separate, indicating that the reaction between the Ti(C,N) and TaC was not carried out to completion during the sintering process, therefore unreacted TaC material was still present within the microstructure.

The TaC lattice parameter changes following densification is given in Table 4-10. The TaC lattice parameter significantly decreased after densification from 4.45Å to 4.34Å for the 48 hour mechanically alloyed sample. This indicated that Ti, N and maybe O had dissolved into the material and a solid solution of Ta-Ti-(C,N) may have formed. The lattice parameter of TiC and TiN are significantly smaller than that of TaC, thus the dissolution of Ti and N into

the crystal lattice of TaC would explain the considerable decrease in its lattice parameter. Consequently, these peaks have been identified as a Ta_{ss} phase.

Table 4-10 also gives the lattice parameter changes of the Ti(C,N) phase following densification. The data showed considerable increase in the Ti(C,N) lattice parameter for the cermet sintered after 48 hour mechanical alloying. For this sample, an increase to 4.35Å was observed thereby indicating the dissolution of Ta, C and probably O into the Ti(C,N) lattice structure.

Table 4-10: Ti(C,N) and TaC lattice parameter changes for the Ti(C,N)-TaC cermets produced after different times of mechanical alloying

Sample	Lattice Parameter (Å)	
	Ti(C,N)	TaC
12h	4.310 ± 0.002	4.440 ± 0.004
24h	4.340 ± 0.003	4.350 ± 0.003
48h	4.350 ± 0.003	4.340 ± 0.003

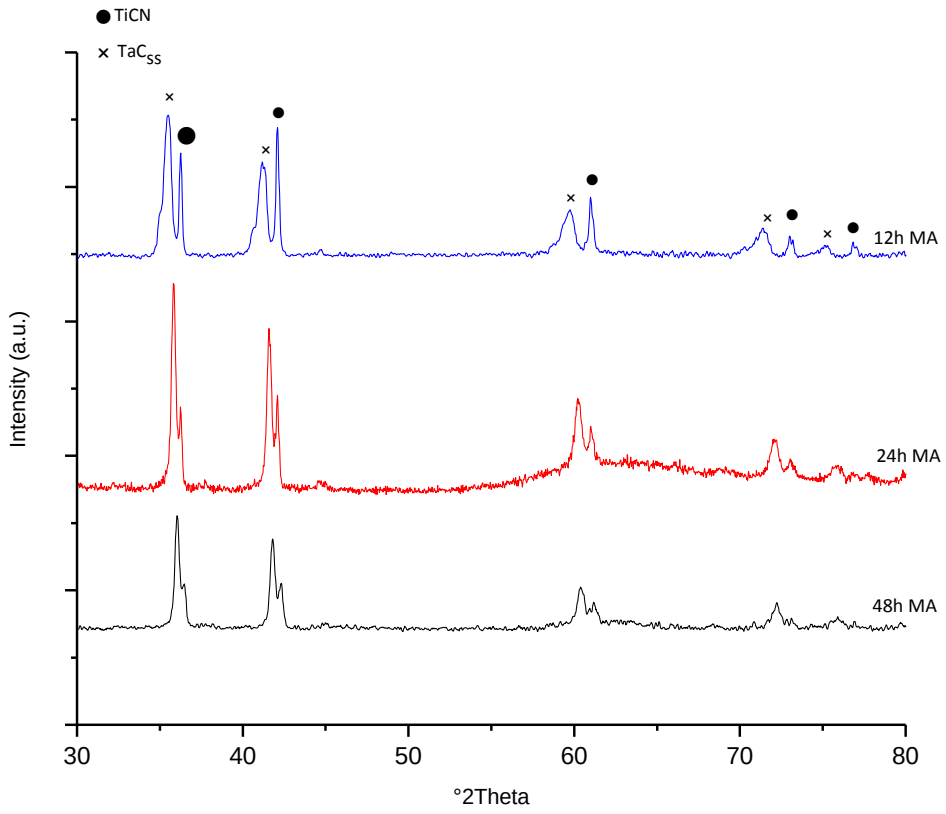


Figure 4-13: XRD profile of the mechanically alloyed Ti(C,N)-TaC powders sintered by SPS at 1500°C

4.3. Microstructural Analysis

4.3.1. Ball-Milled Cermets

The microstructures of the cermets produced after ball-milling mixtures of different powder compositions are shown in Figure 4-14. In general, the micrographs displayed typical core-rim morphology for all ball-milled cermets. However, the characteristics of the core-rim (in terms of size and shape) are different, depending on the composition of the cermet starting powders and the sintering temperature. For Cermets 1-4, the distribution of the Ni binder (bright contrast) in the ceramic phase could be observed. The micrographs also showed different wetting behaviour within these materials. Good wetting of the Ni binder with the Ti(C,N) grains was observed for Cermets 1-3, whereas poor wetting behaviour was displayed in Cermet 4 and 5.

Cermets 2 and 4 contained the same starting powder composition, except that Cermet 4 contained 5wt% less Ni then Cermet 2. From the SEM micrographs, the microstructure of Cermet 4 appeared more refined then that of Cermet 2. For both Cermets 2 and 4, EDX analysis revealed the presence of Ta in the Ni binder. Thus, the evolution of the core-rim morphology occurred via dissolution-reprecipitation processes. Due to the higher solubility of the Ta phase in the Ni binder, during sintering Ta was dissolved in the liquid phase. From this melt, the liquid solution of (Ti,Ta)(C,N) would have precipitated out onto the undissolved TiN-richer Ti(C,N) nuclei.

The micrograph of Cermet 4 also showed the presence of the unreacted Ta phase which was not present in Cermet 2. This suggested that sintering Cermet 2 at 1500°C allowed for the complete reaction between the Ti(C,N) and Ta phases, whereas at 1400°C (i.e. the sintering temperature of Cermet 4) the reaction between Ti(C,N) and Ta was limited and some of the Ta remained undissolved during densification.

For Cermet 5, the core-rim morphology was not as distinct as in the other ball-milled cermets and unreacted Ta could also be observed in the microstructure.

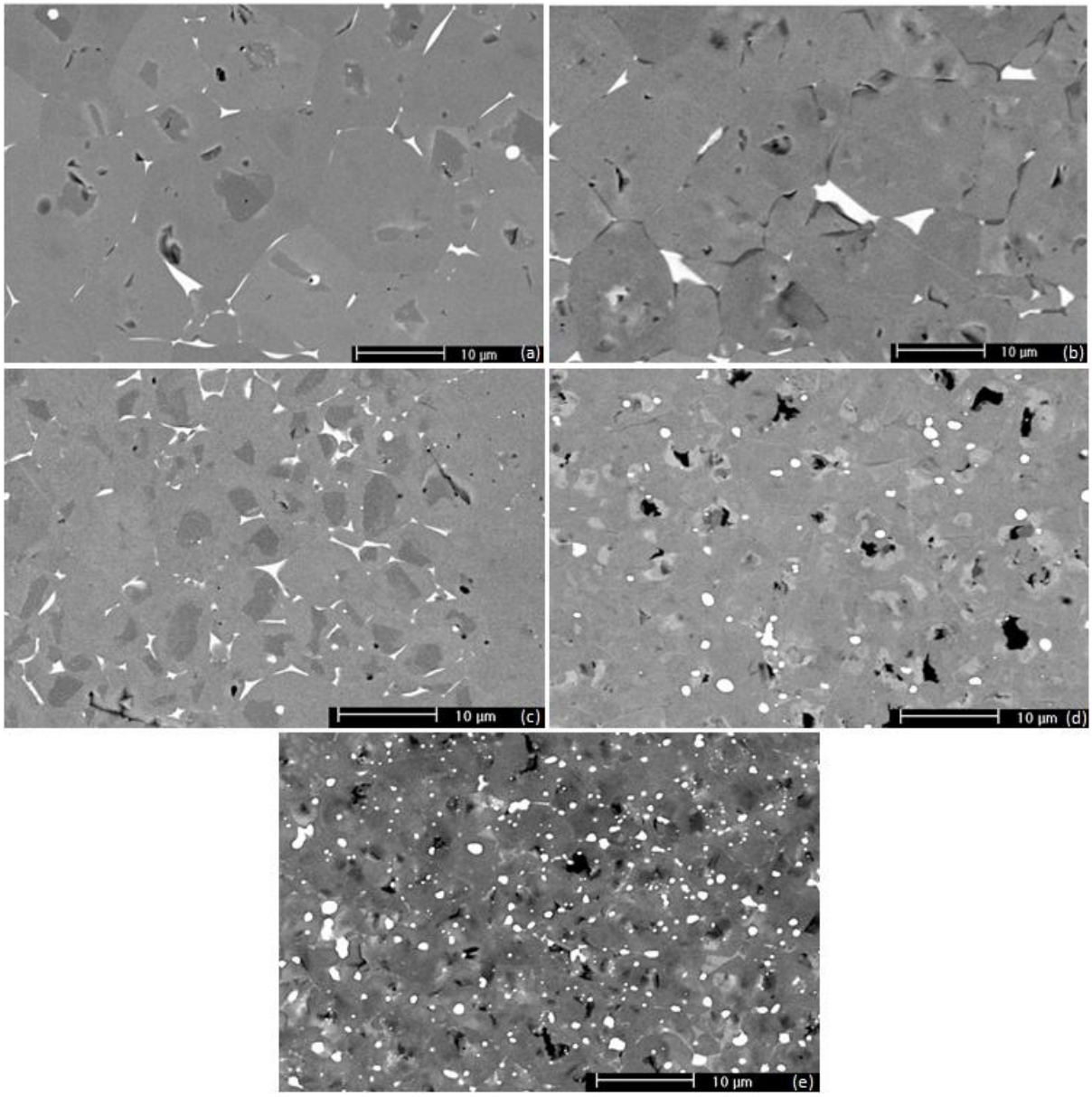
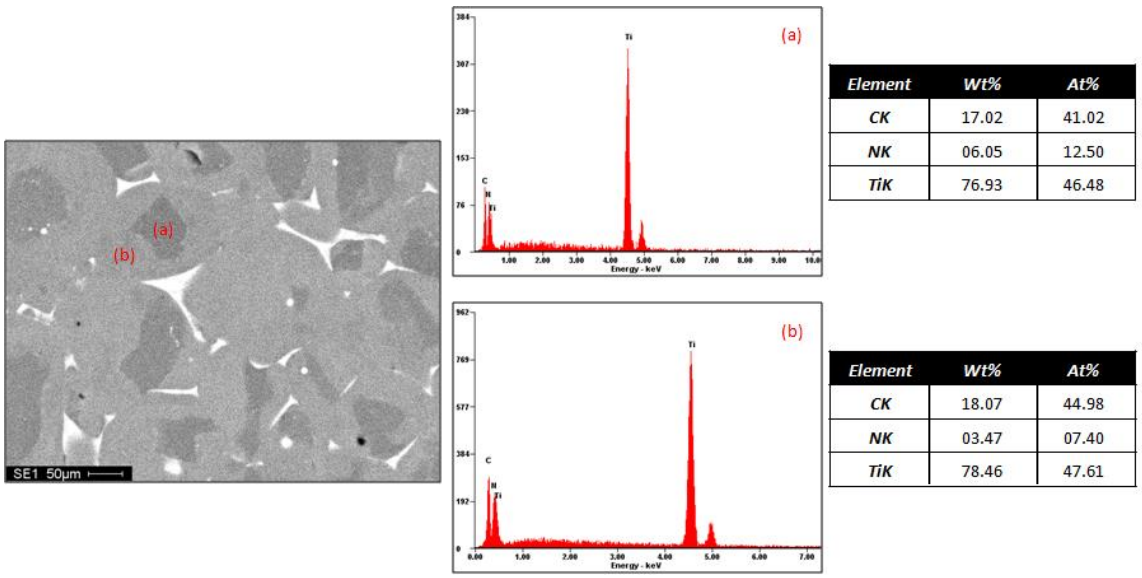


Figure 4-14: SEM (BSE) micrographs of the various cermets sintered by SPS after ball-milling (a) Cermet 1: TiCN-10Ni, (b) Cermet 2: TiCN-Ta-10Ni, (c) Cermet 3: TiCN-5Ni, (d) Cermet 4: TiCN-Ta-5Ni and (e) Cermet 5: TiCN-Ta



Element	Wt%	At%
CK	17.02	41.02
NK	06.05	12.50
TiK	76.93	46.48

Element	Wt%	At%
CK	18.07	44.98
NK	03.47	07.40
TiK	78.46	47.61

Figure 4-15: SEM (SE) image of Cermet 3, with EDS spectra of various mircostructural phases

4.3.2. Mechanically Alloyed Cermets

4.3.2.1. The Ti(C,N)-Ta Mixture

The microstructures of the mechanically alloyed Ti(C,N)-Ta powders are shown in Figure 4-16. Similar to the ball-milled cermets, the microstructure displayed core-rim morphology. The backscattered electron SEM micrographs clearly showed non reacted Ti(C,N) cores, which significantly reduced with increasing mechanical alloying time. EDX analysis shown in Figure 4-17 confirmed that the black core regions comprised only Ti, N and C, while the surrounding contained Ti, Ta, C and N.

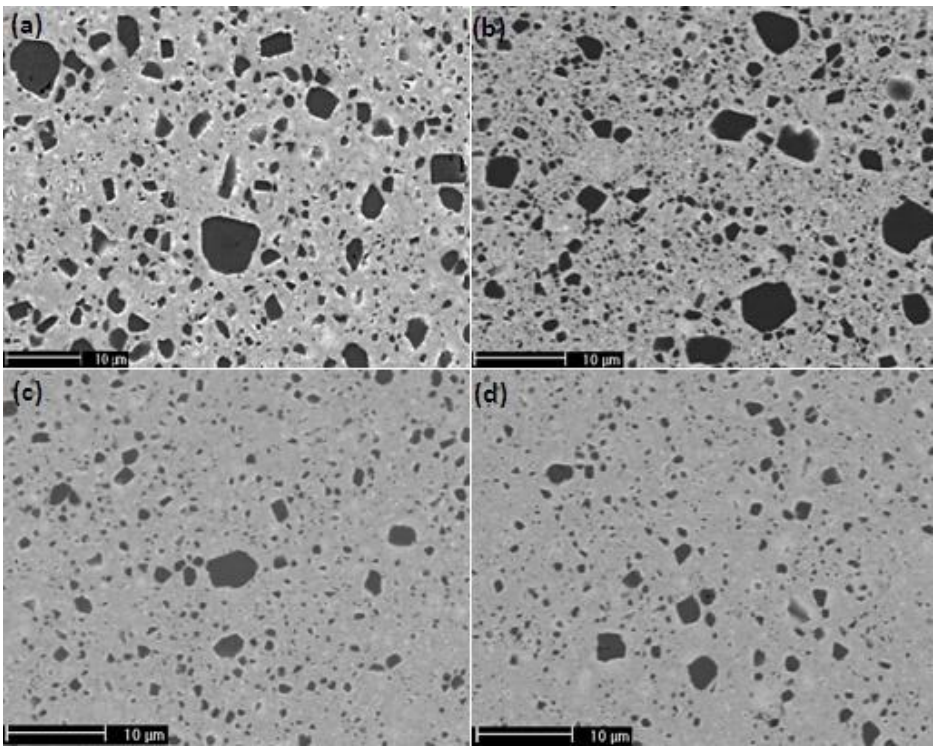


Figure 4-16: SEM (SE) micrographs of the Ti(C,N)-Ta powders sintered at 1500°C after (a) 2 hours MA (b) 4 hours MA (c) 8 hours MA and (d) 12 hours MA

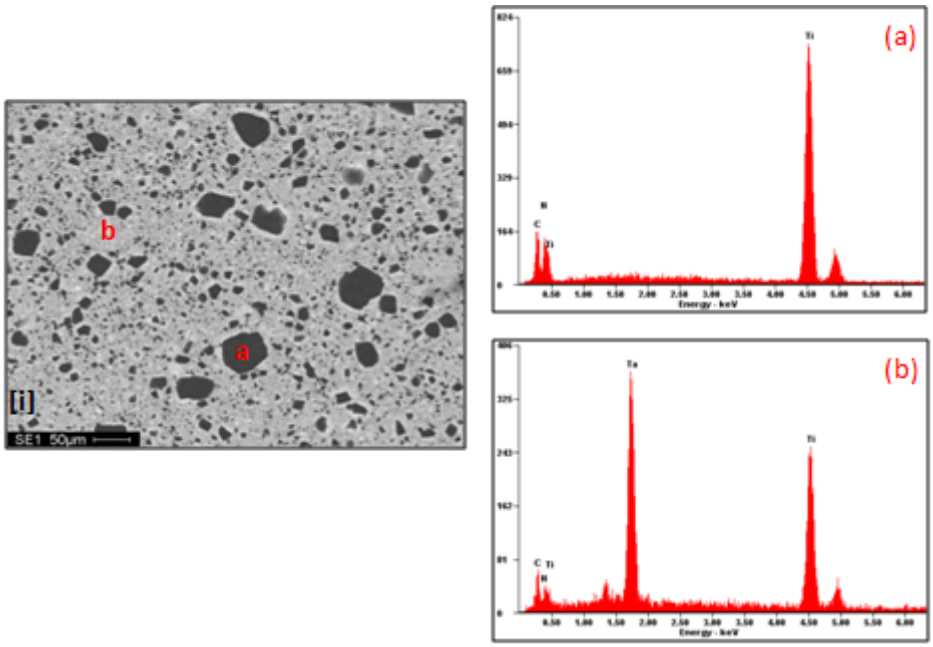


Figure 4-17: SEM (SE) image of Ti(C,N)-Ta cermet prepared by MA, with EDS spectra of various mircostructural phases

4.3.2.2. The Ti(C,N)-TaC Mixture

The SEM micrographs of the mechanically alloyed Ti(C,N)-TaC samples are shown in Figure 4-18. Similar to the mechanically alloyed Ti(C,N)-Ta cermets, the microstructure displayed core-rim morphology. It was evident from the microstructure that the Ti(C,N) phase had not completely reacted during densification. Rather, there are many undissolved Ti(C,N) grains surrounded by solid solution phases consisting of Ta, Ti, C and N. Unlike in the Ti(C,N)-Ta mixture, the size of the Ti(C,N) core did not reduce with prolonged mechanical milling and even after 48 hours, a high amount of large, unreacted Ti(C,N) grains was observed within the microstructure.

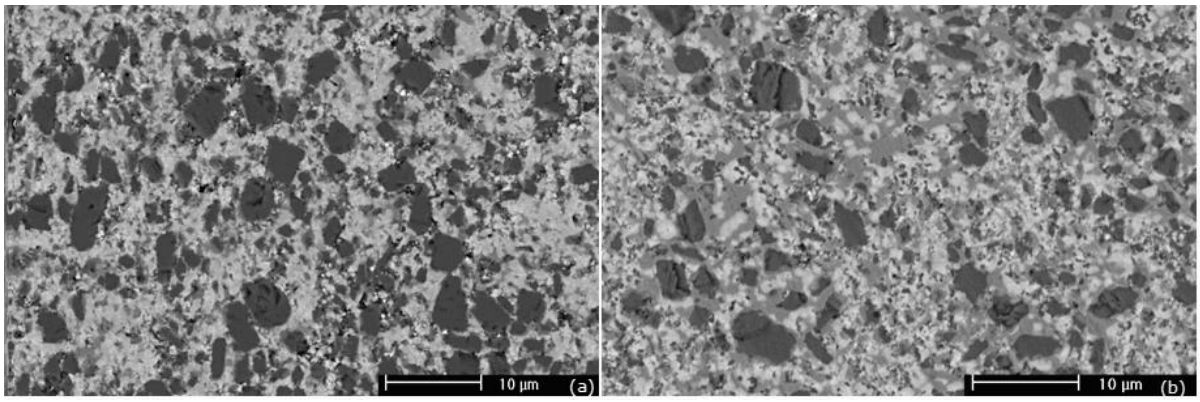


Figure 4-18: SEM (BSE) micrographs of the Ti(C,N)-TaC powders sintered at 1500°C after (a) 24 hours MA and (b) 48 hours MA

4.4. Mechanical Properties

4.4.1. Ball-Milled Cermets

The mechanical properties for the ball-milled cermets are shown in Table 4-11. The effect of binder content, as well as secondary phase additions on the mechanical properties of the Ti(C,N) cermets are illustrated by these results. In general, the mechanical properties increased with decreased binder content and the addition of the secondary tantalum phase. The lowest mechanical properties were obtained for Cermets 1 and 2.

Of the ball-milled cermets, the highest hardness and fracture toughness were found in Cermet 4 containing Ti(C,N), Ta and 5wt% Ni. The hardness and fracture toughness in this material was measured to be 17.8 HV and 6.9 MPa.$m^{1/2}$ respectively.

Table 4-11: Mechanical properties of the various cermets produced after ball-milling

Cermet #	Sample	Hardness (HV_5)	K_{Ic} (MPa.$m^{1/2}$)
Cermet 1	TiCN-10Ni	15.1 ± 0.7	4.3 ± 0.4
Cermet 2	TiCN-Ta-10Ni	15.6 ± 0.2	4.9 ± 0.5
Cermet 3	TiCN-5Ni	16.1 ± 0.3	5.5 ± 0.3
Cermet 4	TiCN-Ta-5Ni	17.8 ± 0.5	6.9 ± 0.5
Cermet 5	TiCN-Ta	17.2 ± 0.6	5.1 ± 0.7

4.4.2. Mechanically Alloyed Cermets

4.4.2.1. The Ti(C,N)-Ta Mixture

Table 4-12 shows the Vickers hardness and fracture toughness of the Ti(C,N)-Ta cermets produced after different times of mechanical alloying. Results showed that both hardness and fracture toughness increased with increasing time of mechanical alloying. After 12 hours mechanical alloying, a significant increase in the mechanical properties of the material was observed. The hardness and fracture toughness was increased to 20 HV_5 and 5.6 $MPa.m^{1/2}$ respectively.

Table 4-12: Mechanical properties of the mechanically alloyed Ti(C,N)-Ta cermets

Cermet #	Sample	Hardness (HV_5)	K_{Ic} ($MPa.m^{1/2}$)
Cermet 6	2h	18.2 ± 0.8	5.0 ± 0.1
Cermet 7	4h	18.7 ± 0.9	5.1 ± 0.1
Cermet 8	8h	19.0 ± 0.8	5.4 ± 0.2
Cermet 9	12h	20.1 ± 0.6	5.6 ± 0.2

4.4.2.2. The Ti(C,N)-TaC Mixture

The Vickers hardness and fracture toughness results for the Ti(C,N)-TaC cermets are given in Table 4-13. The results showed an increase in both hardness and fracture toughness with increasing periods of mechanical alloying. After 48 hours, the hardness and fracture toughness of the cermets increase to 13 HV_5 and 7.4 $MPa.m^{1/2}$ respectively.

Table 4-13: Mechanical properties of the mechanically alloyed Ti(C,N)-TaC cermets

Cermet #	Sample	Hardness (HV_5)	K_{Ic} ($MPa.m^{1/2}$)
Cermet 10	12h	6.5 ± 0.5	4.1 ± 0.4
Cermet 11	24h	8.5 ± 0.9	5.1 ± 0.2
Cermet 12	48h	12.7 ± 0.8	7.4 ± 0.1

Chapter 5: Discussion

5.1. Fundamental Reactions in Mechanical Alloying of Ductile-Brittle and Brittle-Brittle Components

The success of the mechanical alloying process in the production of the (Ti,Ta)(C,N) solid solution relies on the constituents of the starting mixture and optimization of the milling parameters. In this section, the mechanisms of alloying within the ductile-brittle Ti(C,N)-Ta and brittle-brittle Ti(C,N)-TaC systems are discussed and compared.

An early indication to the reaction of Ta/TaC with Ti(C,N) during mechanical alloying was evident by X-Ray diffraction analysis, which provided a convenient and visual representation of the solid state reactions following mechanical alloying. A summary of the results obtained during mechanical alloying of the Ti(C,N)-Ta and Ti(C,N)-TaC mixture is given in Table 5-1.

Table 5-1: Comparison of properties between mechanically alloyed powders and reference materials

Material	Milling time (h)	Ti(C,N) lattice parameter after MA (Å)	TaC lattice parameter after MA (Å)	Crystallite size (nm)	References
Ti(C,N)-Ta	**0**	4.296 ± 0.002	-	54	-
	2	4.299 ± 0.002	-	22	-
	4	4.301 ± 0.003	-	20	-
	8	4.296 ± 0.003	-	13	-
	12	4.292 ± 0.003	-	10	-
Ti(C,N)-TaC	**0**	4.296 ± 0.002	4.453 ± 0.002	54	-
	12	4.295 ± 0.002	4.452 ± 0.002	60	-
	24	4.298 ± 0.003	4.451 ± 0.003	35	-
	48	4.299 ± 0.003	4.450 ± 0.003	33	-
$TiC_{0.7}N_{0.3}$		4.296 ± 0.001	-	-	-
TiC		4.322 ± 0.001	-	-	[**28**]
TiN		4.242 ± 0.001	-	-	[**28**]
TaC		-	4.455 ± 0.001	-	[**90**]
TaN		4.358 ± 0.001	-	-	[**91**]

Considering at first the Ti(C,N)-Ta mixture, as compared to the starting powder mixture X-Ray diffraction analysis (Figure 4-3) showed the progressive disappearance of the Ta phase with increasing mechanical alloying time. After 8 hours of mechanical alloying, the Ta phase had completely merged with neighbouring Ti(C,N) peaks. The disappearance of the tantalum peaks may be attributed to amorphization of the tantalum phase, the destruction of the crystal lattice and/or the solid state diffusion and dissolution of titanium, carbon and nitrogen atoms into the Ta crystal structure.

Compared to the Ti(C,N)-TaC mixture, the XRD data (Figure 4-7) following mechanical alloying showed no distinguishable shift in peak position of the TaC phase with increasing mechanical alloying. After 48 hours mechanical alloying, the TaC phase persisted and still remained well defined. This result is not consistent with those obtained by Zhang *et al*. [**74**] during their investigations to prepare a solid solution of Ti(C,N)-WC-TaC by mechanical alloying. By X-Ray diffraction analysis, the authors showed the complete disappearance of the TaC phase after 88 hours mechanical alloying. Considering that for the current investigations, mechanical alloying was only performed up to 48 hours, it would not be expected that the TaC phase would be completely reacted by the mechanical alloying process. However, even after 49 hours mechanical alloying, Zhang *et al*. [**74**] showed significantly reduced peak intensities and observable shifts in the peak positions of the TaC phase, which was not observed for the current data.

The results obtained by Zhang *et al.* [**74**] may be attributed to the higher ball-to-powder charge weight ratio used (20:1 compared to 10:1 used in our experiments) and/or the lower weight percentage of TaC (10wt% compared to 40wt% used in the current experiments). Consequently, a higher milling intensity and the considerably smaller weight composition of the TaC phase would explain the effects described by the authors [**74**]. In addition, the changes observed from their XRD analysis could also have been due to the formation of oxide phases resulting from the increased reactivity of the material with oxygen, due to the increased surface area of the milled powders.

The changes in the Ti(C,N) phase showed similar trends for both powder mixtures. Broadening of the Ti(C,N) phase peaks with increased mechanical alloying time indicates a decrease in the coherent crystalline domain and the accumulation of lattice strain. This is consistent with crystallite size and lattice strain calculations performed after the different periods of mechanical alloying for the Ti(C,N)-Ta and Ti(C,N)-TaC mixtures, as shown in Figure 5-1.

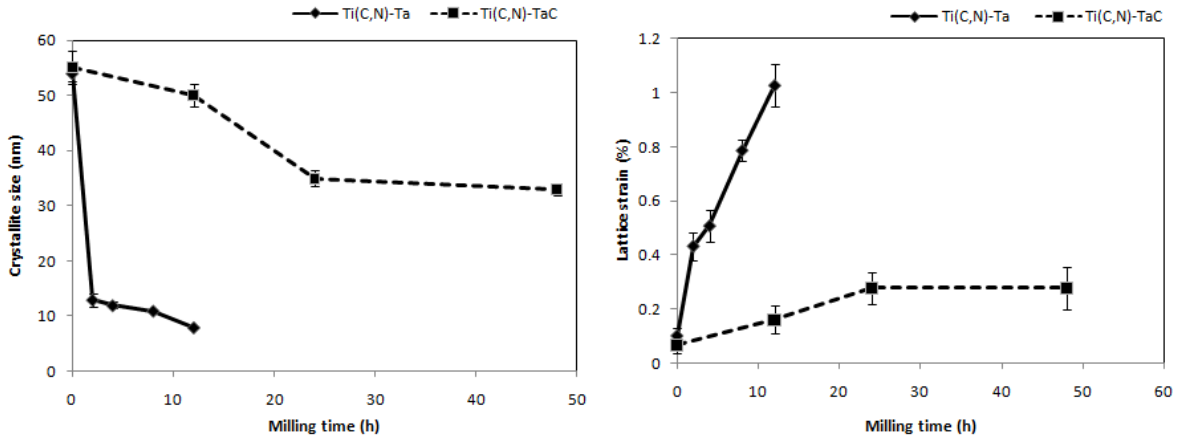


Figure 5-1: Ti(C,N) crystallite size refinement and lattice strain evolution with mechanical alloying of the Ti(C,N)-Ta and Ti(C,N)-TaC mixtures

Accordingly, the data showed that for the Ti(C,N)-Ta mixture, the Ta phase was completely transformed by the mechanical alloying process, whereas the Ti(C,N) phase was only slightly changed, showing only peak broadening. This revealed that a high density of dislocations and defects were introduced into the Ti(C,N) phase as a result of the milling but no significant diffusion of Ta into Ti(C,N) took place. This is in agreement with both the SEM micrographs of the powder and the fact that no change in the Ti(C,N) lattice parameter was observed after milling. However, in the tantalum phase the diffusion of C, N and Ti has probably taken place. This is the direct consequence of the tantalum material being more plastically deformable during milling, whereas plastic deformation of Ti(C,N) is more limited. Consequently, synthesis of the (Ta,Ti)(C,N) phase by mechanical milling included two stages. At first, the ductile tantalum metal powder particles were flattened and welded, and formed lamellar structures by the ball-powder-ball collisions, while the brittle Ti(C,N) particles were fragmented and dispersed into the ductile matrix. As the milling was prolonged, the lamellae was further refined and brittle particles were uniformly dispersed. The increase in

energy stored in the powders by mechanical alloying activated the surface reaction of Ti(C,N) with Ta, allowing formation of a tantalum rich (Ta,Ti)(C,N) solid solution.

Different observations were made for the Ti(C,N)-TaC mixture. The data showed only peak broadening for both the Ti(C,N) and TaC phases after mechanical alloying, thereby indicating the introduction of defects into the material as a result of the mechanical milling process. SEM analysis showed no significant change in the constitution of the powder, except that the individual phases were refined compared to the starting mixtures. In addition, no apparent change in the lattice parameter of the Ti(C,N) and TaC phases were observed after milling, suggesting no dissolution of either the titanium or tantalum atoms into the respective crystal lattices occurred during mechanical milling. Owing to the brittleness of the Ti(C,N) and TaC powders and the low diffusion coefficients in the carbide lattices, the mechanical milling process served only to refine the grain size of the Ti(C,N) and TaC phases, while both phases remained unreacted after 48 hours milling.

The complete dissolution of Ta and TaC into the Ti(C,N) phase took place only during sintering, thereby resulting in a greater increase in the lattice parameter following densification. This result is discussed in Section 5.2.2, where the reactions during sintering are discussed in detail.

5.2. Effect of Composition and Processing on Cermet Sinterability

The microstructure and consequently the resultant physical properties of a cermet material depend strongly on the interactions between the constituent powders during sintering, for both solid state and liquid phase sintering processes. In cermet manufacturing, liquid phase sintering is a necessary processing step, allowing diffusion processes to be accelerated due to the dissolution of the hard phase into the metal binder. Sintering in the solid state occurs also by diffusion, but the rate of mass transport depends on the diffusivity of the constituent materials.

In this section, the fundamental processes occurring during the liquid phase sintering of Ti(C,N)-(Ta)-Ni mixtures are discussed. Furthermore, the influence of mechanical milling on the sinterability of cermet materials are compared with conventional ball-milled cermets, and discussed.

5.2.1. Ni-Binder containing Materials

The densification behaviour for the ball-milled Cermets 3-5 was considerably different (Figure 5-2), and was influenced strongly by the composition of the starting powder mixture.

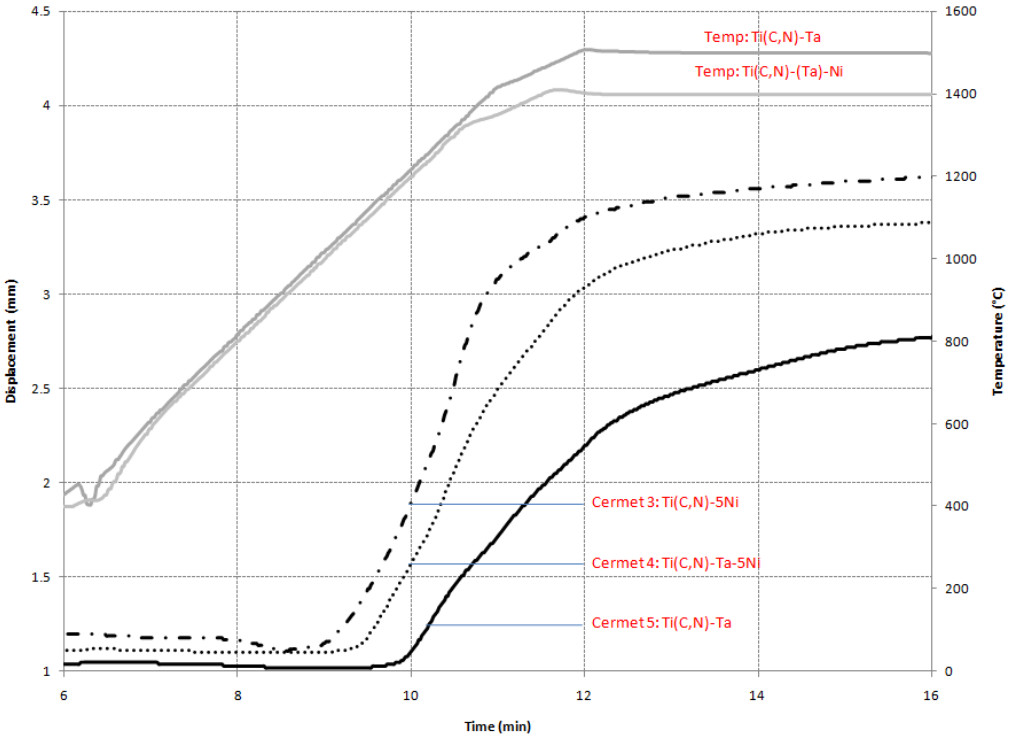


Figure 5-2: Densification curves for Cermet 3, Cermet 4 and Cermet 5

In Cermets 3 and 4, both solid-state and liquid phase sintering processes occur due to the presence of Ni metal in the starting powder mixture. For Cermet 3, which contains Ti(C,N) and Ni as the constituents of the starting powder mixture, densification began at 900°C, after which there was a steep rise in the rate of densification until approximately 1300°C. Above 1300°C (which corresponds to the Ni-C eutectic [**92**]) the liquid phase was formed, at which time the carbide phase dissolved into the liquid binder and the diffusion of atomic species was accelerated through the liquid medium. Upon cooling, the carbide precipitated out onto the undissolved TiN particles and core-rim microstructures are observed (Figure 4-14).

The evolution of the core-rim structure in Ti(C,N)-based cermets was due to dissolution and precipitation reactions occurring during sintering as a result of the different degrees of solubility between the TiN and TiC phases in the binder melt. Ettmayer [**1**] explains that for a nitrogen pressure of 10 mbar at 1773°C, the Ti(C,N) carbonitride is in equilibrium with a nickel melt that contains approximately 8 at.% Ti and 13.3 at.% C, but only 0.002 at.% N. Under the same conditions, TiN is in equilibrium with a nickel melt containing approximately 10 at.% Ti and nearly no nitrogen. Consequently, between these extreme compositional ranges (under identical conditions), Ti(C,N) is in equilibrium with a nickel melt that contains relatively more TiC in liquid solution than TiN.

From the data, it followed that during liquid phase sintering of Ti(C,N)-Ni cermets there would be preferential solubility of TiC in the liquid phase, and the undissolved TiN residues would remain and serve as nuclei for precipitation of the dissolved carbides upon solidification of the liquid phase.

This correlates with the EDX analysis of Cermet 3 shown in Figure 4-15. The data confirmed that although both the core and rim were composed of Ti, C and N elements, the core was slightly more concentrated with nitrogen compared to the rim, whereas the rim had a slightly higher carbon composition. Hence, during sintering, Ti(C,N) reacted with the Ni melt such that TiC was dissolved in the metal binder, leaving a carbon-poor Ti(C,N). The nitrogen rich Ti(C,N) particles remained and served as nucleation sites for the precipitation of the dissolved carbides by Oswald ripening and upon solidification of the liquid phase. This process then gave rise to the core-rim morphology, in which the cores were richer in nitrogen and the rim carbon.

Like Cermet 3, during the sintering of Cermet 4, both solid state and liquid phase sintering processes occur as described above. However, the difference in densification behaviour observed in Figure 5-2was due to the addition of tantalum metal to the starting powder mixture of Cermet 4. As a result, densification started later in Cermet 4 (1100°C compared to 900°C in Cermet 3), and the reactions occurring between the tantalum and nickel phase during initial solid state processes subsequently resulted in the formation of intermediate phases. This follows from the Ni-Ta phase diagram (Figure 5-3 [**92**]) which suggests that for Cermet 4, having a mole ratio of $\frac{\text{Ta}}{\text{Ni+Ta}} \approx 0.7$, at 1400°C, the reaction between the tantalum and nickel phase would result in the formation of Ta_2Ni. Thus, the addition of Ta to Cermet 4 reduced the densification/shrinkage because only an intermediate, or possibly even no melt, was produced in Cermet 4. This may then also explain the poor wetting behaviour (Figure 4-14) observed in the microstructure of Cermet 4 as opposed to Cermet 3. Only with the dissolution of Ta into the Ti(C,N) complex did the residual metallic components become increasingly Ni rich, which at the end of the sintering period may form a liquid phase.

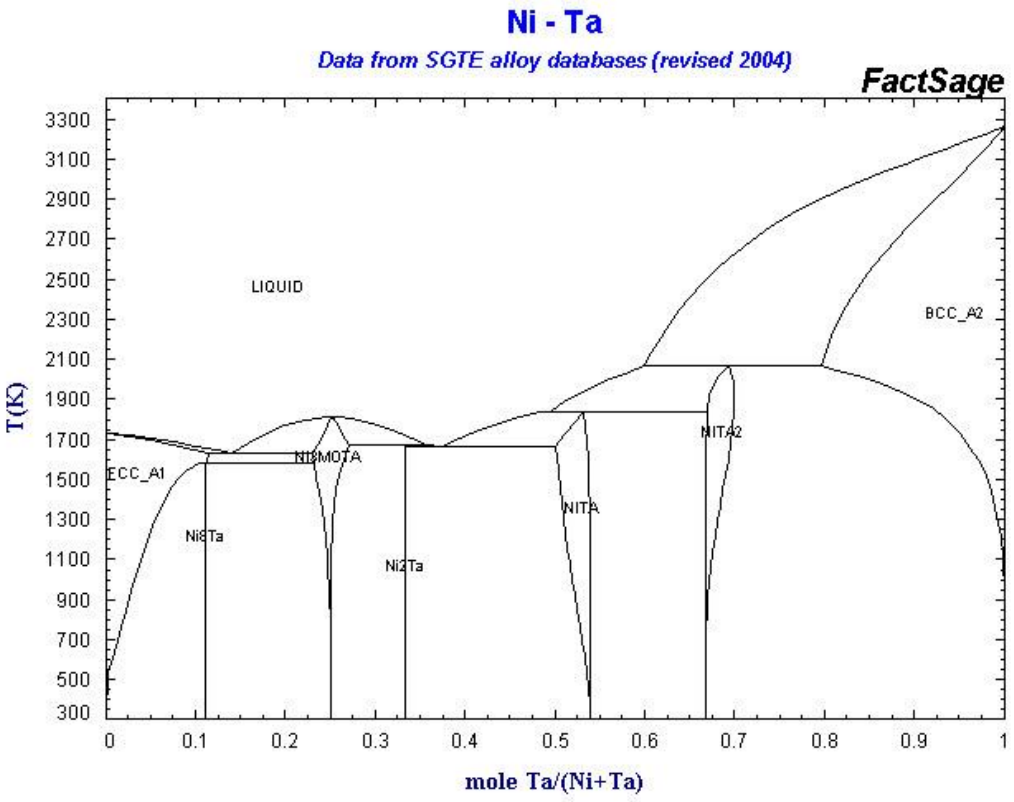


Figure 5-3: Binary Ni-Ta phase diagram [92**]**

Densification in Cermet 5 (Ti(C,N)-Ta) occurred only by solid-state sintering processes, due to the absence of the Ni binder phase. Consequently, densification was reduced in this cermet compared to Cermets 3 and 4, as the densification curve shows considerably lower shrinkage due to the absence of the liquid phase. Densification occurred much later in this sample, at approximately 1200°C, most of which occurred during the isothermal sintering temperature i.e. approximately 40%, opposed to the 15% and 25% densification occurring during the isothermal sintering temperature of Cermets 3 and 4 respectively.

A more detailed analysis of the densification behaviour of Cermet 5 is given in its comparison to the mechanically alloyed cermets in the next section.

5.2.2. Binder-free Materials

A summary of the results obtained for the cermets prepared from mechanically alloyed powders is given in Table 5-2. For comparison, Cermet 5 of the ball-milled samples will be used. In the sections to follow, this sample will hereafter be referred to as 'BM'.

Table 5-2: Summary of results for the mechanically alloyed cermets sintered at 1500°C

Sample Composition	Densification		Phase Composition after Sintering	(Ta,Ti)(C,N) Lattice Parameter (Å)
	g/cm^3	%Theoretical		
Cermet 5 TiCN-Ta BM	6.88 ± 0.22	99.6	(Ta,Ti)(C,N) Ta	4.316 ± 0.001
Cermet 6 TiCN-Ta 2h MA	6.89 ± 0.03	99.7	Ti(C,N) (Ta,Ti)(C,N) Fe	4.328 ± 0.001
Cermet 7 TiCN-Ta 4h MA	6.92 ± 0.01	100	Ti(C,N) (Ta,Ti)(C,N) Fe	4.335 ± 0.004
Cermet 8 TiCN-Ta 8h MA	6.90 ± 0.01	99.9	Ti(C,N) (Ta,Ti)(C,N) Fe	4.334 ± 0.003
Cermet 9 TiCN-Ta 12h MA	6.92 ± 0.01	100	Ti(C,N) (Ta,Ti)(C,N) Fe	4.335 ± 0.001
Cermet 10 TiCN-TaC 12h MA	5.25 ± 0.03	77.3	Ti(C,N) (Ta,Ti)(C,N) Fe	4.310 ± 0.001
Cermet 11 TiCN-TaC 24h MA	5.70 ± 0.02	84.4	Ti(C,N) (Ta,Ti)(C,N) Fe	4.350 ± 0.002
Cermet 12 TiCN-TaC 48h MA	6.72 ± 0.07	99.0	Ti(C,N) (Ta,Ti)(C,N) Fe	4.345 ± 0.002

Although full densification was achieved for the mechanically alloyed Ti(C,N)-Ta powders, Figure 5-4 illustrated significantly different sintering behaviour between the samples. For the 2 hour mechanically alloyed powders, densification started at approximately 900°C. Thereafter, there was a steep rise in densification, which was almost completed before entering the isothermal sintering period. For powders mechanically alloyed longer than 2 hours, there were only slight changes observable in densification behaviour between the 4, 8 and 12 hour samples. For these samples, densification occurred at temperatures slightly higher than 1000°C and the rate of densification was much slower as compared to the 2 hour mechanically alloyed sample. Similar to the 2 hour mechanically alloyed sample, densification was near completion upon reaching the isothermal sintering temperature.

Huang *et al*. [**93**] explained that during the mechanical alloying process, a large number of dislocations and defects are introduced into the material by strong collisions between the balls and powders, which lead to the formation of nano-crystalline particles and large lattice distortion. This large amount of distortion and nano-grain boundaries increase free energy, the atomic cavity and the number of atoms distributed on the nano-grain boundary. Huang *et al*. [**93**] explained that all these effects shorten the diffusion distances between atoms, subsequently improving the sintering process substantially. The authors were able to substantiate this theory by showing enhanced consolidation and reduced sintering temperatures for their nano-crystalline powders produced by mechanical alloying.

These results also correlated with reports by Borrell *et al*. [**94**] who performed spark plasma sintering investigations on TiC_xN_{1-x} powders after mechanical alloying. In their study, the authors found that full densification (99.8%) was obtained at temperatures as low as 1300°C. They attributed the high sinterability of the powders to the refined microstructure and the great amount of induced defects produced during the mechanical milling process. In addition, the improved sinterability could also be attributed to increasing oxygen content, as a result of the mechanical milling process.

By the mechanical alloying of the Ti(C,N)-Ta system in the current study, chemical analysis showed an increase in oxygen content to 1.86 ± 0.07 wt% after 12 hours mechanical alloying. However, the physical properties achieved through solid state sintering of these mechanically alloyed powders suggested that the 1.86 wt% oxygen picked up during milling did not have an adverse effect on the sintering behaviour of the samples. It is commonly

known that the oxide film on the surface of particles significantly influences the densification during the sintering stage [**95**], leading to undesired microstructures and consequently inferior mechanical properties. No oxide phases were present from XRD and SEM analysis following densification, suggesting that the oxygen content in the milled powder was low enough to allow for complete deoxidation during solid state sintering or complete dissolution in the (Ti,Ta)(C,N) lattice. By the former, the oxide film on the milled particle surface was transformed to CO through the reaction between the carbon in the carbide phase and the chemsorbed oxygen on the particle surface, thereby making the surface clean, resulting in the modification of wettability between the particles and subsequently facilitating densification. Alternatively, the oxygen could have been introduced into the lattice of the mixed carbide and produced (Ti,Ta)(C,N,O).

The sintering behaviour of the (Ti,Ta)(C,N) cermet produced without mechanical alloying was significantly different from that of the mechanically alloyed powders (curve 'BM' in Figure 5-4). In this sample, densification started much later (at 1200°C) and required a longer time for completion in comparison to the mechanically alloyed powders. Approximately 40% of the densification occurred during the isothermal sintering period, as opposed to the approximately 5% densification occurring during isothermal sintering of the mechanically alloyed powders.

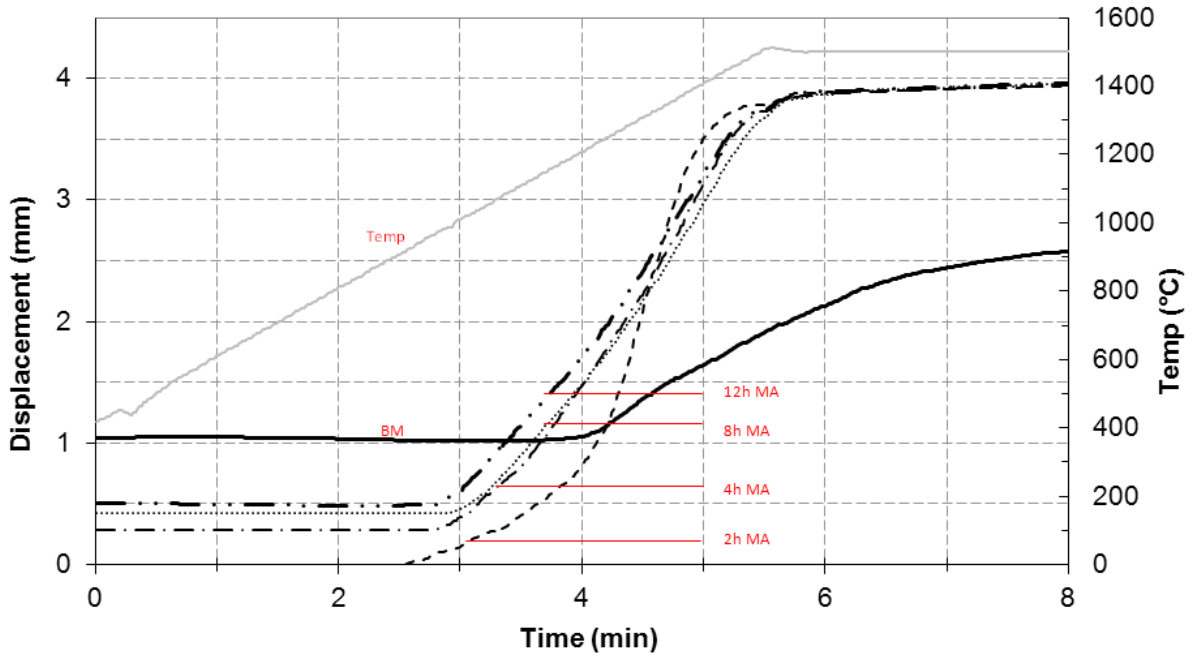


Figure 5-4: Densification curve for the Ti(C,N)-Ta powders sintered after ball-milling and various times of MA

The differences in densification behaviour between the mechanically alloyed powders correspond to the change in phase composition of the starting mixtures. The 2 hour milled powder still showed the presence of the Ta phase by XRD, but with a remarkable shift to lower 2θ angles, thereby indicating that C, N, and most probably Ti, had dissolved into the metallic phase. For samples mechanically alloyed at 4-12 hours, Ta had nearly completely reacted with the Ti(C,N) phase. Consequently, these samples now displayed more ceramic behaviour, thus only limited plastic deformation of the Ta phase during the beginning of sintering occurred. The chemical reaction between the Ta and Ti(C,N) phases had strongly advanced in these powders due to the mechanical alloying process and, as a result, there was reduced reactivity during sintering in comparison to the 2 hour mechanically alloyed powder.

Comparing to the ball milled material, sinterability of the mechanically alloyed powders had greatly improved, despite the lower green density. The ball milled material showed the existence of two phases prior to densification, without remarkable peak broadening or peak shift. This indicated low activation of the powder and accounts for the densification behaviour observed (Figure 5-4).

These findings are further substantiated by the change in the Ti(C,N) lattice parameter after densification in comparison to the starting powders Figure 5-5.

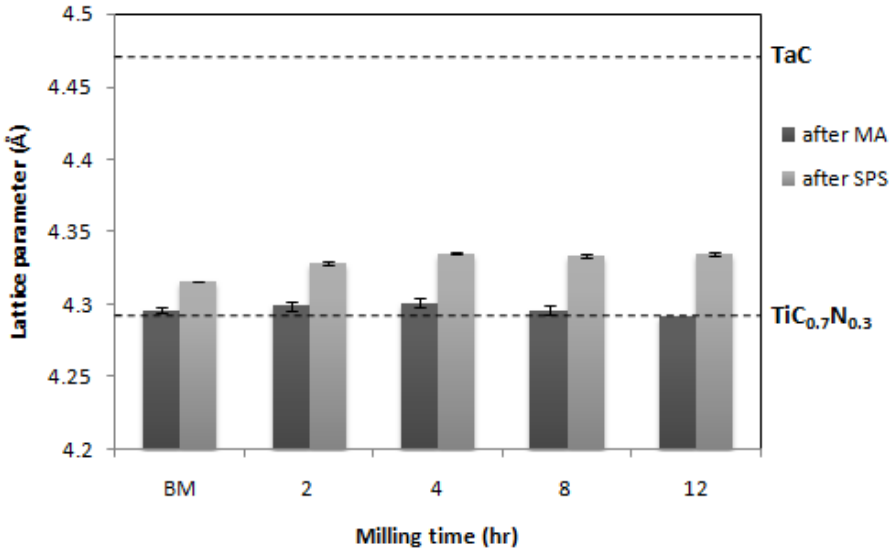


Figure 5-5: Ti(C,N) lattice parameter changes of the BM and Ti(C,N)-Ta mixtures following MA and SPS, including the lattice parameters of the Ti(C,N) and TaC reference materials [28**]- [**90**]**

In Figure 5-5, the lattice parameters for the $TiC_{0.7}N_{0.3}$ and TaC phases are also given. There was significant increase in the lattice parameter of the cubic carbide for both the ball milled and mechanically alloyed samples following densification in comparison to the starting powder. After densification, there was an overall increase to approximately 4.335Å ± 0.003. Following from the results obtained from the densification curves, the difference in lattice parameters between the ball-milled and mechanically alloyed samples was the result of the different degrees of reaction within these samples. XRD analysis of the mechanically alloyed samples (Figure 4-11) showed complete disappearance of the Ta phase after densification. As a result, the introduction of Ta into the Ti(C,N) crystal structure increased its lattice parameter and the resultant (Ti,Ta)(C,N) solid solution exhibited a lattice parameter that was closer to that of the TaC phase (4.45Å [**90**]). Although the addition of 40wt% Ta considerably increased the lattice parameter by the formation of $Ti_{1-x}Ta_x(C,N)_y$, by the same rate as x increased, y decreased and the metal/(C,N) ratio was changed. Theoretically, the stoichiometry for this mixture would be $(Ti_{0.82}Ta_{0.18})(C_{0.57}N_{0.25})$, showing that the anion concentration was diluted (C+N <1) due to the Ta metal addition. Consequently, the lattice parameter of the cubic carbide increased due to the Ta addition, but decreased due to the decrease in the anion concentration (Figure 5-5).

The ball milled sample exhibited the lowest increase in the cubic carbide lattice parameter, which also follows from the degree of reactivity exhibited by this material. From the SEM micrographs (Figure 5-7), a large amount of unreacted pure Ta was still present within the cermet following densification, thereby implying that the reaction between the Ti(C,N) and Ta phases was not carried out to completion. This then accounts for the small increase in the Ti(C,N) lattice parameter.

Following from this, the results obtained for the Ti(C,N)-TaC mixture could also be explained. Considering that tantalum was added as a carbide in this mixture, theoretically it would be expected that the complete reaction between the Ti(C,N) and TaC phase following densification would result in a substantial increase of the Ti(C,N) lattice parameter, to a value that tended to be closer to that of the TaC phase. This follows from the above, where the addition of 40wt% TaC would lead to the formation of the $Ti_{1-x}Ta_x(C,N)_y$ solid-solution, except for this mixture, as x increased, y would remain constant, as the carbide addition would serve to replenish the C, N anion ratio of the Ti(C,N) complex. This is substantiated by considering the stoichiometry of the final solid solution product as $(Ti_{0.83}Ta_{0.17})(C_{0.75}N_{0.25})$,

which showed that the molar ratio of the anion remained constant at 1, when TaC was added to the mixture. Using the law of linearity, the theoretical lattice constant for a (Ti,Ta)(C,N) solid solution phase produced from a 60:40 wt% ratio of Ti($C_{0.7}$ $N_{0.3}$) and TaC should then be: (4.296)(0.6) + (4.455)(0.4) = 4.360Å.

Figure 5-6compares the lattice parameter changes following densification, due to the Ta and TaC additions to the Ti(C,N)-Ta and Ti(C,N)-TaC mixtures respectively. Also given are the initial Ti(C,N) lattice parameter and the theoretical lattice parameter for the ($Ti_{0.83}Ta_{0.17}$)($C_{0.75}N_{0.25}$) solid solution (i.e. 4.360Å) for reference. The data showed that after 12 hours mechanical alloying in both mixtures, the lattice parameter change for the metal addition was significantly greater than for the carbide addition. Again, this follows from the different degrees of reactivity of the constituents during densification. As mentioned, for the Ti(C,N)-Ta mixture, XRD analysis showed the complete reaction of the Ta phase with Ti(C,N), whereas for the Ti(C,N)-TaC mixture, the presence of two individual phases was still distinguishable following densification. This suggests a lower reactivity between the Ti(C,N) and TaC phases, consequently the change in the Ti(C,N) lattice parameter was small. With increased mechanical alloying, the lattice parameter change became more substantial, so that for the 48 hour mechanically alloyed powders, the lattice parameter increased to 4.345Å, closer to the theoretically determined value (4.360Å) compared to the Ti(C,N)-Ta mixture (4.335Å). This sample however, still showed the presence of the TaC phase by XRD and SEM (Figure 5-7) analysis. This suggests that only partial reaction between the Ti(C,N) and TaC phases was achieved during densification. Consequently, the formation of the ($Ti_{0.83}Ta_{0.17}$)($C_{0.75}N_{0.25}$) solid solution was incomplete and thus the lattice parameter for the Ti(C,N)-TaC mixture did not correspond to the theoretically determined lattice constant (4.360Å).

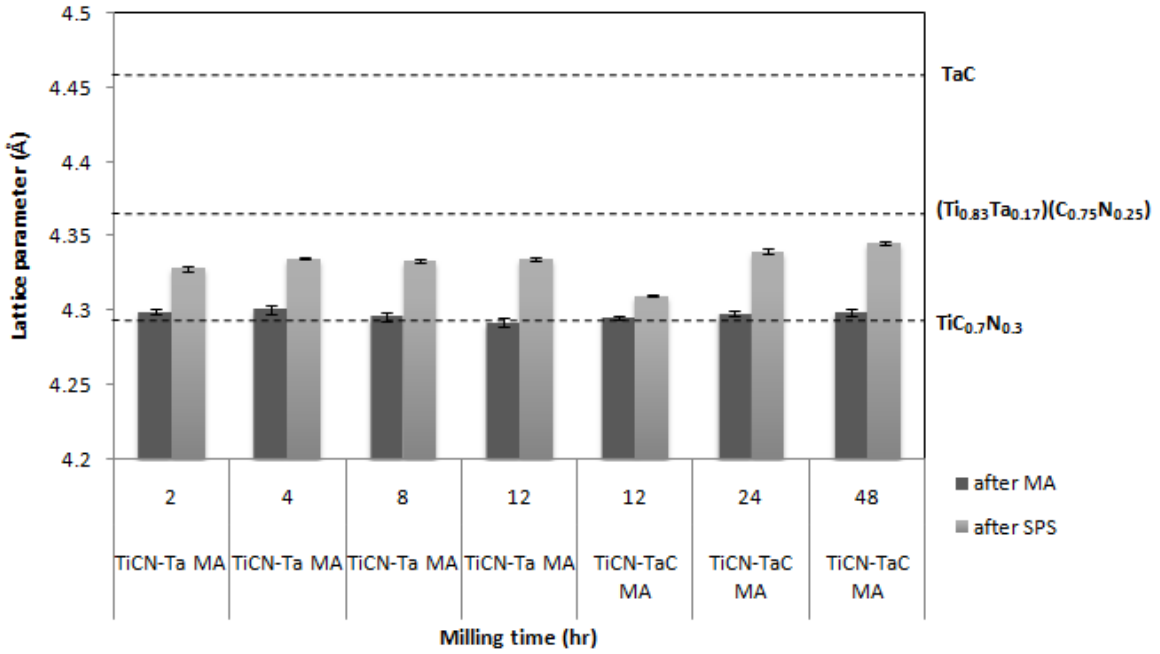


Figure 5-6: Ti(C,N) lattice parameter changes for the Ti(C,N)-Ta and Ti(C,N)-TaC mixtures following MA and SPS

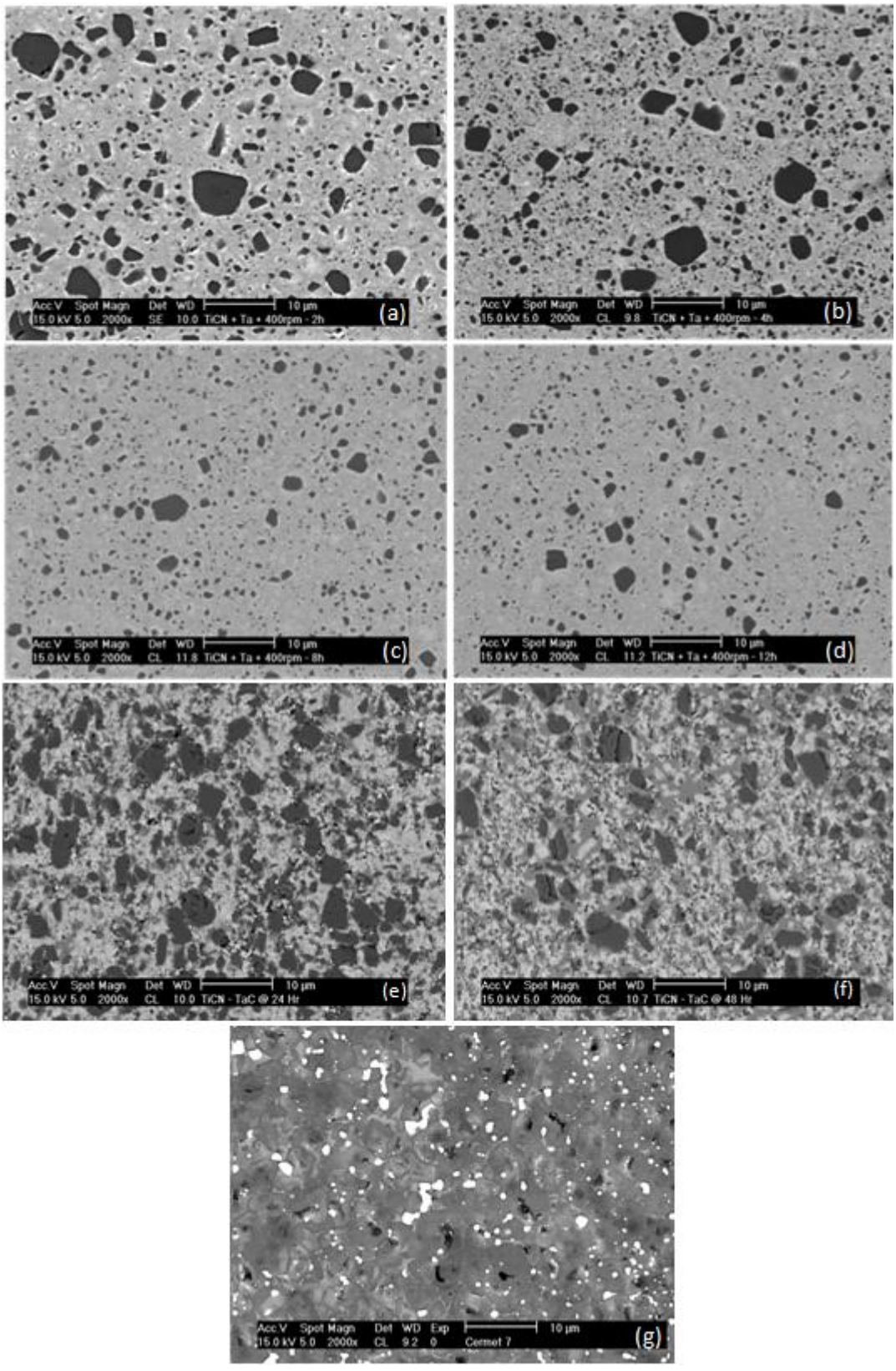


Figure 5-7: Microstructures of binder-free Ti(C,N)-based cermets (a) Ti(C,N)-Ta MA 2Hr, (b) Ti(C,N)-Ta MA 4Hr, (c) Ti(C,N)-Ta MA 8Hr, (d) Ti(C,N)-Ta MA 12Hr, (e) Ti(C,N)-TaC MA 24Hr, (f) Ti(C,N)-TaC MA 48Hr and (g) Ti(C,N)-Ta BM

5.3. Effect of Composition and Processing on the Microstructural and Mechanical Properties of Ti(C,N)-based Cermets

The mechanical properties of cermets depend not only on their starting compositions but also on their microstructural features such as grain size, grain size distribution, phase volume fractions, morphology etc., which evolve during sintering [**96**]. In this section, the microstructures of ball-milled and mechanically alloyed cermets are compared, and the influence of their microstructural features on the resultant mechanical properties is discussed.

5.3.1. Ni-Binder containing Materials

The mechanical properties of the Ni-bonded Ti(C,N)-based cermets are influenced by the amount of nickel binder in the starting composition, as well as secondary phase additions. This, coupled with the processing parameters and resultant microstructural features, would account for the hardness and fracture toughness results shown in Figure 5-8.

The results showed that the lowest hardness and fracture toughness were found in Cermets 1 and 2, whereas the highest properties were found in Cermet 4. These results can be readily understood by considering the composition of the cermets as well as their processing parameters. Both Cermets 1 and 2 contained the highest amount of Ni (10wt% as compared to 5wt% in Cermets 3 and 4) and were sintered at higher temperatures (1500°C compared to 1400°C in Cermets 3 and 4).

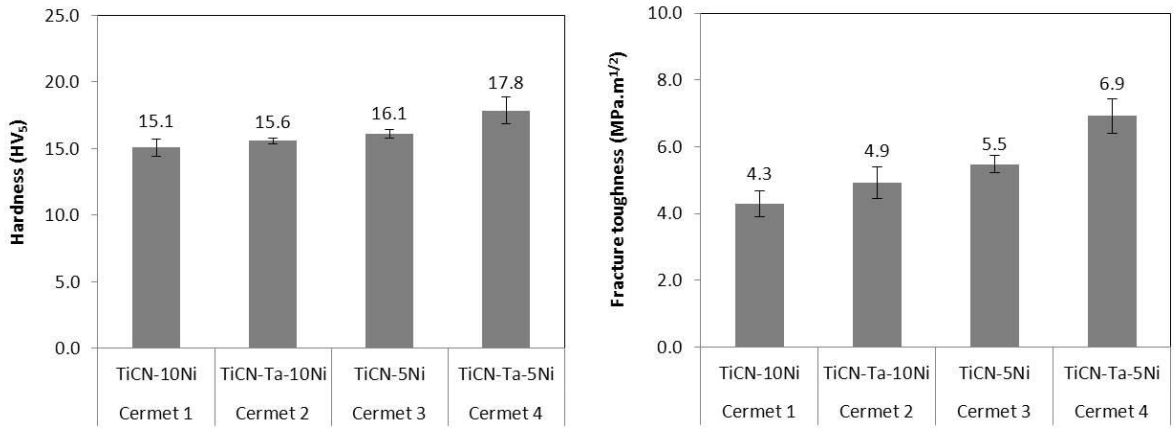


Figure 5-8: Mechanical properties of the Ni-binder containing Ti(C,N)-based cermets

Initially, the poor hardness and fracture toughness obtained for Cermets 1 and 2 were attributed to the low degree of densification as compared to Cermets 3 and 4. However, upon further investigation, it was found that the higher porosity values calculated for Cermets 1 and 2 were not observed from the SEM micrographs (Figure 4-14). Consequently, the low densification values obtained for Cermets 1 and 2 cannot be substantiated by porosity. The lack of correlation between density and porosity can be explained by taking into account the effect of liquid exudation. Alvarez and Sanchez [**97**] explain exudation as the phenomenon occurring during liquid phase sintering, where the liquid generated during sintering is squeezed out of compacts through the clearance between the graphite punches and die. This has been observed in other Ti(C,N) cermets processed by SPS [**98**]. As a result of liquid exudation, the theoretical density decreased and the densities of Cermet 1 and 2 were in reality higher than those values calculated for these materials.

Thus, the mechanical properties obtained for Cermets 1 and 2 were subsequently attributed primarily to the higher sintering temperature used for the densification of these materials. The higher sintering temperature contributed to the poor mechanical properties by influencing their microstructural characteristics. The large grain and rim sizes observed in the microstructures of Cermets 1 and 2 (compared to Cermets 3 and 4) may be attributed to the Ostwald ripening effect being dominant during sintering at high temperatures. During sintering, a well-known phenomenon accompanying the dissolution-precipitation process is the progressive growth of larger grains at the expense of smaller ones [**99**]. This phenomenon is commonly referred to as Ostwald ripening and occurs because the solubility of a grain varies inversely to its size. Thus, smaller grains tend to dissolve more readily and hence the liquid surrounding them is richer in solute concentration than the liquid surrounding larger grains. This difference in solute concentration gives rise to a driving force for mass transport of solutes from small grains to larger ones via diffusion through the liquid binder phase. As a result, larger grains grow at the expense of smaller ones and the mean grain size increases [**100**], [**101**].

For Cermets 1-4, grain growth was promoted due to the existence of the metallic melt. In addition, for Cermets 1 and 2, the grain growth mechanisms were further accelerated due to the higher sintering temperature employed for these samples. Consequently, with increasing sintering temperature, Ostwald ripening became more and more influential and dominated rim growth at sufficiently high temperatures. By the microstructures observed

for cermets 1 and 2, it is understood that Ostwald ripening processes dominated rim growth during sintering of these materials at 1500°C, which inevitably served to coarsen their microstructures thereby leading to their inferior mechanical properties as compared to Cermets 3 and 4.

Excessive rim growth via Ostwald ripening could be avoided by using a temperature regime where rim growth via solute-precipitation prevails (i.e. by keeping the sintering temperature to not more than 1480°C). Another advantage of keeping the sintering temperature low is the avoidance of the denitrification processes, which become significant when sintering nitrogen-containing cermets at sufficiently high temperatures (i.e. ≥ 1500°C) and is dependant of the sintering atmosphere [**102**]-[**103**]. Denitrification occurred in Cermets 1 and 3, which only contained Ti(C,N) and Ni. This was substantiated by the slight change in the Ti(C,N) lattice parameter following densification and earlier evidence that denitrification occurs during the reaction between the Ti(C,N) phase and the binding metal [**89**]. When Ti(C,N)-based cermets were produced by SPS at temperatures above 1350°C, Feng *et al*. [**104**] also observed an increase in the Ti(C,N) lattice parameter. After taking into account the metallurgical reactions during sintering, the elemental distribution in the various phases, crystal structure and the orientational relationships between the inner and outer rims, these authors finally concluded that the expansion of the lattice at temperatures ranging from 1350°C to 1430°C was attributed to the removal of nitrogen from Ti(C,N). Park *et al*. [**105**] demonstrated that the growth rate of Ti(C,N) is slower than that of TiC, due to the fact that nitrogen further stabilises the TiC phase. The solubility of $Ti(C_{1-x}N_x)$ in the metal decreases with an increase in nitrogen content at high temperatures (e.g. 1500°C). This has been shown to retard the dissolution and subsequently the coarsening of the Ti(C,N) in the Ni melt, thereby resulting in a refined microstructure. It then follows that the denitrification effect in Cermets 1 and 3 would result in the destabilization of the Ti(C,N) phase, as the loss of nitrogen would increase the solubility of the TiC phase in the Ni melt and subsequently enhance grain and rim growth. All these effects would then contribute to the coarse microstructures observed, and subsequently accounts for the inferior mechanical properties obtained for these materials.

Consequently, the superior mechanical properties obtained for Cermet 4 were due to the optimization of the processing parameters i.e. reducing the concentration of the binder

material, lowering the sintering temperature to prevent Ostwald ripening processes and the addition of the secondary tantalum phase to reduce dissolution of the TiC and refine the microstructure.

5.3.2. Binder-free Materials

The hardness and fracture toughness of both the ball-milled and mechanically alloyed binder-free Ti(C,N)-based cermets are given in Figure 5-9. The data show that cermets produced from mechanically alloyed Ti(C,N)-Ta powders possess superior hardness and fracture toughness properties compared to conventional ball-milled cermets. This is due to the nature of the mechanical alloying process, allowing for the production of a fine microstructure (as seen in Figure 5-7(a)-(d)) and fast diffusion of alloying elements into the cubic carbide.

In addition, the influence of the Ni binder can readily be observed when comparing the ball-milled binder-containing and binder-free materials i.e. Cermets 4 and 5 respectively. Binder additions to Ti(C,N)-based cermets improved densification through liquid phase sintering, as well as improving material toughness. The results showed that the hardness and toughness properties of Cermet 4 were improved due to the Ni addition as compared to Cermet 5. The addition of the binder to Cermet 4 increased crack interactions with both the solid solution rim and the binder phases, thereby resulting in enhanced toughness compared to Cermet 5.

Considering that the hardness of TaC (1800 kg/mm^2) is significantly higher than that of metallic Ta (110 kg/mm^2), the hardness values obtained for cermets produced from the Ti(C,N)-TaC powder were expected to be higher than both the ball-milled and mechanically alloyed Ti(C,N)-Ta powders as a result of the TaC addition. However, Figure 5-9 shows that significantly poor hardness was obtained for the Ti(C,N)-TaC mixture, although fracture toughness greatly outweighed both the ball-milled and mechanically alloyed Ti(C,N)-Ta powders.

However, these results are consistent with the microstructures obtained during sintering of these materials. As mentioned before, only partial reactivity between the Ti(C,N) and TaC phases occurred during sintering. Consequently, the solid solution phase was present to a lesser extent in the Ti(C,N)-TaC material and a larger amount of unreacted Ti(C,N) cores

were present in the microstructure (Figure 5-7(e)-(f)) following sintering. This, together with the lower densities obtained for the Ti(C,N)-TaC cermets, may account for the lower hardness achieved for these samples compared to the Ti(C,N)-Ta materials.

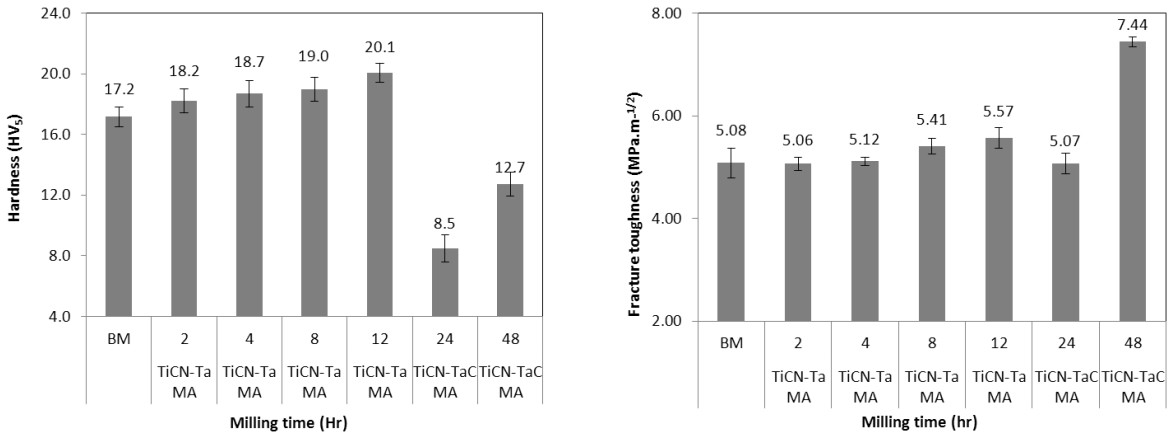


Figure 5-9: Mechanical properties of the binder-free Ti(C,N)-based cermets

Chapter 6: Conclusions

Formation of the (Ti,Ta)(C,N) solid solution phase has been observed as a result of mechanically alloying ductile-brittle Ti(C,N) and tantalum powders. Significant reduction in crystallite size of the Ti(C,N) phase was obtained within the first few hours of mechanical alloying, thereafter the rate of reduction slowed down. The metallic Ta strongly deformed and reacted with the surface of the Ti(C,N), forming a fine grained phase containing (Ta,Ti)(C,N). However, the main amount of the Ti(C,N) remained unreacted during the milling process. The preparation of the (Ti,Ta)(C,N) solid solution phase was more effective when prepared from a mixture of Ti(C,N) and Ta powder, then by the mechanical alloying of hard and brittle Ti(C,N) and TaC powders. Owing to the brittleness of the powders and the low diffusion coefficients in the carbide lattices, the mechanical alloying process served only to refine the grain size of the Ti(C,N) and TaC phases, whilst both phases remained unreacted after 48 hours of mechanical alloying.

The use of the reaction sintering approach for the preparation of the binder free (Ta,Ti)(C,N) cermet using Ta and Ti(C,N) powders significantly improves the densification behaviour and reduces the sintering temperature. In additional, the mechanical alloying improved the sinterability of the Ti(C,N)-Ta powders and full densification was obtainable in solid state following mechanical alloying, using FAST/SPS technique with temperatures as low as 1500°C. Cermets produced of the mechanically alloyed Ti(C,N)-Ta powders showed a fine microstructure, with complete dissolution of Ta into the Ti(C,N) phase following sintering. Consequently, the cermets possessed superior mechanical properties, as compared to conventional ball milled sintered cermets. Only partial dissolution was achieved during sintering of the mechanically alloyed Ti(C,N)-TaC powders. Consequently, poor densification was obtained in these samples, which served to lower the mechanical properties.

Chapter 7: References

1 Ettmayer P, Kolaska H, Lengauer W, Dreyert K. Ti(C,N) Cermets - Metallurgy and Properties. Int J. of Refractory Metals & Hard Materials. 1995;13(6):343-351.

2 Zhou SQ, Zhao W, Xiong WH. Microstructure and Properties of the cermets based on Ti(C,N). In: J. Salem GHWF. Mechanical properties and processing of ceramic binary, ternary and composite systems. John Wiley & Sons; 2008.

3 Ahn SY, S.W. Kim, Kang S. Microstructure of Ti(CN)–WC–NbC-Ni cermets. J. Am. Ceram. Soc.. 2001;84(4):843-849.

4 Ahn SY, Kang S. Formation of Core/Rim Structures in Ti(C, N)-WC-Ni Cermets via a Dissolution and Precipitation Process. J. Am. Ceram. Soc. 2000;83(6):1489-1494.

5 Ahn S, Kang S. Effect of various carbides on the dissolution behavior of Ti(C0.7N0.3) in a Ti(C0.7N0.3)–30Ni system. International Journal of Refractory Metals and Hard Materials. 2001;19(4-6):539-545.

6 P.N. T, Wedlake RJ. In Proceedings of the International Conference on Recent Developments in Speciality Steels and Hard Materials. Vol 173. Pretoria: Pergamon, Oxford; 1983.

7 Wentorf RH, Vries RCD, Bundy FP. Sintered Super- Hard Materials. Science 208. 1980;873.

8 Ardo AJD, Garcia CI, Laible RM, Eriksson U. A better way to assess machinability. Am. Machinist. 1993;137(5):33-35.

9 Suryanarayana C. Mechanical Alloying and Milling. Progress in Materials Science. 2001;46:1-184.

10 Santhanam AT. Application of transition metal carbides and nitrides in industrial tools. In: Oyama ST. The chemistry of transition metal carbides and nitrides. London: Chapman & Hall; 1996.

11 Storms EK. The refractory carbides. New York: Academic Press; 1967.

12 Toth LE. Transition Metal Carbides and Nitrides. New York: Academic Press; 1971.

13 Storms EK. The Refractory Carbides. 1st ed. New York: Academic Press; 1967.

14 Kwona DH, Hongb SH, Kim BK. Fabrication of ultrafine TaC powders by mechano-chemical process. Materials Letters. 2004;58:3863-3867.

15 Palomar FE, Zambrano P, Gómez MI, Colás R, Castillo A. Tungsten Carbide and Tantalum Carbide Coatings on Machining Tools. Ingeniería mecánica tecnología y desarrollo. 2009;3(2):55-59.

16 Holleck H. Material selection for hard coatings. Journal of Vacuum Science and Technology A. 1986;4 (6):2661-2669.

17 MOAK RDKaDP. Hot Hardness of Selected Borides, Oxides and Carbides to 19OOC. Journal of The American Ceramic Society. 1967;50(6):290-296.

18 DeArdo AJ, Garcia CI, Laible RM, Eriksson U. A better way to assess machinability. Am. Machinist. 1993;137(5):33-35.

19 Salem JA, Hilmas G, Fahrenholtz W. Mechanical Properties and Processing of Ceramic Binary, Ternary, and Composite Systems. Ceramic Engineering and Science Proceedings. 2009.

20 Liu N, Xu YD, Li H, Chen MH, Zhou J, Xie F, Yang HD. Cutting and wearing characterisitics of TiC-based cermets cutters with nano-TiN addition. Journal of Materials Processing Technology. 2005;161(3):478-484.

21 Pastor H. Titanium-carbonitride-based hard alloys for cutting tools. Mater. Sci. and Eng. 1988;A105:401-409.

22 Tobioka M, Shimizu Y, Isobe K, Kitagawa N, Nomura T, Takahashi K. High toughness cermet and a process for the production of the same. 1988. September 6.

23 Matsubara H, Sakuma T. Microstructure and mechanical properties of titanium carbonitride base cermets. Sintering '87. 1988;2:1269-1274.

24 Gruss WW. Cermets. In: Metals Handbook. 9th ed. 1993. p. 90-97.

25 Zhang S. Titanium carbonitride-based cermets: processes and properties. Materials Science and Engineering. 1993;163A:141-148.

26 Weast RC, editor. Handbook of Chemistry and Physics. 66th ed. CRC Press Inc; 1986.

27 Neumann G, Kieffer R, Ettmayer P. Uber das System TiC-TiN-TiO. Monatshefie fur Chemie. 1972;103:1130-1137.

28 Shimada M, Suzuki T, Koizumi M. Fabrication and characterization of $TiC_{1-x}N_x$ ($0 \leq x \leq l$) and $Mo_2B_{2-x}C_x$ ($x = 0, 1.0, 2.0$) by high-pressure hot-pressing. Mater Lett. 1983;1(5/6):175-177.

29 Moskowitz D, Terner LL, Jr MH. Some physical and metal-cutting properties of titanium carbonitride base materials. Science of Hard Materials. 1984 605-617.

30 Parikh NM, Humenik M. Cermets: II, Wettability and Microstructure Studies in Liquid-Phase Sintering. Journal of the American Ceramic Society. 1957;40(9):315-320.

31 Chaoa S, Liua N, Yuana Y, Xua CHY, Shia M, Feng J. Microstructure and mechanical properties of ultrafine Ti(CN)-based cermets fabricated from nano/submicron starting powders. Ceramics International. 2005;31:851-862.

32 Lindahl P, Rose AE, Gustafson P, Rolander U, Andre HO. Effect of pre-alloyed raw materials on the microstructure of a (Ti,W)(C, N)–Co cermet. International Journal of Refractory Metals and Hard Materials. 2000;18:273-279.

33 Xiong J, Guo Z, Shen B, Cao D. Fracture origin and intrinsic strength of ultra-fine TiC0.7N0.3-based cermet. International Journal of Refractory Metals & Hard Materials. 2007;25:256-262.

34 Gong J, Pan X, Miao H, Zhao Z. Effect of metallic binder content on the microhardness of TiCN-based cermets. Materials Science and Engineering. 2003;A359:391-395.

35 Kumar AS, Durai AR, Sornakumar T. Machinability of hardened steel using alumina based ceramic cutting tools. International Journal of Refractory Metals & Hard Materials. 2003;21:109-117.

36 Rolander U, Weinl G, Zwinkels M. Effect of Ta on structure and mechanical properties of (Ti,Ta,W)(C,N)–Co cermets. International Journal of Refractory Metals and Hard Material. 2001;19(4-6):325-328.

37 Chase MW, editor. NIST-JANAF Thermochemical Tables. 4th ed. 1998.

38 Dizaji VR, Rahmani M, Sani MF, Nemati Z, Akbari J. Microstructure and cutting performance investigation of Ti(C, N)-based cermets containing various types of secondary carbides. International Journal of Machine Tools & Manufacture. 2007;47:768-772.

39 Kumar BVM, Ramkumar J, Basu B, Kang S. Electro-discharge machining performance of TiCN-based cermets. International Journal of Refractory Metals & Hard Materials. 2007;25:293-299.

40 Kumar BVM, Basu B. Mechanisms of material removal during high temperature fretting

of TiCN–Ni based cermets. International Journal of Refractory Metals & Hard Materials. 2008;26:504-513.

41 Kang S, Park DS, Lee YD. Effect of carbides on the microstructure and properties of Ti(C,N)-based ceramics. Journal of American Ceramics Society. 1999;82(11):3150-3154.

42 Tret'yakov VL, Mashevskaya VL. Effect of tantalum on the properties and microstructure of hard alloys based on titanium carbonitride. Powder Metallurgy and Metal Ceramics. 1999;38(1-2):64-67.

43 Gruss WW. Cermets. In: Metals Handbook. 9th ed. Vol 16. 1989. p. 90-97.

44 El-Eskandarany MS. Mechanical alloying for fabrication of advanced engineering materials. Noyes Publications/William Andrew Publishing; 2001.

45 Huang B, Fan J, Liang S, Qu X. The rheological and sintering behavior of W–Ni–Fe nano-structured crystalline powder. Journal of Materials Processing Technology. 2003;137:177-182.

46 Lahiri I, Bhargava S. X-ray powder diffraction line profile analysis of mechanically alloyed Cu–Cr powder. Materials Science and Technology. 2009;25(4):520-526.

47 Benjamin JS. Scientific American. 1976;234(5):40–48.

48 Gordo E, Velasco F, Anton N, Torralba JM. Wear mechanisms in high speed steel reinforced with (NbC)p and (TaC)p MMC. Wear. 2000;239:251–259.

49 Gordo E, Parra E, Ruiz-Nava EM, Torralba JM. Approach to the development of high-carbide content high-speed-steel matrix composites. New Developments in Powder Technology. 2001 1355–1360.

50 Fogagnolo JB, Ruiz-Navas EM, Robert MH, Torralba JM. 6061 Al reinforced with silicon nitride particles processed by mechanical milling. Scripta Materialia. 2002;47:243–248.

51 Matteazzi P, Caer GL. Room-Temperature Mechanosynthesis of Carbides by Grinding of Elemental Powders. Journal of the American Ceramic Society. 1991;74(6):1382-1390.

52 Gu DD, Meiners W, Hagedorn YC, Wissenbach K, Poprawe R. Structural evolution and formation mechanisms of TiC/Ti nanocomposites prepared by high-energy mechanical alloying. Journal of physics D: Applied physics. 2010;43:1-11.

53 Gu DD, Shen YF. Advanced Engineering Materials. 2009;11:573-578.

54 Choi CJ. Preparation of ultra®ne TiC±Ni cermet powders by mechanical alloying. Journal

of Materials Processing Technology. 200;140:127-132.

55 Bolokang AS. A comparison of the mechanically alloyed (V,W)C and (V,W)C–Co powders. Journal of Alloys and Compounds. 2009;477:905-908.

56 Zhu S, Ma J, Zhang M, Wu C. Mechanical Alloying: For Formation of Nanocomposite WC/MgO Materials. Advances in Nanocomposites- Synthesis, Characterization and Industrial Applications. 883-908.

57 Unal N. The effect of boron carbide addition on the structural and mechanical properties of tungsten matrix composites. MSc Thesis. Istanbul Technical University; 2006.

58 Perng ZHCaTP. Instant formation of Ti N by reactive milling of Ti in nitrogen. Materials Science Forum. 1997;121:235-238.

59 M. Kis-Varga DLB. Materials Science Forum. 1996;465:225-227.

60 Soni PR. Mechanical Alloying: Fundamentals and Applications. Cambridge International Science Publishing; 2001.

61 A. Calka, J.I. Nikolov, B.W. Ninham. In: DeBarbadillo JJ. Mechanical alloying for structural applications. Materials Park: ASM International; 1993. p. 189-195.

62 Gordo E, Gómez B, Torralba EMRNaJM. Influence of milling parameters on the manufacturing of Fe–TiCN composite powders. Journal of Materials Processing Technology. 2005;162(163):59-64.

63 Maurice DR, Courtney TH. The Physics of Mechanical Alloying" A First Report. Metallurgical Transactions. 1990;21A:289-303.

64 Harris JR. Mathematical modeling of mechanical alloying. Ph.D. Thesis. University of Nottingham ; 2002.

65 Benjamin JS, Violin TE. The Mechanism of Mechanical Alloying. Metallurgical Transactions. 1974;5:1929-1934.

66 Aikin BJM, Courtney TH. The Kinetics of Composite Particle Formation During Mechanical Alloying. Metallurgical Transactions. 1993;24A:647-657.

67 Harris CC. On the Limit of Comminution. Trans. AIME. 1967;238:17-30.

68 CC K. Nanostructured Mater. 1993;2:109-129.

69 Lee PY, Yang JL, Lin HM. Amorphization behaviour in mechanically alloyed Ni-Ta

powders. Journal of Material Science. 1998;33(1):235-239.

70 Benjamin JS. Mechanical alloying - A perspective. Metal Powder Report. 1990;45(2):122-127.

71 Gilman PS, Benjamin JS. Mechanical Alloying. Annual Review of Materials Science 1983;13:279–300.

72 Davis RM, Koch CC. Scripta Metall. 1987;21:305-310.

73 Davis RM, McDermott B, Koch CC. Metallurgical Transactions. 1988;A19:2867-2874.

74 Zhang S, Khor KA, Lii L. Preparation Of Ti(C,N)-WC-TaC Solid Solution By Mechanical Alloying Technique. Journal of Materials Processing Technology. 1995;48:779-784.

75 Maweja K, Cornish LA, Can N. Transformation and alloying mechanisms in sub-stoichiometric titanium carbonitrides - tungsten high energy ball milled powders. Int. Journal of Refractory Metals and Hard Materials. 2011;29:312-319.

76 Schaffer GB, McCormick PG. Mechanical alloying. Materials Forum. 1992;16:91-97.

77 McCormick PG, Wharton VN, Royhani MM, Schaffer GB. Microcomposites and Nanophase Materials. Pennsylvania: Warrendale; 1991.

78 Lu L, Lai MO, Zhang S. Synthesis of Cu-based shape memory alloy powder. Mater. Week. 1994;94(2-6):517-522.

79 Lu L, Lai MO, Zhang S. Diffusion in mechanical alloying. Journal of Materials Processing Technology. 1997;67:100-104.

80 Schaffer GB, McCormick PG. Mechanical alloying. Materials Forum. 1992;16:91-97.

81 Lu L, Lai MO. Formation of new materials in solid state by mechanical alloying. Mater. Design. 1994;16:33-39.

82 Porter DA, Easterling KE. Phase Transformation in Metals and Alloys. 1980 66-68.

83 Atkinson HV, Rickinson BA. Hot isostatic processing. In: Wood J, editor. The Adam Hilger Series on New Manufacturing Processes and Materials. Bristol: Philadelphia and New York; 1991. p. 34-38.

84 Cullity BD. Elements of X-Ray Diffraction. Addison-Wesley; 1965.

85 Klug HP, Alexander LE. X-Ray diffraction procedures for polycrystalline and amorphous materials. Wiley-Interscience; 1974.

86 Angerera P, Yub LG, Khorb KA, Korba G, Zalitec I. Spark-plasma-sintering (SPS) of

nanostructured titanium carbonitride powders. Journal of the European Ceramic Society. 2005;25:1919-1927.

87 D. K. SHETTY IGW. On estimating fracture toughness of cemented carbides from Palmqvist crack sizes. Journal of Materials Science Letters. 1986;5:365-368.

88 Frage NR, Gurevich YG, Sokolova EV, Leonovich BI. The interaction of titanium carbonitride with iron and nickel. Russian MetalL(English translation). 1989;4:171-175.

89 Fukuhara M, Mitani H. On the sintering of Ti(C,N)-30 wt% Ni and TiNx-TiCy-30 wt% Ni mixed powder compacts. Journal of Japan Society Powder Metallurgy. 1980;27(4):125-129.

90 Storms EK. The Refractory Carbides. 1967: Academic Press; New Yors.

91 Alekseev ES, Arkhipw RG, Popova SV. Band Structure of the Metastable F.G.C. Tantalum Nitride. Physica status solidi. 2006;90(2):133-136.

92 SGTE - SGTE Alloy Phase Diagrams. [Internet]. Available from: http://www.crct.polymtl.ca/fact/phase_diagram.php?file=Ni-Ta.jpg&dir=SGTE.

93 Huang B, Fan J, Liang S, Qu X. The rheological and sintering behavior of W–Ni–Fe nano-structured crystalline powder. Journal of Materials Processing Technology. 2003;137:177-182.

94 Borrell A, Fernandez A, Torrecillas R, Cordoba JM, Aviles MA, Gotorz FJ. Spark Plasma Sintering ofUltrafine TiCxN1-x Powders Synthesized by a Mechanically Induced Self-Sustaining Reaction. Journal of American Ceramic Society. 2010;93(8):2252-2256.

95 Raichenko AI, Khandros LL, Muravskii NA. The sintering of compacts from powders with particles in different conditions. Translated from Poroshkovaya Metallurgiya. 1969;11(83):26-30.

96 Liu N, Chao S, Huang X. Effects of TiC/TiN addition on the microstructure and mechanical properties of ultra-fine grade Ti (C, N)–Ni cermets. Journal of the European Ceramic Society. 2006;26:3861-3870.

97 Alvarez M, Sánchez JM. Spark plasma sintering of Ti(C,N) cermets with intermetallic binder phases. International Journal of Refractory Metals & Hard Materials. 2007;25:107-118.

98 Alvarez M, Sánchez JM, Etxeberria J, Bourgeois L, G. Barbier JH. In: Kneringer G,

Rödhammer P, Wildner H, editors. Proceedings of 16th international plansee seminar 2005; 2005; Plansee Holding AG. p. 419-433.

99 German RM. Sintering Theory and Practice. New York: Wiley; 1996.

100 Burton WK, Cabrera N, Frank FC. The Growth of Crystals and the Equilibrium Structure of their Surfaces. Philosophical Transactions of the Royal Society of London, Series A, Mathematical and Physical Sciences. 1951;243:299-358.

101 Cahn JW. On the Morphological Stability of Growing Crystal. Oxford: Symposium Publications Division, Pergamon Press; 1967.

102 Fukuhara M, Mitani H. Phase Relationship and Denitrification during the Sintering Process of TiN-Ni Mixed Powder Compacts. Transactions of the Japan Institute of Metals. 1980;21:211-218.

103 Ueki M, Saito T, Suzuki H. Sinterability of Nitrogen Contained TiC-Mo2C-Ni Cermet. Journal of the Japan Society of Powder and Powder Metallurgy. 1989;36:371-373.

104 Feng P, Xiong W, Yu L, Zheng Y, Xia Y. Phase evolution and microstructure characteristics of ultrafine Ti(C,N)-based cermet by spark plasma sintering. International Journal of Refractory Metals & Hard Materials. 2004;22:133-138.

105 Park S, Kang S. Toughened ultra-fine (Ti,W)(CN)–Ni cermets. Scripta Materialia. 2005;52:129-133.

106 Phasha M, Maweja K, Babst C. Mechanical alloying by ball milling of Ti and Mg elemental powders: Operation condition considerations. Journal of Alloys and Compounds. 2010;492(1-2):201-207.

107 Bilyk II. Potentialities of carbonitrides as the hard constituent of sintered hard alloys. Poroshk Metal. 1972;6:49-54.

108 Wentorf RH, Vries RCD, Bundy FP. Sintered superhard materials. Science. 1980; 208:873-880.

109 Tomlinson PN, Wedlake RJ. Proceedings of the International Conference on Recent Developments in Speciality Steels and Hard Materials.; 1983; Pretoria. p. 173.

110 Bezhenaar NP. Physiochemical interactions between cubic boron nitride and aluminium during high-pressure sintering. Journal of Superhard Materials. 1999;21(2):2-9.

111 Benko E. Proc World Ceramic Congress. In: Vincenzini P, editor. Techna; 1995; Firenze.

p. 1430-45.

112 Rong XZ, Tsurumi T, Fukunaga O, Yano T. High-pressure sintering of cBN-TiN-Al composite for cutting tool application. Diamond and Related Materials. 2002;11:280-286.

113 Sahin Y. Comparison of tool life between ceramic and cubic boron nitride (CBN) cutting tools when machining hardened steels. Journal of materials processing technology. 2009;209(7):3478-3489.

114 Diniz AE, Oliveria AJ. Hard turning of interrupted surfaces using CBN tools. J. Mater. Process. Technol. 2008;195:275-281.

115 Chou YK, Evans CJ, Barash MM. Experimental investigation on CBN turning of hardened AISI 52100 steel. Journal of Materials Processing Technology. 2002;124:274-283.

116 Chung-Chen T, Hong H. Comparison of the tool life of tungsten carbide coated by multi-layer TiCN and TiAlCN for end mills using the Taguchi method. Journal of Materials Processing Technology. 2002;123:1-4.

117 Rong XZ, O. Fukunaga. Sintering of cubic boron nitride with added aluminium at high pressure and temperatures. Advanced Materials. 1993.

118 Calos NJ, Forrester JS, Schaffer GB. The mechanisms of combustion and continuous reactions during mechanical alloying. Journal of Solid State Chemistry. 2001;158(2):268-278.

119 Mazurovsky V, M.Zinigrad, Zinigrad A, Leontiev L, Lisin V. The phenomenological model of non-equilibrium crystallization and strengthening-phase-formation processes in the weld. 2003 155-167.

120 Pierson HO. Handbook of Refractory Carbides and Nitrides. 1st ed. Park Ridge NJ: Noyes; 1960.

121 Maouche D, Louail L, Ruterana P, Maamache M. Formation and stability of di-transition-metal carbides TixZr1-xC, TixHf1-xC and HfxZr1-xC. Computational Materials Science. 2008;44:347-350.

122 Ozturk B, Fruehan RJ. Thermodynamics of inclusion formation in Fe-Ti-C-N alloys. Metallurgical. Metallurgical Trans. B. 1990;21:879-884.